

## **General Disclaimer**

### **One or more of the Following Statements may affect this Document**

- This document has been reproduced from the best copy furnished by the organizational source. It is being released in the interest of making available as much information as possible.
- This document may contain data, which exceeds the sheet parameters. It was furnished in this condition by the organizational source and is the best copy available.
- This document may contain tone-on-tone or color graphs, charts and/or pictures, which have been reproduced in black and white.
- This document is paginated as submitted by the original source.
- Portions of this document are not fully legible due to the historical nature of some of the material. However, it is the best reproduction available from the original submission.

Prepared by:


Guidance and Control Group  
The Bendix Corporation

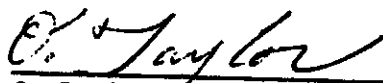
THE BENDIX  
CORPORATION


GUIDANCE SYSTEMS  
DIVISION  
DENVER OPERATIONS

FLOATED PALLET  
DEFINITION STUDY

Approved by:

  
S. Calvin Rybak  
Program Manager

  
O. Taylor  
Technical Manager

  
M. Brown  
Manager,  
Denver Operations

FINAL REPORT

APRIL 1975

VOLUME III  
RETENTION/SUSPENSION  
SYSTEMS, PALLET  
COMMON MODULE  
CONFIGURATION STUDY

PREPARED FOR:

GEORGE C. MARSHALL  
SPACE FLIGHT CENTER  
HUNTSVILLE, ALABAMA

NASA CONTRACT NO.  
NAS8-30889

### FOREWORD

This final report is submitted in accordance with the requirements of NASA-GSFC, Contract No. NAS8-30889. The report includes:

- Volume I - Evaluation of Alternate Telescope Pointing Schemes
- Volume II - Suspended Pallet Pointing Performance Study
- Volume III - Retention/Suspension Systems, Pallet Common Module Configuration Study

## CONTENTS

	<u>Page</u>
Foreword. . . . .	ii
Contents. . . . .	iii
 1. INTRODUCTION. . . . .	 1-1
1.1 General . . . . .	1-1
1.2 Study Objectives. . . . .	1-1
1.3 Method of Approach and Principal Assumptions. . . . .	1-2
1.4 Suggested Additional Effort. . . . .	1-2
 2. SUMMARY . . . . .	 2-1
 3. VEHICLE DESCRIPTION . . . . .	 3-1
3.1 Space Shuttle System Description. . . . .	3-1
3.2 Orbiter/Pallet System . . . . .	3-1
3.2.1 Orbiter . . . . .	3-1
3.2.2 Pallet. . . . .	3-6
 4. PALLET SUSPENSION SYSTEM. . . . .	 4-1
4.1 General . . . . .	4-1
4.2 Summary . . . . .	4-1
4.3 Discussion. . . . .	4-1
4.3.1 Design Objectives . . . . .	4-1
4.3.2 Isolator Attachment Region. . . . .	4-1
4.3.3 System Geometry Study . . . . .	4-3
4.3.4 Single Point Suspension . . . . .	4-4
4.3.5 Two Point Suspension Containing the Center of Mass . . . . .	4-7
4.3.6 Three Point Suspension Containing the Center of Mass. . . . .	4-15
4.3.7 Four Point Suspension . . . . .	4-22
4.3.8 Damping . . . . .	4-29
4.3.9 Isolator Study. . . . .	4-31
4.3.10 System/Isolator Selection . . . . .	4-33
4.3.11 Four Point Suspension Using Gas Filled Bellows . . . . .	4-33
4.3.12 Suspension System Evaluation. . . . .	4-49
4.4 Conclusion. . . . .	4-62
 5. PALLET RETENTION SYSTEM . . . . .	 5-1
5.1 General . . . . .	5-1
5.2 Summary . . . . .	5-1
5.3 Discussion. . . . .	5-1
5.3.1 Design Objectives . . . . .	5-1

## CONTENTS (Continued)

	<u>Page</u>
5.3.2 Release At the Orbiter Trunnions. . . . .	5-2
5.3.3 Splitting the Mounting Shaft. . . . .	5-2
5.3.4 Movable Mounting Shaft. . . . .	5-2
5.4 Conclusion. . . . .	5-7
 6. CONTROL MOMENT GYROSCOPE (CMG) INSTALLATION . . .	 6-1
6.1 General . . . . .	6-1
6.2 Summary . . . . .	6-1
6.3 Discussion. . . . .	6-1
6.3.1 Design Objectives . . . . .	6-1
6.3.2 Installation Study. . . . .	6-1
6.3.3 CMG Isolation System. . . . .	6-3
6.3.4 Support Frame With Two CMGs . . . . .	6-3
6.3.5 Support Frame With Four CMGs. . . . .	6-3
6.3.6 Installation. . . . .	6-6
6.4 Conclusion. . . . .	6-6
 7. EXPERIMENT MOUNT AND ERECTION . . . . .	 7-1
7.1 General . . . . .	7-1
7.2 Summary . . . . .	7-1
7.3 Experiment Base Mount Installation. . . . .	7-1
7.3.1 Support Frame . . . . .	7-1
7.3.2 Installation. . . . .	7-1
7.4 Line of Sight Errors Due to Mounting	
Misalignments . . . . .	7-1
7.4.1 Error Propagation for the Inside Out	
Gimbal System (IOG) . . . . .	7-3
7.4.2 Error Propagation for the Classical	
Gimbal System . . . . .	7-8
7.5 Gimbal Motions Required for an Arbitrary	
Line of Sight Adjustment. . . . .	7-14
7.5.1 Gimbal Motions of the IOG System. . . . .	7-16
7.5.2 Gimbal Motions of the Classical System. . . .	7-18
7.6 Conclusions . . . . .	7-20
 8. PALLET COMMON MODULE CONFIGURATION. . . . .	 8-1
8.1 General . . . . .	8-1
8.2 Summary . . . . .	8-1
8.3 Discussion. . . . .	8-1
8.3.1 Design Objectives . . . . .	8-1
8.3.2 Suspension System Installation. . . . .	8-1
8.3.3 Retention System Installation . . . . .	8-4
8.3.4 Control Moment Gyroscope Installation . . . .	8-4

## CONTENTS (Continued)

		<u>Page</u>
8.4	Control Moment Gyroscope Installation . . . . .	8-4
8.5	Conclusion. . . . .	8-7
9.	REFERENCES. . . . .	9-1
 <u>Figure</u>		
2-1	Logical Flow of the Performance of the Study. . .	2-2
3-1	Space Shuttle Flight System . . . . .	3-2
3-2	Orbiter/Pallet Configuration. . . . .	3-3
3-3	Orbiter Related to the Inertial Coordinate System. . . . .	3-5
3-4	Pallet System . . . . .	3-8
4-1	Isolator Attachment Region. . . . .	4-2
4-2	Single Point Offset Below the Pallet - Sign Convention for Forces and Moments . . . . .	4-5
4-3	Two Point Suspension at the Sides of the Pallet - Sign Convention for Forces and Moments . . . . .	4-9
4-4	Two Point Suspension at the Ends of the Pallet - Sign Convention for Forces and Moments . . . . .	4-13
4-5	Three Point Suspension Containing the Center of Mass on a YZ Plane - Sign Convention for Forces and Moments. . . . .	4-16
4-6	Three Point Suspension Containing the Center of Mass on a Skewed Plane - Sign Convention for Forces and Moments. . . . .	4-19
4-7	Four Point Suspension Containing the Center of Mass - Sign Convention for Forces and Moments . . . . .	4-24
4-8	Four Point Suspension Offset Above the Pallet - Sign Convention for Forces and Moments. . . . .	4-28
4-9	Four Point Suspension Containing the Center of Mass Gas Filled Bellows Isolators. . . . .	4-35
4-10	Gas Filled Bellows. . . . .	4-39
4-11	Center of Mass Offset . . . . .	4-50
4-12	X Offset Center of Mass . . . . .	4-52
4-13	Y Offset Center of Mass . . . . .	4-53
4-14	Z Offset Center of Mass . . . . .	4-54
5-1	Locked Position . . . . .	5-3
5-2	Unlocked Position . . . . .	5-4
5-3	Cargo Bay Main Longeron Retention Point Mounting Shaft Extended Position. . . . .	5-5

## CONTENTS (Continued)

		<u>Page</u>
5-4	Cargo Bay Main Longeron Retention Point	
	Mounting Shaft Retracted Position . . . . .	5-6
5-5	Engagement Sequence . . . . .	5-8
6-1	Bendix MA-2300 Double Gimbal Control Moment	
	Gyroscope . . . . .	6-2
6-2	Support Frame With Two CMGs . . . . .	6-4
6-3	Support Frame With Four CMGs. . . . .	6-5
7-1	Experiment Base Mount Installation. . . . .	7-2
7-2	Relation of the Ideal Pointed Coordinates to the Base Coordinates For the Inside Out Gimbal. . . . .	7-4
7-3	Relation of the Ideal Pointed Coordinates to the Base Coordinates For the Classical Gimbal Arrangement. . . . .	7-10
7-4	Relation of the Initial and Adjusted Lines of Sight. . . . .	7-15
8-1	Pallet Common Module. . . . .	8-2
8-2	Suspension System - Gas Filled Bellows Aft Left-Hand Location. . . . .	8-3
8-3	Retention System - Movable Mounting Shafts. . . .	8-5
8-4	Four Control Moment Gyroscopes on a Single Pallet. . . . .	8-6

### Table

3-1	Orbiter/Pallet Vehicle Mass Properties. . . . .	3-4
3-2	Orbiter Mass Properties . . . . .	3-7
3-3	Pallet Mass Properties. . . . .	3-7
4-1	Single Point Suspension Offset Below the Pallet Natural Frequencies and Spring Constants. . . .	4-8
4-2	Two Point Suspension At the Sides of the Pallet Natural Frequencies and Spring Constants. . . .	4-12
4-3	Two Point Suspension At the Ends of the Pallet Natural Frequencies and Spring Constants. . . .	
4-4	Three Point Suspension on a YZ Plane Natural Frequencies and Spring Constants. . . . .	4-18
4-5	Three Point Suspension on a Skewed Plane Natural Frequencies and Spring Constants. . . .	4-23
4-6	Four Point Suspension Containing the Center of Mass Natural Frequencies and Spring Constants . . . . .	4-26
4-7	Four Point Suspension Offset Above the Pallet Natural Frequencies and Spring Constants. . . .	4-30

CONTENTS (Concluded)

		<u>Page</u>
4-8	Summary - Performance Characteristics of the Suspension Systems and Isolators. . . . .	4-34
4-9	Four Point Suspension - Gas Filled Bellows Natural Frequencies, Damping Ratios, Spring Constants, Damping Constants . . . . .	4-36
4-10	Bellows Design Features . . . . .	4-44
4-11	Spring Constant Sensitivity . . . . .	4-56
4-12	Damping Sensitivity . . . . .	4-58
4-13	Weight and Volume . . . . .	4-61



## 1. INTRODUCTION

1.1 General - With the maturation of the space shuttle concept using a reusable launch vehicle for earth orbital missions, two divergent modes of operation have been defined. One mode involves the use of the shuttle as a logistics vehicle placing free flying experiment packages in orbit and replacing, repairing or servicing existing packages. In addition it will perform a crucial role as a manned experiment base, remaining in earth orbit from 7 to 30 days performing various experiments with equipment mounted in the payload bay.

Current assessments of the experiments proposed for operation in low earth orbit in conjunction with a manned vehicle indicate that nearly 45 percent of the payloads require pointing accuracy greater than that afforded by the orbiter capability using the Reaction Control System (RCS) and 39 percent have requirements exceeding the capabilities of the orbiter under the direct control of Control Moment Gyroscopes (CMGs). One concept under study to meet these higher accuracy pointing requirements is to mount the experiment packages to a pallet structure which in turn is attached to the orbiter through a suspension system which isolates the pallet from the disturbances arising in the orbiter occurring during periods of instrument operation.

The study described in this report involves the definition and evaluation of the pallet suspension system, a compatible pallet retention system and a pallet common module configuration. The latter includes the installation of Control Moment Gyroscopes (CMGs), an experiment universal base mount and the definition of experiment erection motions and tolerances.

1.2 Study Objectives - The objectives of the study were the following:

- a. Selection of a suspension system and definition of the isolator that best satisfies the overall mission requirements.
- b. Definition of a retention system that minimizes structural modifications to existing pallet designs and that best satisfies the overall mission requirements.
- c. Definition of a pallet common module that will be used for various missions.
- d. Installation of the CMGs on the pallet common module.

- e. Development of an approach to install the experiment universal base mount on the pallet common module and definition of the motions and tolerances of the experiment erection.

All of the above objectives were met during the course of the study.

1.3 Method of Approach and Principal Assumptions - The approach followed in this study throughout was to make use of state-of-the-art technology. A primary consideration in the selection of the suspension system and definition of the isolator was the availability of mathematical design data in order to obtain a cost effective system. Likewise the definition of a retention system minimizes structural modifications to existing pallet designs.

The orbiter as defined in mid-1974 along with pallet designs of the latter part of 1974 were the configurations used.

1.4 Suggested Additional Effort - The following additional investigations affecting the floated pallet common module are suggested:

- a. Review the instruments and payload experiment combinations which are candidates for the floated pallet to determine center of mass envelopes as they affect the suspension system.
- b. Investigate the relative motions of the pallet/orbiter mounting points as they affect the suspension system and the retention system.

## 2. SUMMARY

The floated pallet definition study consisted of three related but separate studies. The first was an evaluation of alternate pointing systems for orbiter experimental instrumentation, the results of which are presented in volume I of this final report. The second was the pallet pointing performance study treated in volume II. The third was a hardware conceptual design study including pallet suspension and retention systems, experiment erection, CMG mounting, etc., with results presented in this volume of the final report. Figure 2-1 is a diagram of the logical flow of activity during the performance of the retention/suspension systems, pallet common module configuration study.

The basic requirements under which this study was performed are shown as block 0 on the diagram. The contract statement of work defines all tasks and schedules. Input data for the study included baseline shuttle data, particularly payload interface information required for pallet mounting and mass properties. Pallet data included mass properties, structural and dimensional data and typical experiment layouts. The mission requirements applicable to this study included the suspension system performance and the retention system constraints.

The study was initiated with block 1, the pallet suspension system study. The suspension system performance requirements were applied to various configurations with results given in section 4. Next the retention system constraints study, shown as block 2, were applied to existing pallet designs with results given in section 5. The impact of the suspension system and the retention system to the existing pallet design, shown as blocks 5 and 6, was defined with results given in section 8.

In parallel with the suspension system and the retention system studies a CMG support equipment configuration study, shown in block 3, and an experiment mount and erection study, shown in block 4, were performed. The CMG support equipment configuration study was also performed in parallel with the control system study presented in volume II. Results of the CMG support equipment configuration study are given in section 6 and results of the experiment mount and erection study are given in section 7.

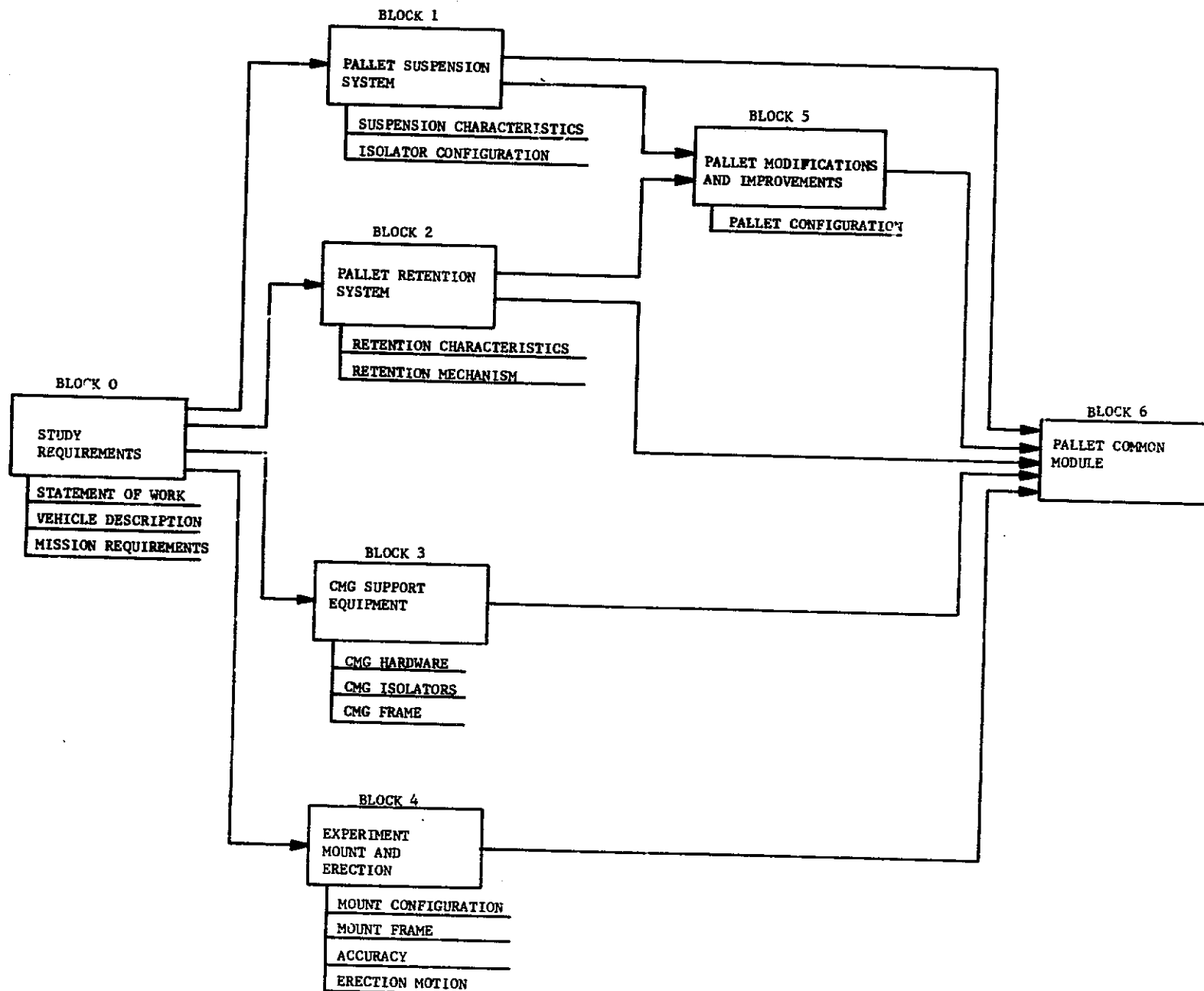


Figure 2-1. Logical Flow of the Performance of the Study

### 3. VEHICLE DESCRIPTION

3.1 Space Shuttle System Description - There are three main components which comprise the space shuttle flight system; the orbiter, an external tank containing the ascent propellants to be used by the orbiter main engines, and two Solid Rocket Boosters (SRBs). The space shuttle flight system is shown in figure 3-1. The SRBs and the orbiter main engines fire in parallel, providing thrust for lift-off. The SRBs are jettisoned when the fuel is exhausted and the orbiter main engines continue firing until the vehicle reaches the desired suborbital conditions where the external tank is jettisoned. At this time the Orbital Maneuvering Subsystem (OMS) is fired to place the orbiter in the desired orbit.

The orbiter portion shown in figure 3-1 is a reusable vehicle which delivers and retrieves payloads, conducts orbital operations, and returns to a land base in a manner similar to that of an aircraft. Typical orbital missions are designed for operations of up to 7 days. However, orbiter design does not preclude missions of up to 30 days.

3.2 Orbiter/Pallet System - Payloads are carried by the orbiter in the payload bay (figure 3-1). The payload used for this study is a floated pallet which is connected to the orbiter through vibration isolators. The orbiter and payload are considered to be rigid bodies. Figure 3-2 is an overall view of the orbiter/pallet combined configuration.

Each isolator suspension point is assumed to exhibit linear compliance, viscous damping and friction along each axis with no rotational effects or cross-coupling. The design goal of the suspension is to have uncoupled rotational and translational isolation with equal natural frequencies.

Mass properties of the orbiter/pallet configuration are given in table 3-1. All center-of-mass locations are given referenced to an Inertial (I) coordinate system, which has its origin located at the nose of the external tank. Figure 3-3 shows the location of the orbiter with respect to the I coordinate system. As shown, the centerline of the payload bay is 400 inches above the inertial axis.

3.2.1 Orbiter - Once the orbiter has reached the desired orbit, attitude control is maintained by the Reaction Control System (RCS) or by some control mechanism which has been placed in the payload bay. Through use of the RCS system, the orbiter is capable of achieving and maintaining any attitude to a certain degree of accuracy. If more accurate pointing is required for a particular experiment, then pointing capability must be included within the

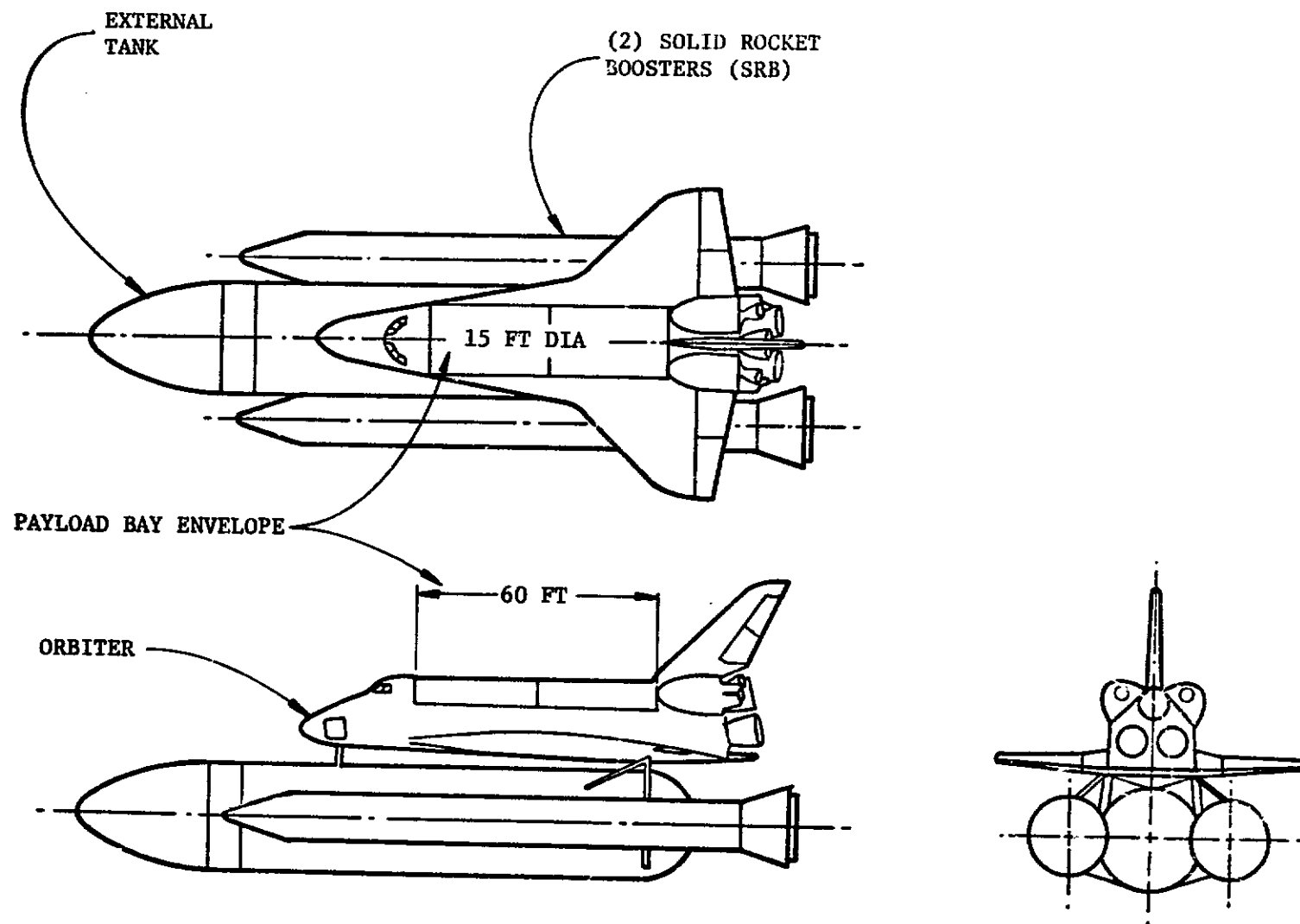


Figure 3-1. Space Shuttle Flight System

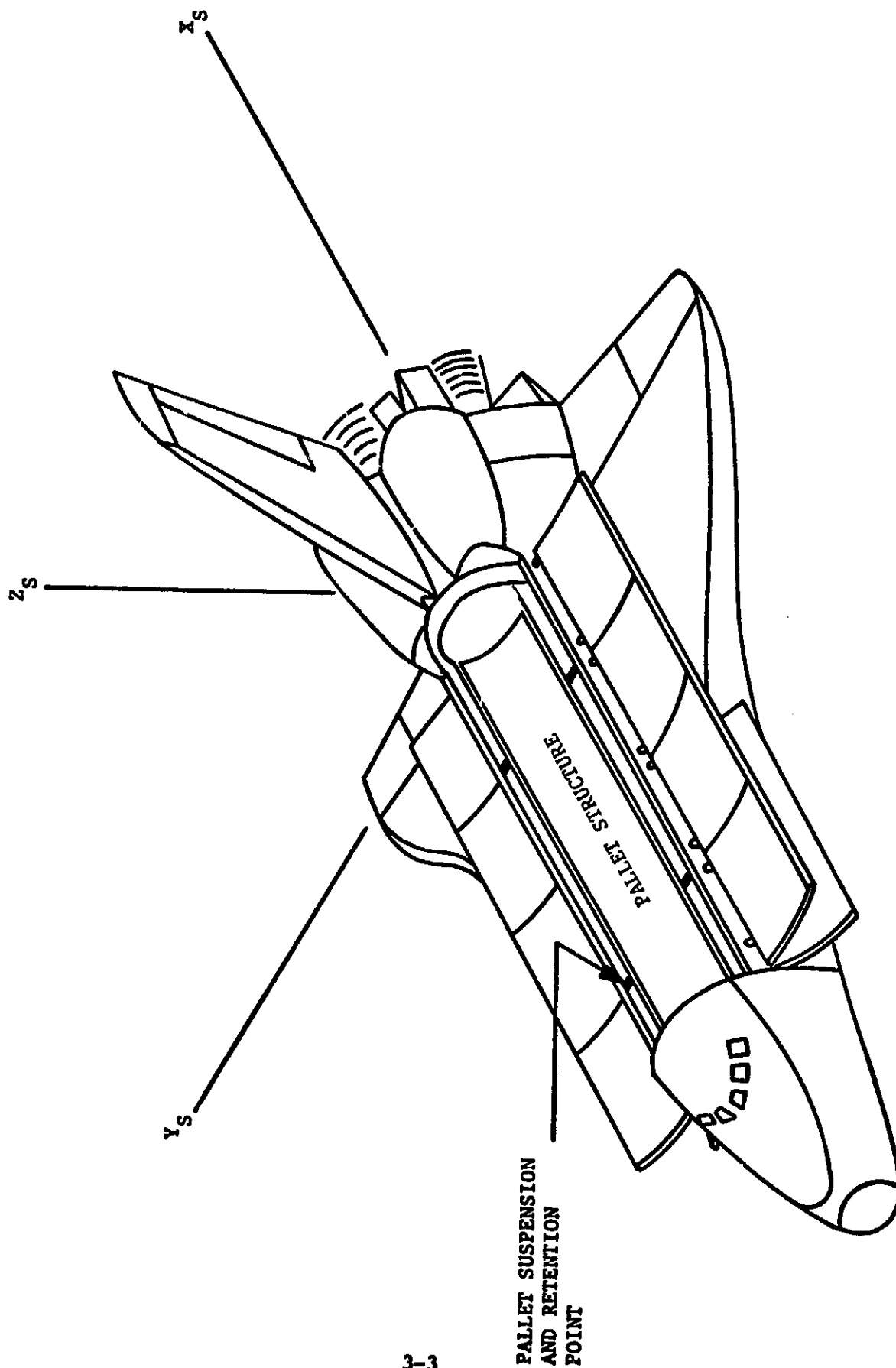


Figure 3-2. Orbiter/Pallet Configuration

Table 3-1. Orbiter/Pallet Vehicle Mass Properties

Mass = 82,430 kg	
Center-of-Mass wrt I Coordinate System (27.97, 0.0027, 9.54) meters	
$I_{xx} = 1,010,359 \text{ kg-m}^2$	$I_{xy} = -9,491 \text{ kg-m}^2$
$I_{yy} = 7,400,759 \text{ kg-m}^2$	$I_{xz} = 266,419 \text{ kg-m}^2$
$I_{zz} = 7,614,979 \text{ kg-m}^2$	$I_{yz} = -3,118 \text{ kg-m}^2$



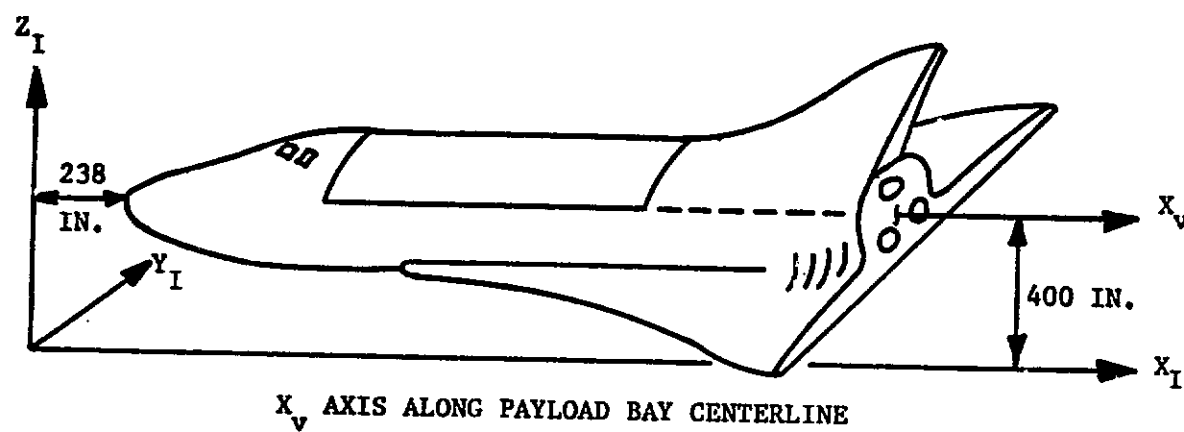


Figure 3-3. Orbiter Related to the Inertial Coordinate System

experiment, or the entire payload pallet may be accurately stabilized. The method chosen to increase pointing capability for the present study is to control the pointing of the pallet via the use of a CMG cluster.

Mass properties for the orbiter are defined with respect to the orbiter center of mass and are given in table 3-2.

3.2.2 Pallet - Experiment equipment will be mounted on the pallet. When performing experiments, it is undesirable to allow the orbiter RCS system to fire. Therefore, the pallet will be controlled by the CMG cluster which provides pallet pointing to within one sec. Since the orbiter will also be controlled by the CMGs via the isolators, the RCS deadband should not be exceeded and no firings should occur.

The pallet will consist of mechanically coupled segments attached to the orbiter through the isolators. There will be a separate retention system which will support the pallet during launch and descent. Once in orbit, the retention system will be disengaged and the pallet will float on the isolators.

Figure 3-4 is a pictorial diagram of the pallet.

Mass properties for the pallet are defined in table 3-3 with respect to the pallet center of mass.

Table 3-2. Orbiter Mass Properties

Mass=71,452 kg	
Center-of-Mass wrt I Coordinate System (28.24,0.005,9.46) meters	
$I_{xxs}=986,497 \text{ kg-m}^2$	$I_{xys}=-8,135 \text{ kg-m}^2$
$I_{yys}=7,219,756 \text{ kg-m}^2$	$I_{xzs}=256,250 \text{ kg-m}^2$
$I_{zys}=738,652 \text{ kg-m}^2$	$I_{yzs}=-4,067 \text{ kg-m}^2$

Table 3-3. Pallet Mass Properties

Mass=10,974 kg	
Center-of-Mass wrt I Coordinate System (26.22,0.01,10.06) meters	
$I_{xyp}=21,292 \text{ kg-m}^2$	$I_{xyp}=-991 \text{ kg-m}^2$
$I_{yyp}=138,839 \text{ kg-m}^2$	$I_{xzp}=-1,231 \text{ kg-m}^2$
$I_{zyp}=135,444 \text{ kg-m}^2$	$I_{yzp}=903 \text{ kg-m}^2$

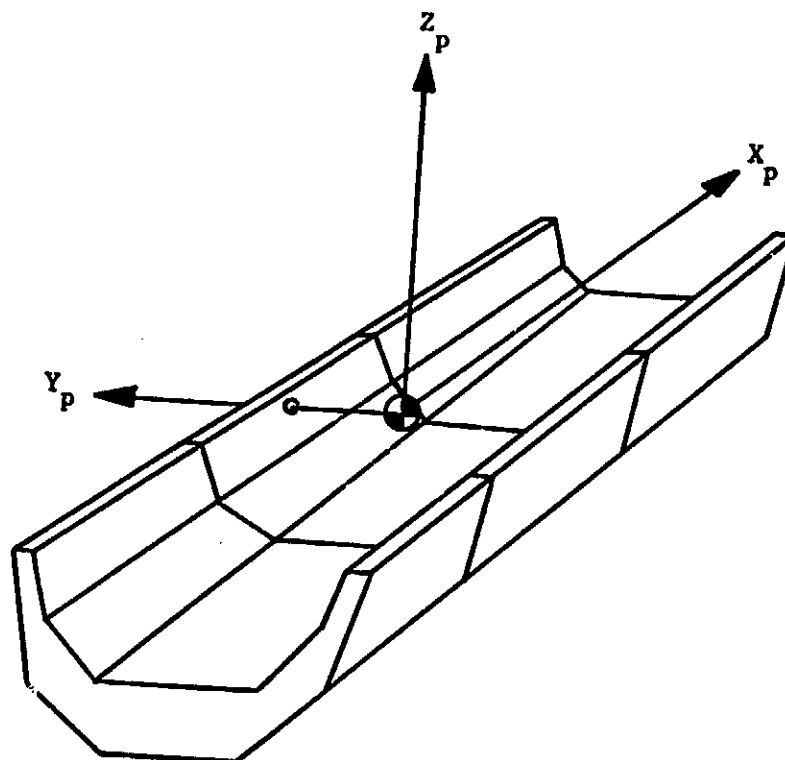


Figure 3-4. Pallet System

#### 4. PALLET SUSPENSION SYSTEM

4.1 General - This section specifically deals with the number and type of isolators required and their location relative to the pallet center of mass.

4.2 Summary - Single point, two point, three point, and four point suspension systems were analyzed to determine if the systems could achieve the design goal of 0.1 Hz natural frequency in all axes for both rotation and translation. Wire rope helical springs, elastomeric isolators, solid wire helical or cantilever springs, and gas filled bellows were analyzed to determine if these configurations could achieve the design goal of the suspension system. The four point suspension system utilizing gas filled bellows was selected as the suspension system which most nearly meets the design objectives. None of the suspension systems can exactly meet the primary design objective of equal natural frequencies in all axes.

#### 4.3 Discussion

4.3.1 Design Objectives - The suspension system shall be locked out during launch and descent of the orbiter, i.e., the suspension system shall allow the pallet retention system to support the pallet during launch and descent. The suspension system shall be active during mission data acquisition and while the pallet retention system is disengaged. The suspension system shall provide the following performance characteristics during mission data acquisition in accordance with reference 1.

Natural Frequency      0.1 Hz in all axes

Damping                      10% of critical

The suspension system shall be compatible with the control system in accordance with volume II. The configuration and location of the suspension system shall not restrict experiment arrangements within the payload volume of the pallet. The suspension system shall be stable through the temperature range from -60° C to +70° C without a thermal control system.

4.3.2 Isolator Attachment Region - The isolator attachment region as shown in figure 4-1 was derived from reference 2. Reference 2 specifies permissible pallet retention loads in specified directions only, i.e., Y axis loads at the lower centerline (axis 1 of figure 4-1) and X and Z axes loads at the longerons (axes 2 of figure 4-1). However, these permissible pallet retention loads are extremely high compared to the anticipated loading through the

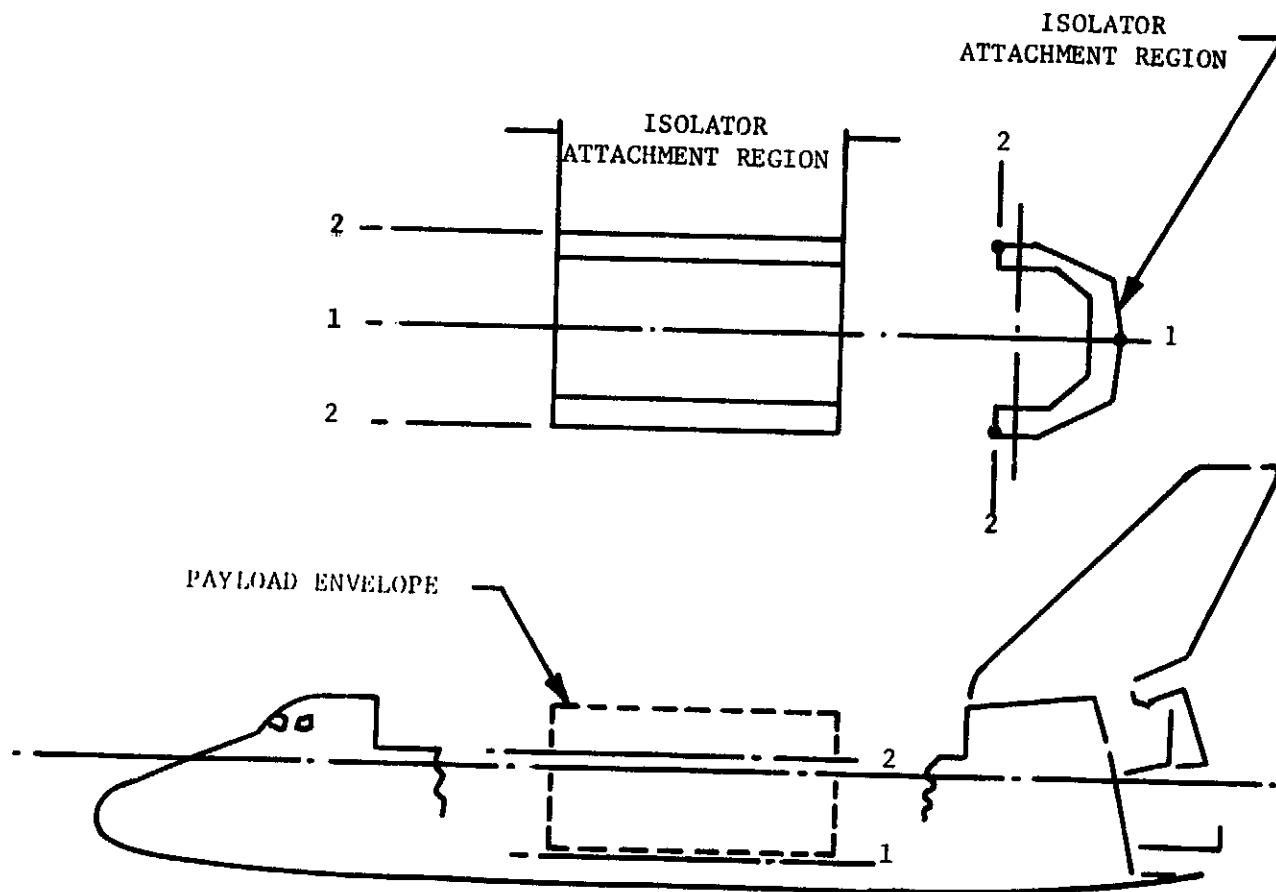


Figure 4-1. Isolator Attachment Region

suspension system. Therefore it is assumed that a suspension system can be mounted adjacent to the outer surfaces of the pallet and the inner surfaces of the orbiter as shown in figure 4-1. Also it is assumed that the loading through the suspension system can be reacted by the orbiter in any direction. These assumptions allow the suspension system to be independent of the pallet retention system.

4.3.3 System Geometry Study - The suspension system geometry study performs analyses on these systems:

4.3.4 Single Point Suspension

4.3.5 Two Point Suspension

4.3.6 Three Point Suspension

4.3.7 Four Point Suspension

Systems with more than four point suspension were not considered since no rationale could be found for these levels of systems. Wire rope helical springs, elastomeric isolators, solid wire helical springs, gas filled bellows, and cantilever springs were analyzed to determine if these configurations could achieve the design objectives.

One design objective of the suspension system is that the natural frequencies of the system shall be the same in all six degrees of freedom. To achieve this, the system must be decoupled, i.e., motion in any one axis must not induce motion in any one of the other five axes. For a decoupled system, the point of convergence of the suspension system's lines of action, the elastic center, must be coincident with the center of mass of the suspended body. Additionally, for a symmetrical system with more than one isolator, the distance between isolators for a particular axis must be equal to twice the radius of gyration for that axis. Two constraints on the mounting geometry are therefore that the system be decoupled and that the isolators be properly spaced. In conducting the geometry study, certain systems could not meet these two criteria. The isolator spring constants and spacing were then selected to give the best conformance to the design objectives, i.e., 0.1 Hz natural frequency and degree of approach towards equality of natural frequencies, for each degree of freedom.

In the analyses, the orbiter/pallet system has been simplified to a spring mass system where the pallet is the suspended rigid mass and the orbiter is the fixed rigid base. This approach is reasonable for the purposes of this study based on the fact that the weight of the orbiter is much larger than the pallet weight.

In the analyses, impedance concepts are used to determine the equations of motion with the coordinate system about the pallet center of mass. Additionally, since the level of damping is low (.1 of critical) the damped natural frequency is very nearly equal to the undamped natural frequency and is assumed to be equal in the analyses.

#### 4.3.4 Single Point Suspension

4.3.4.1 Single Point Containing the Center of Mass - A direct approach to achieve a decoupled suspension system is to place a single point system at the pallet center of mass. As indicated in the mass properties, table 3-3, the pallet center of mass lies very nearly on the pallet centerline within the experiment payload section of the pallet. Although structure could be configured to support the system, the design objective of not restricting experiment positioning cannot be achieved.

4.3.4.2 Single Point Offset Below the Pallet - This approach positions a single point system between the pallet and the orbiter below the pallet center of mass as shown in figure 4-2. This system will have coupling of the X translation and Y rotation modes and also the Y translation and X rotation modes. Coupling will result in rocking (translation plus rotation) natural frequencies about the X and Y axes. The equations of motion are:

$$\begin{aligned}\Sigma F_x & -m\omega^2 X + (X - L_z \theta_y) K_x = F'_x \\ \Sigma M_y & -I_{yy} \omega^2 \theta_y + K_{ry} \theta_y - (X - L_z \theta_y) A K_x = 0 \\ \Sigma F_y & -m\omega^2 Y + (Y - L_z \theta_x) K_y = 0 \\ \Sigma M_x & -I_{xx} \omega^2 \theta_x + K_{rx} \theta_x - (Y - L_z \theta_x) A K_y = 0 \\ \Sigma F_z & -m\omega^2 Z + Z K_z = 0 \\ \Sigma M_z & -I_{zz} \omega^2 \theta_z + K_{rz} \theta_z = 0\end{aligned}$$

Determinants are used to solve the simultaneous equations for displacement and rotation. The natural frequencies are those frequencies which make the denominators equal to zero. Since the Z axis translational and rotational motions are decoupled, solution of the  $F_z$  and  $M_z$  equations yields:



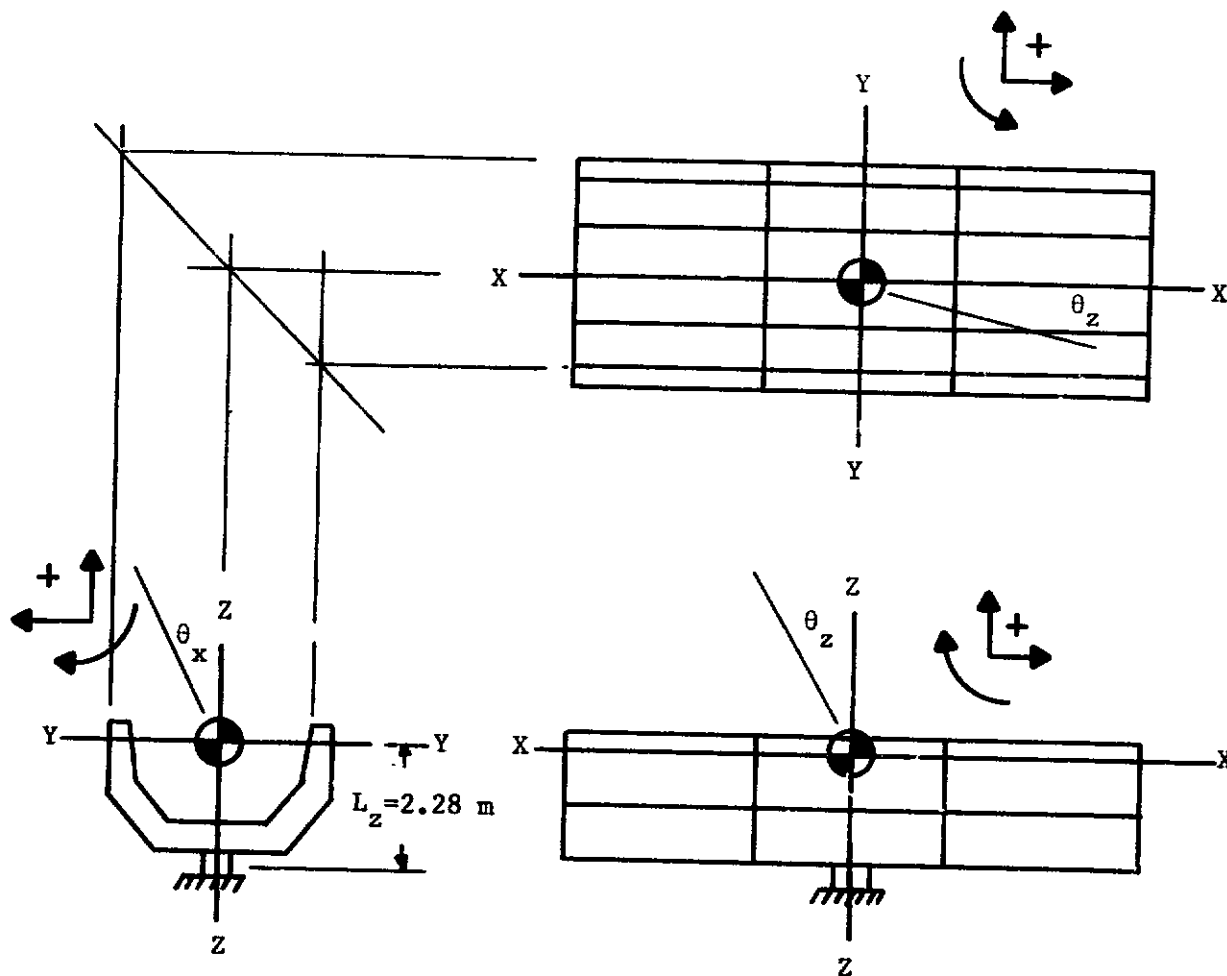


Figure 4-2. Single Point Offset Below the Pallet -  
Sign Convention for Forces and Moments

$$\omega_z = \left[ \frac{K_z}{m} \right]^{1/2}$$

for Z translation and:

$$\omega_{rz} = \left[ \frac{K_{rz}}{I_{zz}} \right]^{1/2}$$

for Z rotation. To simplify the solution of the  $F_x$  and  $M_y$  equations, divide the  $F_x$  equation by  $K_z$  and the  $M_y$  equation by  $K_z R_y^2$ , where  $R_y^2$  is the radius of gyration, and substitute  $\omega_z/m = \omega_z^2$ . The result will be the rocking natural frequencies expressed as a ratio to the Z axis natural frequency

$$\left(\frac{\omega}{\omega_z}\right)^4 - \left(\frac{K_{ry}}{K_z R_y^2} + \frac{L_z^2 K_x}{R_y^2 K_z} + \frac{K_x}{K_z}\right) \left(\frac{\omega}{\omega_z}\right)^2 + \frac{K_x K_{ry}}{K_z^2 R_y^2} = 0$$

For a decoupled system  $K_{ry}/K_y = R_y^2$  and  $K_y = K_x$ ; therefore let  $K_{ry}/K_x = R_y^2$  and the equation becomes:

$$\left(\frac{\omega}{\omega_z}\right)^4 - \left(\frac{L_z^2 + 2R_y^2}{R_y^2}\right) \left(\frac{K_x}{K_z}\right) \left(\frac{\omega}{\omega_z}\right)^2 + \left(\frac{K_x}{K_z}\right)^2 = 0$$

A design objective is to obtain equal frequencies, therefore the equation can be used to obtain  $K_x$  when  $\omega/\omega_z = 1$ . The equation will also yield a second  $\omega$ .

The same approach to the solution of the  $F_y$  and  $M_x$  equations yields:

$$\left(\frac{\omega}{\omega_z}\right)^4 - \left(\frac{L_z^2 + 2R_x^2}{R_x^2}\right) \left(\frac{K_y}{K_z}\right) \left(\frac{\omega}{\omega_z}\right)^2 + \left(\frac{K_y}{K_z}\right)^2 = 0$$

The data are listed in table 4-1.

4.3.4.3 Single Point Offset at the End of the Pallet - This approach is to position a single point system at one end of the pallet with one axis in line with the center of mass. This system will have coupling of the Y translation and Z rotation modes and also the Z translation and Y rotation modes. Coupling will result in rocking (translation plus rotation) natural frequencies about the Y and Z axes. A large structure would be required at the end of the pallet and thus the design objective of not restricting experiment positioning cannot be achieved.

#### 4.3.5 Two Point Suspension Containing the Center of Mass

4.3.5.1 Two Points at the Sides of the Pallet - This approach is to position the axis of two isolators in line with the center of mass and each isolator on the sides of the pallet as shown in figure 4-3. This system is decoupled. To achieve equal natural frequencies the isolators must have equal spring constants and the distance  $2L_y$  between the isolators for a particular axis must be equal to twice the radius of gyration for that axis.

The equations of motion are:

$$\begin{aligned}\Sigma F_x & -m\omega^2 X + 2K_x X = F'_x \\ \Sigma M_x & -I_{xx}\omega^2 \theta_x + 2K_z L_y^2 \theta_x = 0 \\ \Sigma F_y & -m\omega^2 Y + 2K_y Y = 0 \\ \Sigma M_y & -I_{yy}\omega^2 \theta_y + K_{ry} \theta_y = 0 \\ \Sigma F_z & -m\omega^2 Z + 2K_z Z = 0 \\ \Sigma M_z & -I_{zz}\omega^2 \theta_z + 2K_x L_y^2 \theta_z = 0\end{aligned}$$

Solution of the  $F_x$  and  $M_x$  equations yields:

$$\omega_x = \frac{2K_x}{m}^{1/2}$$

Table 4-1. Single Point Suspension Offset Below the Pallet  
Natural Frequencies and Spring Constants

AXIS	TRANSLATIONAL NATURAL FREQUENCY Hz	ROTATIONAL NATURAL FREQUENCY Hz	AXIAL SPRING CONSTANT N/m	ROTATIONAL SPRING CONSTANT N-m/rad
X	0.10, 0.05	0.10, 0.02	2,296	1,849
Y	0.10, 0.02	0.10, 0.05	953	29,048
Z	0.10	0.10	4,332	53,471

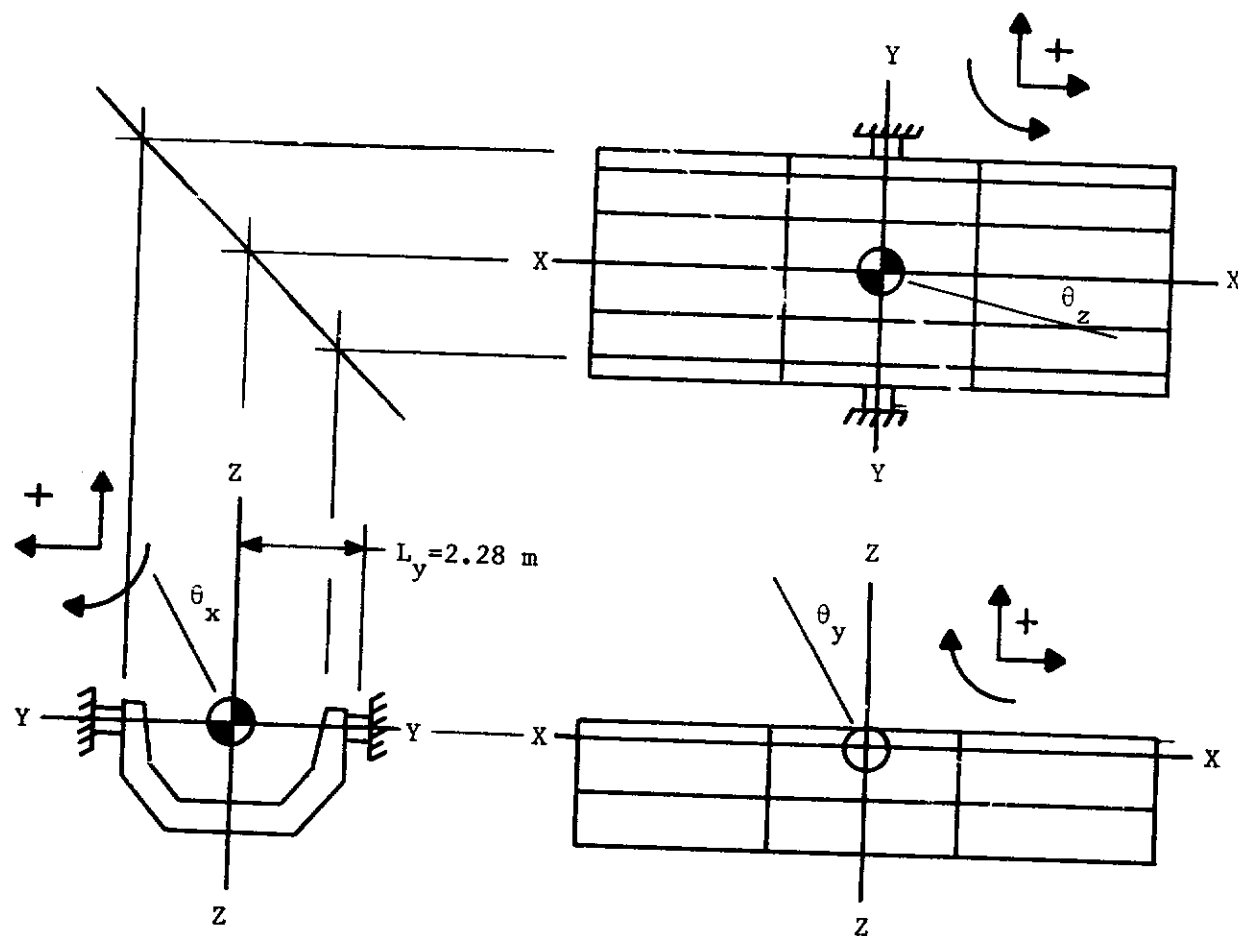


Figure 4-3. Two Point Suspension at the Sides of the Pallet - Sign Convention for Forces and Moments

for X translation and

$$\omega_{rx} = \left[ \frac{2K_z L_y^2}{I_{xx}} \right]^{1/2}$$

for X rotation. Solution of the  $F_y$  and  $M_y$  equations yields:

$$\omega_y = \left[ \frac{2K_y}{m} \right]^{1/2}$$

for Y translation and

$$\omega_{ry} = \left[ \frac{K_{ry}}{I_{yy}} \right]^{1/2}$$

for Y rotation. Solution of the  $F_z$  and  $M_z$  equations yields:

$$\omega_z = \left[ \frac{2K_z}{m} \right]^{1/2}$$

for Z translation and

$$\omega_{rz} = \left[ \frac{2K_x L_y^2}{I_{zz}} \right]^{1/2}$$

for Z rotation.

For equal natural frequencies the requirements of  $L_y$  are evaluated. Using  $\omega_x$  and  $\omega_{rz}$  equations and solve for  $L_y$  yields:

$$L_y = \left[ \frac{I_{zz}}{m} \right]^{1/2} = \left[ \frac{135,444}{10,974} \right]^{1/2} = 3.51 \text{ m}$$

Using  $\omega_z$  and  $\omega_{rx}$  equations and solve for  $L_y$  yields:

$$L_y = \left[ \frac{I_{xx}}{m} \right]^{1/2} = \left[ \frac{21,292}{10,974} \right]^{1/2} = 1.39 \text{ m}$$

The spacing of 3.51 m exceeds the allowable space between the pallet and the orbiter. The spacing of 1.39 m would place the isolators within the experiment payload section and the design objective of not restricting experiment positioning cannot be achieved.

Using  $L_y = 2.28$  m results in at least two of the natural frequencies not equal to the remaining four. Selection of equal translational natural frequencies results in unequal X and Z axes rotational natural frequencies. Selection of equal rotational natural frequencies results in unequal X and Z axes translational natural frequencies. The data of these two alternate selections are shown in table 4-2.

Other combinations are possible by varying the spring constants. However, it appears more reasonable to configure the system for equal rotational natural frequencies or equal translational natural frequencies.

**4.3.5.2 Two Points At the Ends of the Pallet** - This approach positions the axis of two isolators in line with the center of mass and each isolator on the ends of the pallet as shown in figure 4-4. The same analysis is used for the end-mounted system as that used for the side-mounted system (section 4.3.5.1).

The equations of motion are:

$$\begin{aligned}
 \Sigma F_x & \quad -m\omega^2 X + 2K_x X = F'_x \\
 \Sigma M_x & \quad -I_{xx}\omega^2 \theta_x + K_{rx} \theta_x = 0 \\
 \Sigma F_y & \quad -m\omega^2 Y + 2K_y Y = 0 \\
 \Sigma M_y & \quad -I_{yy}\omega^2 \theta_y + 2K_z L_x^2 \theta_y = 0 \\
 \Sigma F_z & \quad -m\omega^2 Z + 2K_z Z = 0 \\
 \Sigma M_z & \quad -I_{zz}\omega^2 \theta_z + 2K_y L_x^2 \theta_z = 0
 \end{aligned}$$

Using  $L_x = 4.57$  m results in at least two of the natural frequencies not equal to the remaining four. In the analysis, the translational natural frequencies were made identical and then the rotational frequencies made identical; it was not possible to have all the frequencies identical. As previously, it was assumed that the X axis rotational and translational frequencies could be made equal since they are independent of the other isolator spring constants. The data are shown in table 4-3. As indicated, very good agreement exists between all three axes rotational and translational natural

Table 4-2. Two Point Suspension At the Sides of the Pallet  
Natural Frequencies and Spring Constants

AXIS	TRANSLATIONAL NATURAL FREQUENCY Hz	ROTATIONAL NATURAL FREQUENCY Hz	AXIAL SPRING CONSTANT N/m	ROTATIONAL SPRING CONSTANT N-m/rad
X	0.10	0.17	2,166	-
Y	0.10	0.10	2,166	54,811
Z	0.10	0.06	2,166	-
X	0.15	0.10	5,143	-
Y	0.10	0.10	2,166	54,811
Z	0.06	0.10	808	-



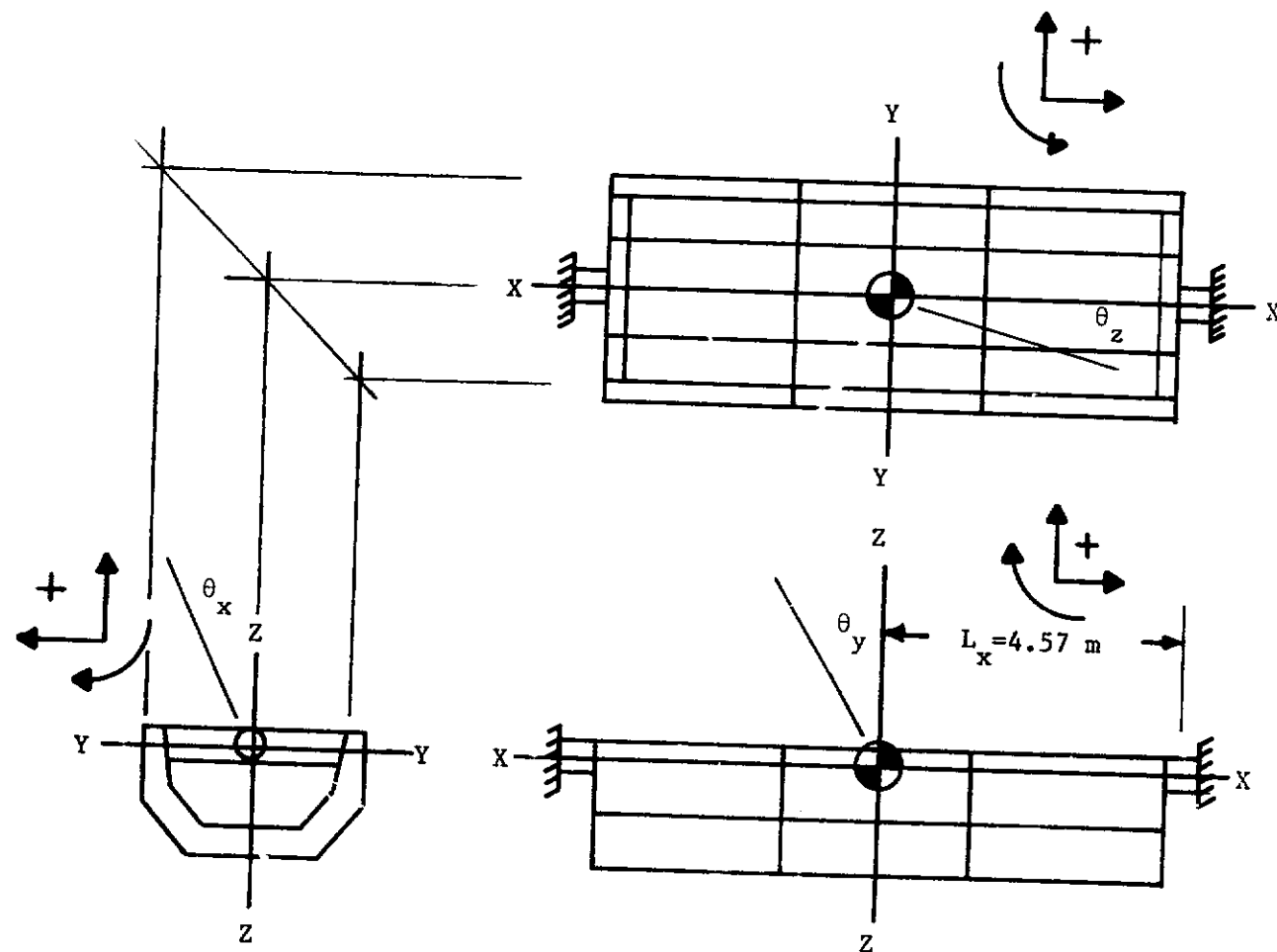


Figure 4-4. Two Point Suspension at the Ends of the Pallet - Sign Convention for Forces and Moments

Table 4-3. Two Point Suspension At the Ends of the Pallet  
Natural Frequencies and Spring Constants

AXIS	TRANSLATIONAL NATURAL FREQUENCY Hz	ROTATIONAL NATURAL FREQUENCY Hz	AXIAL SPRING CONSTANT N/m	ROTATIONAL SPRING CONSTANT N-m/rad
X	0.10	0.10	2,166	13,378
Y	0.10	0.13	2,166	-
Z	0.10	0.13	2,166	-
X	0.10	0.10	2,166	13,378
Y	0.08	0.10	1,280	-
Z	0.08	0.10	1,312	-

frequencies; however, large structure would be required at both ends of the pallet and thus the design objective of not restricting experiment positioning cannot be achieved.

#### 4.3.6 Three Point Suspension Containing the Center of Mass

4.3.6.1 Three Points on a YZ Plane - This approach positions three isolators in a YZ plane containing the center of mass as shown in figure 4-5. The two in line isolators each have spring constants  $K_x, K_y, K_z$  while the single isolator has spring constants  $K_{1x}, K_{1y}$  and rotation is resisted by axial deflection of the isolators. The equations of motion are:

$$\Sigma F_x \quad -Xm\omega^2 + X[2K_x + K_{1x}] - \theta_y(2K_x L_z - K_{1x} L_{1z}) = F'_x$$

$$\Sigma F_y \quad -Ym\omega^2 + Y[2K_y + K_{1y}] - \theta_x(-2K_y L_z + K_{1y} L_{1z}) = 0$$

$$\Sigma F_z \quad -Zm\omega^2 + Z[2K_z] = 0$$

$$\Sigma M_x \quad \theta_x(-I_{xx}\omega^2 + 2K_z L_y^2 + 2K_y L_z^2 + K_{1y} L_{1z}^2) - Y(2K_y L_z - K_{1y} L_{1z}) = 0$$

$$\Sigma M_y \quad \theta_y(-I_{yy}\omega^2 + 2K_x L_z^2 + K_{1x} L_{1z}^2) - X(-2K_x L_z + K_{1x} L_{1z}) = 0$$

$$\Sigma M_z \quad \theta_z(-I_{zz}\omega^2 + 2K_x L_y^2) = 0$$

Decoupling of the system can be achieved by the spring constant relationships:

$$2K_x L_z - K_{1x} L_{1z} = 0$$

$$-2K_y L_z + K_{1y} L_{1z} = 0$$

Solution of the decoupled equations of motion yields:

$$\omega_x = \left[ \frac{2K_x (L_z + L_{1z})}{mL_z} \right]^{1/2}$$

for X translation,

$$\omega_y = \left[ \frac{2K_y (L_z + L_{1z})}{mL_z} \right]^{1/2}$$

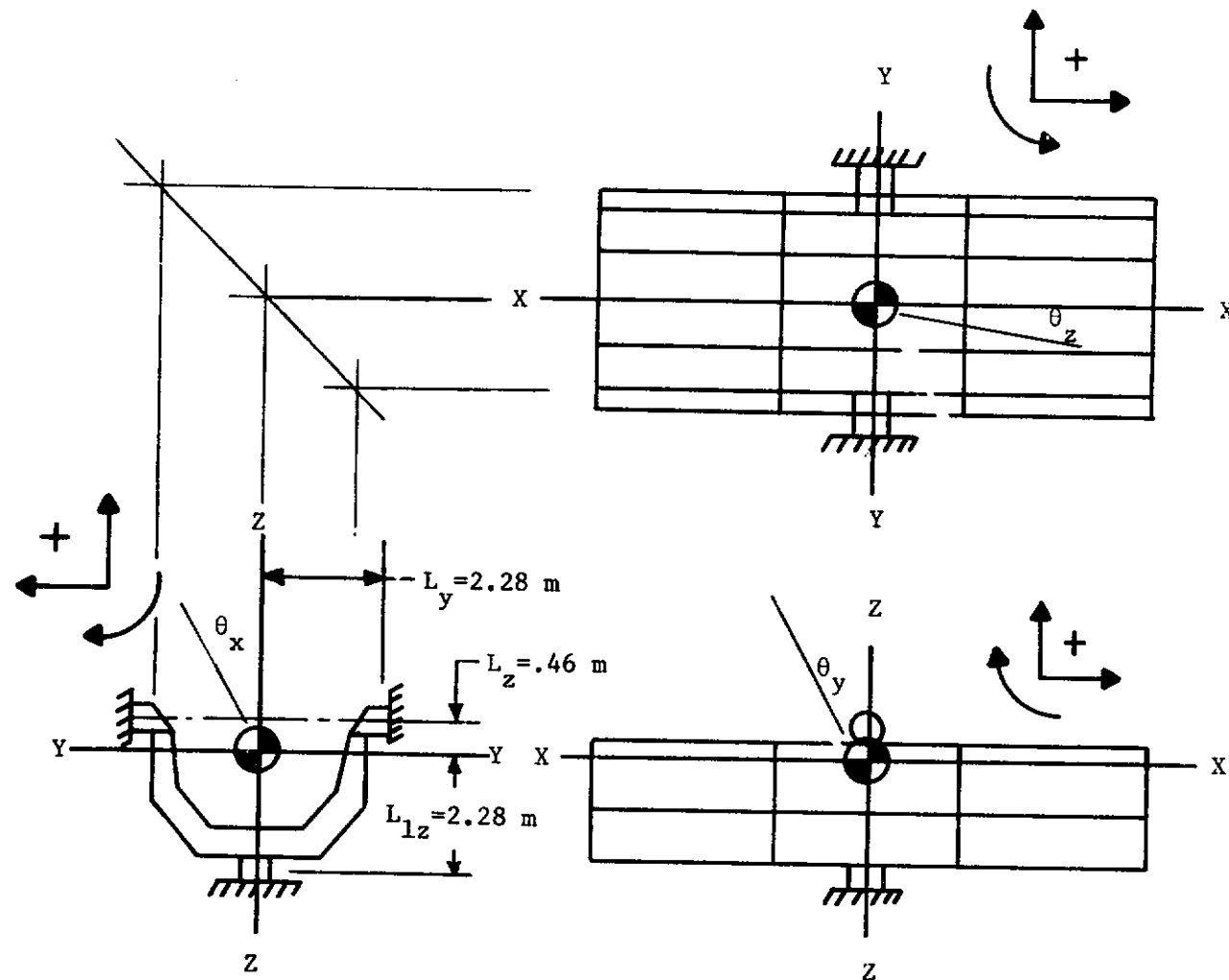


Figure 4-5. Three Point Suspension Containing the Center of Mass on a YZ Plane - Sign Convention for Forces and Moments

for Y translation,

$$\omega_z = \left[ \frac{2K_z}{m} \right]^{1/2}$$

for Z translation,

$$\omega_{rx} = \left[ \frac{2K_y (L_z^2 + L_{1z} L_z) + 2K_z L_y^2}{I_{xx}} \right]^{1/2}$$

for X rotation,

$$\omega_{ry} = \left[ \frac{2K_x (L_z^2 + L_z L_{1z})}{I_{yy}} \right]^{1/2}$$

for Y rotation and,

$$\omega_{rz} = \left[ \frac{2K_x L_y^2}{I_{zz}} \right]^{1/2}$$

for Z rotation.

Clearly the  $\omega_x$ ,  $\omega_{ry}$ , and  $\omega_{rz}$  equations are dependent upon only one spring constant,  $K_x$ . Therefore equal translational natural frequencies can be selected and the rotational natural frequencies can be determined. The data are listed in table 4-4. As indicated by the data, the system is very soft in Y and Z axes rotation. A second analysis based on Z axis rotation equal to 0.10 Hz is included.

**4.3.6.2 Three Points on a Skewed Plane** - This approach positions three isolators in a skewed plane containing the center of mass as shown in figure 4-6. The two inline isolators are parallel to the Y axis and each have spring constants  $K_x, K_y, K_z$ , while the single isolator has spring constants  $K_{1x}, K_{1y}, K_{1z}$  and rotation is resisted by axial deflection of the isolators. The equations of motion are:

$$\Sigma F_x - X m \omega^2 + X(2K_x + K_{1x}) - \theta_y (2K_x L_z - K_{1x} L_{1z}) = F'_x$$

$$\Sigma F_y - Y m \omega^2 + Y(2K_y + K_{1y}) - \theta_x (-2K_y L_z + K_{1y} L_{1z}) - \theta_z (2K_y L_x - K_{1y} L_{1x}) = 0$$

$$\Sigma F_z - Z m \omega^2 + Z(2K_z + K_{1z}) - \theta_y (2K_z L_x - K_{1z} L_{1x}) = 0$$

Table 4-4. Three Point Suspension on a YZ Plane  
Natural Frequencies and Spring Constants

AXIS	TRANSLATIONAL NATURAL FREQUENCY Hz	ROTATIONAL NATURAL FREQUENCY Hz	IN LINE ISOLATORS AXIAL SPRING CONSTANT N/m	SINGLE ISOLATOR AXIAL SPRING CONSTANT N/m
X	0.10	0.11	364	147
Y	0.10	0.01	364	147
Z	0.10	0.03	2,166	-
X	0.17	0.11	5,143	2,075
Y	0.10	0.05	364	147
Z	0.10	0.10	2,166	-

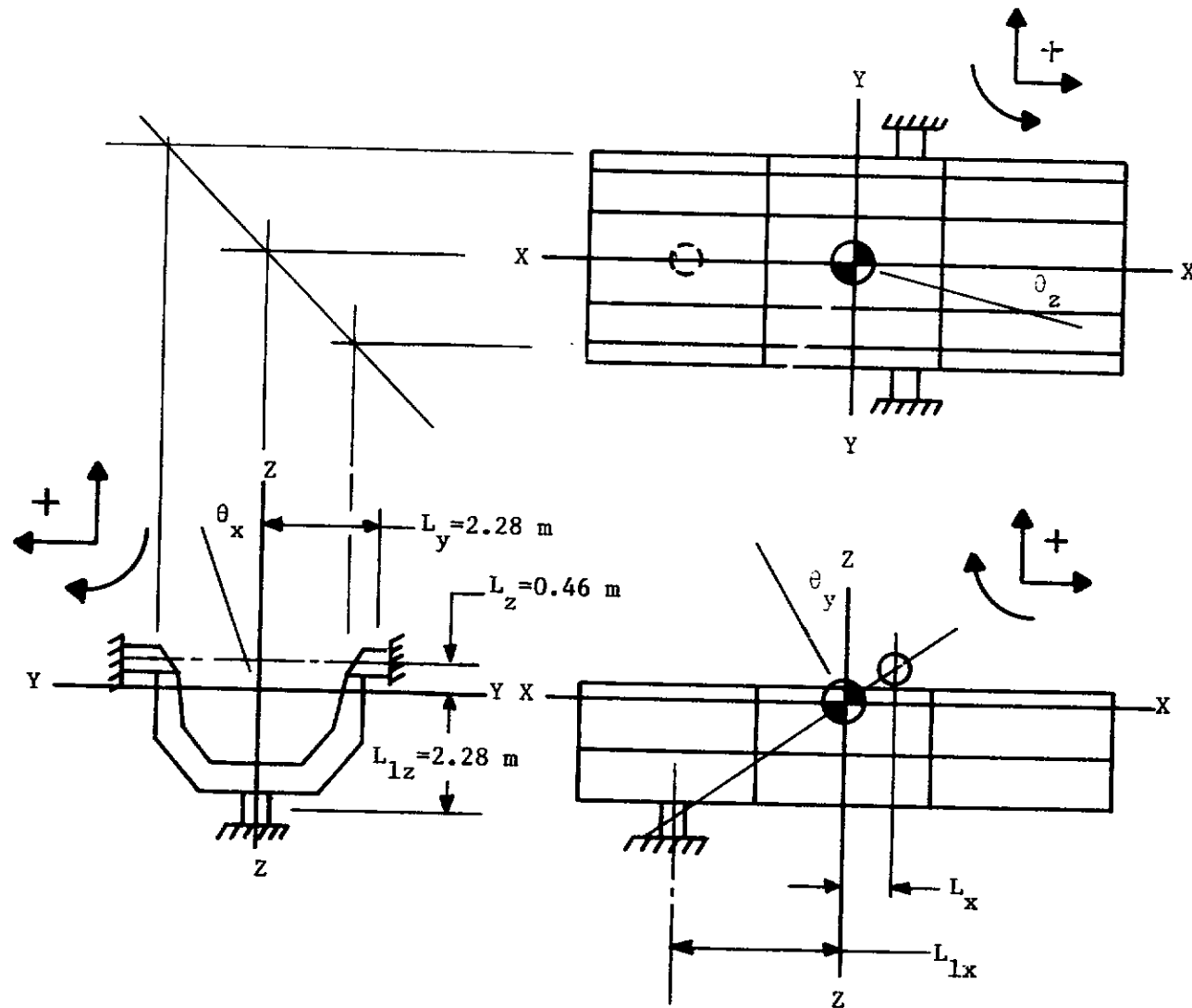


Figure 4-6. Three Point Suspension Containing the Center of Mass on a Skewed Plane - Sign Convention for Forces and Moments

$$\begin{aligned}
\Sigma M_x \quad 0_x (-I_{xx} \omega^2 + 2K_z L_y^2 + 2K_y L_z^2 + K_{ly} L_{lz}^2) - 0_z (2K_y L_x L_z + K_{ly} L_{lx} L_{lz}) \\
+ Y (2K_y L_z - K_{ly} L_{lz}) = 0 \\
\Sigma M_y \quad 0_y (-I_{yy} \omega^2 + 2K_x L_z^2 + K_{lx} L_{lz}^2 + 2K_z L_x^2 + K_{lz} L_{lx}^2) - X (2K_x L_z - K_{lx} L_{lz}) \\
+ Z (2K_z L_x - K_{lz} L_{lx}) = 0 \\
\Sigma M_z \quad 0_z (-I_{zz} \omega^2 + 2K_x L_y^2 + 2K_y L_x^2 + K_{ly} L_{lx}^2) - 0_x (2K_y L_x L_z + K_{ly} L_{lx} L_{lz}) \\
- Y (2K_y L_x - K_{ly} L_{lx}) = 0
\end{aligned}$$

Partial decoupling of the system can be achieved by the spring constant relationships:

$$2K_x L_z - K_{lx} L_{lz} = 0$$

$$2K_y L_z - K_{ly} L_{lz} = 0$$

$$2K_y L_x - K_{ly} L_{lx} = 0$$

$$2K_z L_x - K_{lz} L_{lx} = 0$$

Also to maintain the center of mass in the plane of the isolators the spacing relationships are:

$$\frac{L_x}{L_z} = \frac{L_{lx}}{L_{lz}} = \frac{L_x + L_{lx}}{L_z + L_{lz}}$$

Determinants are used to solve the simultaneous equations for displacement and rotation. The natural frequencies are those frequencies which make the denominator equal to zero. Solution of the  $F_x$  and  $M_y$  equations yields:

$$\omega_x = \left[ \frac{2K_x (L_z + L_{lz})}{m L_{lz}} \right]^{1/2}$$

for X translation and



$$\omega_{ry} = \left[ \frac{2L_z (L_z + L_{1z}) (K_x L_{1z}^2 + K_z L_{1x}^2)}{L_{1z}^2 I_{yy}} \right]^{1/2}$$

for Y rotation.

Solution of the  $F_y$  and  $F_x$  equations yields:

$$\omega_y = \left[ \frac{2K_y (L_z + L_{1z})}{m L_{1z}} \right]^{1/2}$$

for Y translation and

$$\omega_z = \left[ \frac{2K_z (L_z + L_{1z})}{m L_{1z}} \right]^{1/2}$$

for Z translation.

Since the translational natural frequencies can be made equal, the axial spring constants will be equal. To simplify the solution of the  $M_x$  and  $M_z$  equations, each equation is divided by  $K R_1^2$  where  $R_1^2$  is the radius of gyration of the axis and  $K = K_x = K_y = K_z$ ; also note that

$$\frac{K}{m} = \frac{\omega_t^2 L_{1z}}{2(L_{1z} + L_z)}$$

where  $\omega_t$  is the translational natural frequency.

$$\begin{aligned} \Sigma M_x \quad \theta_x \left[ -\left(\frac{\omega}{\omega_t}\right)^2 + \frac{L_{1z} L_y^2}{(L_{1z} + L_z) R_{xx}^2} + \frac{L_{1z} L_z}{R_{xx}^2} \right] - \theta_z \left( \frac{L_z L_{1x}}{R_{xx}^2} \right) &= 0 \\ \Sigma M_z \quad \theta_z \left[ -\left(\frac{\omega}{\omega_t}\right)^2 + \frac{L_{1z} L_y^2}{(L_{1z} + L_z) R_{zz}^2} + \frac{L_z L_{1x}^2}{L_{1z} R_{zz}^2} \right] - \theta_x \left( \frac{L_z L_{1x}}{R_{zz}^2} \right) &= 0 \end{aligned}$$

The solution of these equations yields the ratio of the rotational to translational natural frequencies as a function of  $L_{1x}$  spacing.

$$\frac{\omega}{\omega_t} = \left[ \frac{3.12 + .02L_{1x}^2 + (5.85 - .08L_{1x}^2 + .0004L_{1x}^4)^{1/2}}{2} \right]^{1/2}$$

When  $L_{1x}=0$  the system is in the YZ plane and is the configuration of section 4.3.6.1.  $L_{1x}$  is chosen to be 4.0 m which is close to the end of the pallet. The data are listed in table 4-5. As indicated by the performance data there is no advantage in skewing the suspension plane about the center of mass.

#### 4.3.7 Four Point Suspension

4.3.7.1 Four Points on a XY Plane Containing the Center of Mass - This approach positions four isolators in a XY plane containing the center of mass as shown in figure 4-7. Each isolator has spring constants  $K_x, K_y, K_z$  and rotation is resisted by axial deflection of the isolators. The equations of motion are:

$$\begin{aligned} \Sigma F_x & -Xm\omega^2 + X[4K_x] = F'_x \\ \Sigma F_y & -Ym\omega^2 + Y[4K_y] = 0 \\ \Sigma F_z & -Zm\omega^2 + Z[4K_z] = 0 \\ \Sigma M_x & -\theta_x I_{xx} \omega^2 + \theta_x (4K_z L_y^2) = 0 \\ \Sigma M_y & -\theta_y I_{yy} \omega^2 + \theta_y (4K_z L_x^2) = 0 \\ \Sigma M_z & -\theta_z I_{zz} \omega^2 + \theta_z (4K_y L_x^2) + \theta_z (4K_x L_y^2) = 0 \end{aligned}$$

Solution of the equations yields:

$$\omega_x = \left[ \frac{4K_x}{m} \right]^{1/2}$$

for X translation,

$$\omega_y = \left[ \frac{4K_y}{m} \right]^{1/2}$$

for Y translation,

Table 4-5. Three Point Suspension on a Skewed Plane  
Natural Frequencies and Spring Constants

AXIS	TRANSLATIONAL NATURAL FREQUENCY Hz	ROTATIONAL NATURAL FREQUENCY Hz	IN LINE ISOLATORS AXIAL SPRING CONSTANT N/m	SINGLE ISOLATOR AXIAL SPRING CONSTANT N/m
X	0.10	0.17, 0.08	364	147
Y	0.10	0.03	364	147
Z	0.10	0.17, 0.08	364	147

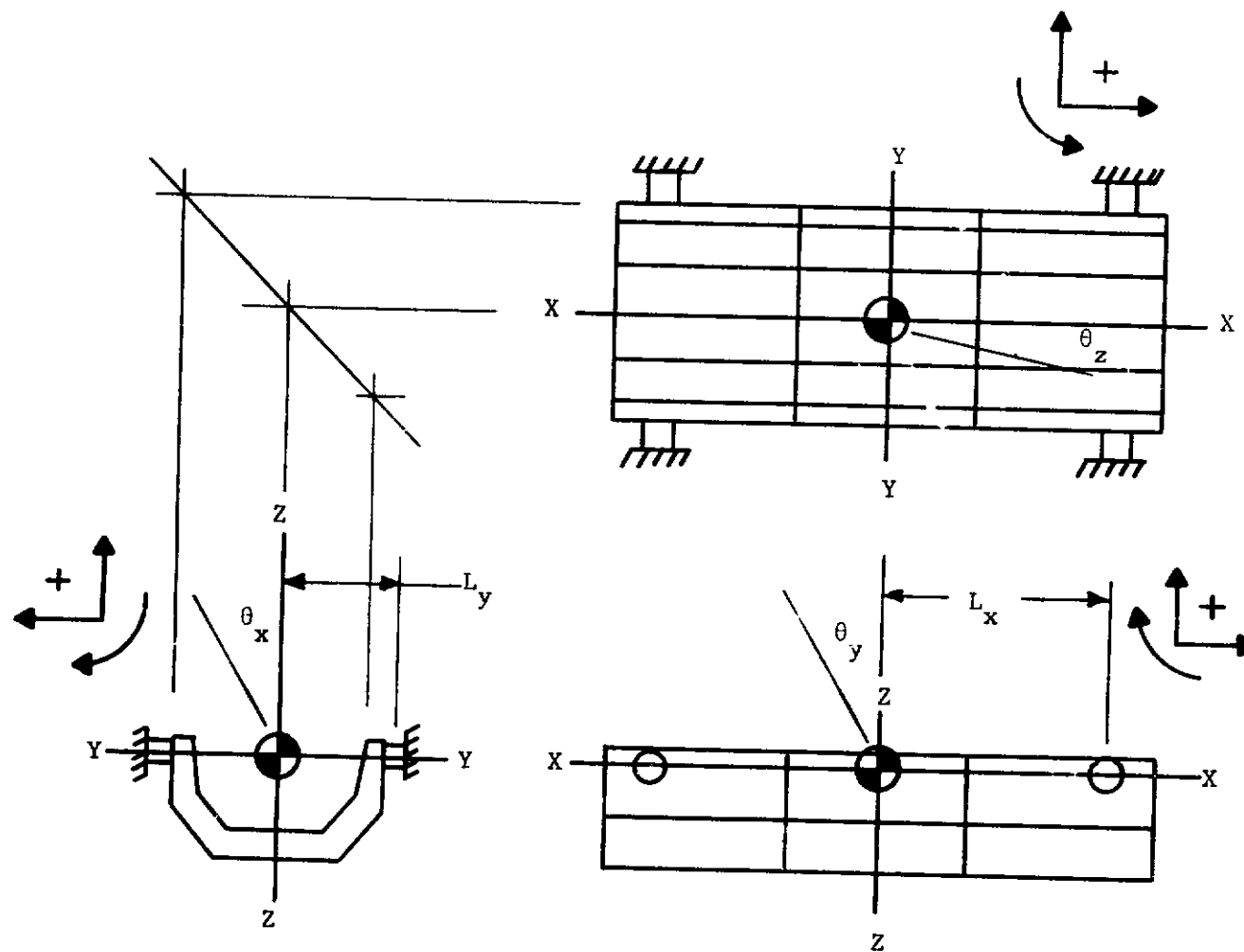


Figure 4-7. Four Point Suspension Containing the Center of Mass - Sign Convention for Forces and Moments

$$\omega_z = \left[ \frac{4K_z}{m} \right]^{1/2}$$

for Z translation,

$$\omega_{rx} = \left[ \frac{4L_y^2 K_z}{I_{xx}} \right]^{1/2}$$

for X rotation,

$$\omega_{ry} = \left[ \frac{4L_x^2 K_z}{I_{yy}} \right]^{1/2}$$

for Y rotation and,

$$\omega_{rz} = \left[ \frac{4L_x^2 K_z + 4L_y^2 K_z}{I_{zz}} \right]^{1/2}$$

for Z rotation.

Clearly equal translational natural frequencies can be selected and the rotational natural frequencies can be determined. To achieve equal frequencies in all axes, the spacing constants  $L_x$  and  $L_y$  are:

$$L_y = \left[ \frac{I_{xx}}{m} \right]^{1/2} = \left[ \frac{21,292}{10,974} \right]^{1/2} = 1.39 \text{ m}$$

$$L_x = \left[ \frac{I_{yy}}{m} \right]^{1/2} = \left[ \frac{138,839}{10,974} \right]^{1/2} = 3.56 \text{ m}$$

The  $L_y = 1.39 \text{ m}$  spacing would place the isolators within the payload experiment section. The  $L_x = 3.56 \text{ m}$  spacing is compatible with the length of the pallet. However, for equal Z axis rotational natural frequency:

$$\left[ L_x^2 + L_y^2 \right]^{1/2} = \left[ \frac{I_{zz}}{m} \right]^{1/2} = \left[ \frac{135,444}{10,974} \right]^{1/2} = 3.51 \text{ m}$$

This spacing  $3.51 \text{ m}$  is not compatible with  $L_y = 1.39 \text{ m}$  and  $L_x = 3.56 \text{ m}$ . Therefore equal natural frequencies in all axes cannot be achieved.

Various combinations of spring constants and isolator spacing can be evaluated. The data of three combinations are listed in table 4-6. Configuration 1 is based on equal translational frequencies and  $L_y = 1.39 \text{ m}$ ,  $L_x = 3.56 \text{ m}$ ; configuration 2 is based on equal

Table 4-6. Four Point Suspension Containing the Center of Mass  
Natural Frequencies and Spring Constants

CONFIGURATION	AXIS	SPACING m	TRANSLATIONAL NATURAL FREQUENCY Hz	ROTATIONAL NATURAL FREQUENCY Hz	AXIAL SPRING CONSTANT N/m
1	X	3.56	0.10	0.10	1,084
1	Y	1.39	0.10	0.10	1,084
1	Z	0.00	0.10	0.11	1,084
2	X	3.66	0.10	0.16	1,084
2	Y	2.28	0.10	0.10	1,084
2	Z	0.00	0.10	0.12	1,084
3	X	3.66	0.08	0.10	719
3	Y	2.28	0.08	0.06	719
3	Z	0.00	0.06	0.10	404

translational frequencies and selected isolator spacings; configuration 3 is based on X and Z axes equal rotational frequencies and selected isolator spacing.

#### 4.3.7.2 Four Points on a XY Plane Offset Above the Pallet -

This approach positions four isolators in a XY plane offset from the center of mass as shown in figure 4-8. This system would attach to the pallet and orbiter longerons. Each isolator has spring constants  $K_x, K_y, K_z$  and rotation is resisted by axial deflection of the isolators. The equations of motion are:

$$\Sigma F_x \quad -Xm\omega^2 + X4K_x + \theta \frac{4K_x L}{x} = F'_x$$

$$\Sigma F_y \quad -Ym\omega^2 + Y4K_y + \theta \frac{4K_y L}{y} = 0$$

$$\Sigma F_z \quad -Zm\omega^2 + Z4K_z = 0$$

$$\Sigma M_x \quad \theta_x (-I_{xx}\omega^2 + 4K_z L_y^2 + 4K_y L_z^2) + Y4K_y L_z = 0$$

$$\Sigma M_y \quad \theta_y (-I_{yy}\omega^2 + 4K_z L_x^2 + 4K_x L_z^2) + X4K_x L_z = 0$$

$$\Sigma M_z \quad \theta_z (-I_{zz}\omega^2 + 4K_y L_x^2 + 4K_x L_y^2) = 0$$

Solution of the  $F_z$  and  $M_z$  equations yields:

$$\omega_z = \left[ \frac{4K_z}{m} \right]^{1/2}$$

for Z translation and,

$$\omega_{rz} = \left[ \frac{4K_y L_x^2 + 4K_x L_y^2}{I_{zz}} \right]^{1/2}$$

for Z rotation.

To simplify the solution of the remaining equations, each force equation is divided by  $K_z$  and each moment equation is divided by  $K_z R_{ii}^2$ , where  $R_{ii}$  is the radius of gyration of the axis; also note that

$$\frac{K_z}{m} = \frac{\omega_z^2}{4}$$

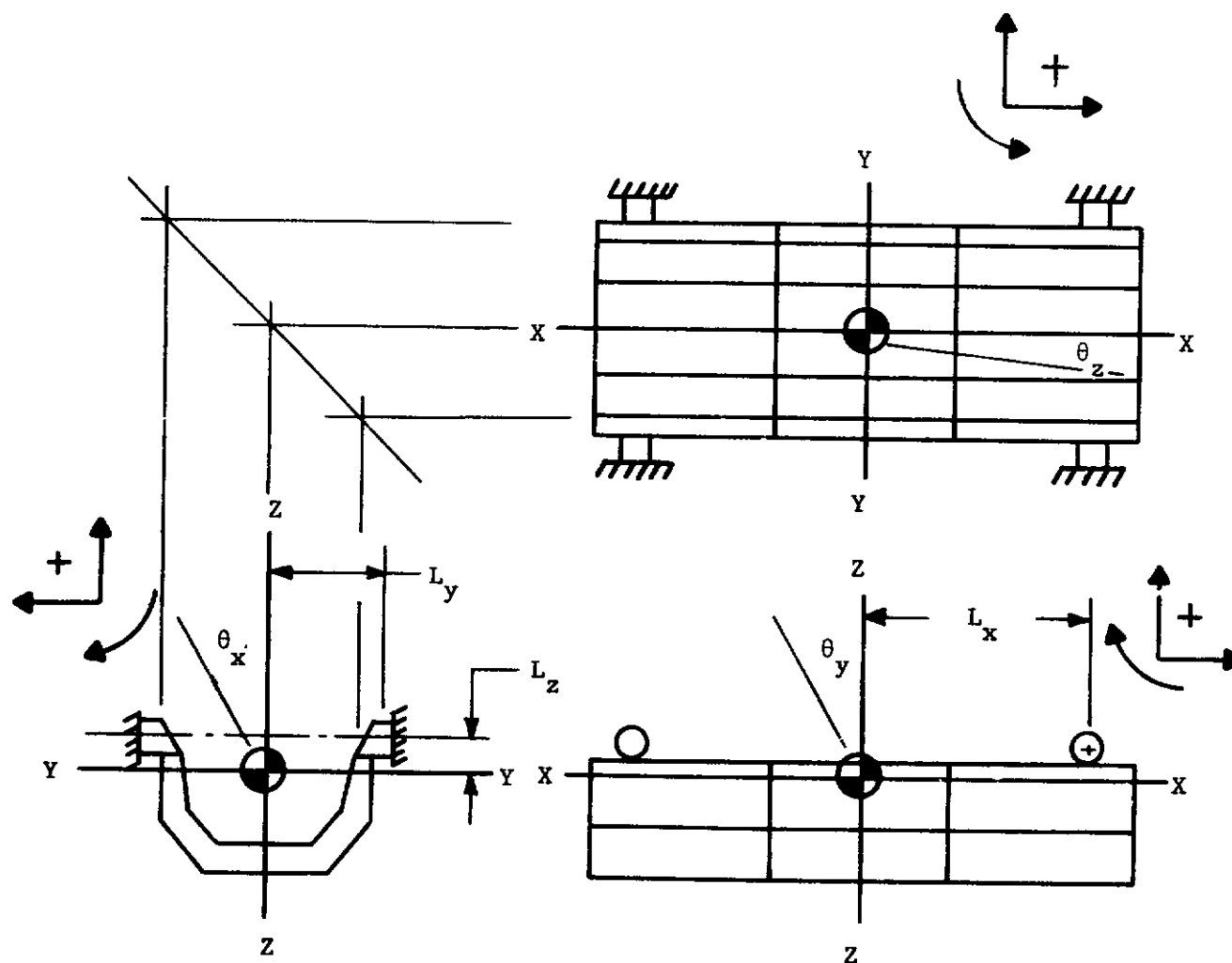


Figure 4-8. Four Point Suspension Offset Above the Pallet - Sign Convention for Forces and Moments



The solution of the equations yields the rocking natural frequencies as a ratio to the Z axis natural translational frequency.

$$\left(\frac{\omega}{\omega_z}\right)^4 - \left(\frac{L_x^2}{R_{yy}^2} + \frac{L_z^2 K_x}{R_{yy}^2 K_z} + \frac{K_x}{K_z}\right) \left(\frac{\omega}{\omega_z}\right)^2 + \frac{L_x^2 K_x}{R_{yy}^2 K_z} = 0$$

For X axis translation coupled with the Y axis rotation and:

$$\left(\frac{\omega}{\omega_z}\right)^4 - \left(\frac{L_y^2}{R_{xx}^2} + \frac{L_z^2 K_y}{R_{xx}^2 K_z} + \frac{K_y}{K_z}\right) \left(\frac{\omega}{\omega_z}\right)^2 + \frac{L_y^2 K_y}{R_{xx}^2 K_z} = 0$$

For Y axis translation coupled with the X axis rotation.

Various combinations of spring constants and natural frequencies can be evaluated. The data of two combinations are listed in table 4-7. Configuration 1 is based on Z axis translational frequency equal to Z axis rotational frequency and  $K_x$  equal to  $K_y$ ; configuration 2 is based on the ratios equal to 1.0.

4.3.8 Damping - Natural frequencies of the various suspension systems have been expressed as functions of geometry and spring constants. The design objective for damping is based on 10 percent of critical damping. Translational critical damping is:

$$C_c = 2m\omega$$

Rotational critical damping is:

$$C_{rc} = 2I\omega_r$$

For all the suspension systems analyzed the damping constants are:

$$C = .2m\omega$$

for translation and

$$C_r = .2I\omega_r$$

for rotation. Since damping is a function of natural frequencies specific damping constants are easily defined and will be specified only for the recommended isolator design.

Table 4-7. Four Point Suspension Offset Above the Pallet  
Natural Frequencies and Spring Constants

CONFIGURATION	AXIS	SPACING m	TRANSLATIONAL NATURAL FREQUENCY Hz	ROTATIONAL NATURAL FREQUENCY Hz	AXIAL SPRING CONSTANT N/m
1	X	3.66	0.10,0.08	0.17,0.08	719
1	Y	2.28	0.17,0.08	0.10,0.08	719
1	Z	0.46	0.10	0.10	1,084
2	X	3.66	0.12,0.10	0.17,0.10	1,514
2	Y	2.28	0.17,0.10	0.12,0.10	1,159
2	Z	0.46	0.10	0.13	1,084

#### 4.3.9 Isolator Study

4.3.9.1 Elastomeric Isolators - Stock elastomeric isolators manufactured by Barry Controls and Lord Manufacturing Co. were investigated. Stock isolators cannot meet the requirements of the suspension systems analyzed.

The method of sizing an elastomeric isolator to specific requirements involves a trial and error development approach. This is due to several performance characteristics of elastomers.

- a. Typical elastomers have nonlinear load vs deflection curves.
- b. Hysteretic damping is a function of the compound; damping ratios range from 0.05 to 0.15.
- c. Elastomers are temperature sensitive; at low temperatures, below  $-60^{\circ}\text{C}$ , they become stiff and brittle while at high temperatures,  $+150^{\circ}\text{C}$ , they become soft.
- d. The shape of the isolator can be varied to achieve various performances; tension, compression, shear and rotational loading each require different approaches to the shape.

Elastomeric isolators specifically designed for any of the suspension systems would have nonlinear spring constants and hysteretic damping. A thermal control system would be required for stable performance.

4.3.9.2 Wire Rope Helical Springs - Stock wire rope helical springs manufactured by Aeroflex Laboratories, Inc. were investigated. Stock springs cannot meet the requirements of the suspension systems analyzed.

The method of sizing a wire rope helical spring involves a trial and error development approach. This is due to limited design data plus the following performance characteristics of stock springs.

- a. Stock springs have nonlinear load vs deflection curves.
- b. Compression, shear and compression roll loading of stock springs have hysteresis response.
- c. Stock springs have high, 15 percent to 20 percent, friction damping.

Wire rope helical springs specifically designed for any of the suspension systems would have nonlinear hysteresis responses plus high friction damping. Therefore the use of wire rope helical springs is not recommended for this application.

4.3.9.3 Solid Wire Springs - Solid wire springs are manufactured by many spring companies and can be sized to specific requirements. The approach to sizing these springs is based on mathematical data with several performance characteristics.

- a. Various configurations have linear spring constants.
- b. Open loop helical and cantilever springs have very small hysteretic damping factors: .5 percent.
- c. Closed loop helical springs will have friction damping factors as high as 20 percent.
- d. Metal wire springs are insensitive to the temperature range.

Solid wire springs specifically designed for any of the suspension systems would have linear spring constants but nearly zero damping. To overcome the low damping, additional dampers would be required.

Friction dampers similar to those used in stock solid wire spring isolators could be developed.

Electrodynamic dampers based on a conductor in a magnetic field are feasible. However, the presence of magnetic fields would require shielding.

Viscous dampers based on fluid/gas flow would require a closed system due to the vacuum environment.

4.3.9.4 Gas Filled Bellows - Metal bellows are manufactured by several companies in various configurations. Servometer Corporation manufactures electrodeposited nickel bellows for a variety of applications. The approach to sizing a gas filled bellows is based on mathematical data using several performance parameters.

- a. Spring constants are linear.
- b. Viscous damping is based on gas flow through a circular orifice.
- c. Metal bellows are insensitive to the temperature range.

Gas filled metal bellows specifically designed for either the three point or four point suspension systems would have linear spring constants plus viscous damping.

#### 4.3.10 System/Isolator Selection

4.3.10.1 Performance - The performance characteristics of the suspension systems and isolators are summarized in table 4-8. The selection of the suspension system and isolator is based on this data. The systems which restrict experiment placement are rejected. Since there are no evident advantages to systems with coupling they are rejected.

The decoupled three point suspension is soft for Y axis rotation because of the location of the two inline isolators. Since the location of the isolators cannot be improved this system can be rejected.

The two point suspension at the sides of the pallet has reasonable performance. However, the isolator configuration is questionable due to the high torsional spring constants required compared to the soft linear spring constants required. Of the isolators investigated, the elastomeric isolator would be the most likely to achieve the desired performance. Since elastomer performance varies with temperature, a thermal control would be required.

The decoupled four point suspension has reasonable performance. A gas filled bellows can be configured to achieve the translational stiffness required. By combining three bellows at right angles an isolator can be configured to achieve the required isolation and damping.

Therefore the selection of the decoupled four point suspension utilizing gas filled bellows is recommended.










#### 4.3.11 Four Point Suspension Using Gas Filled Bellows

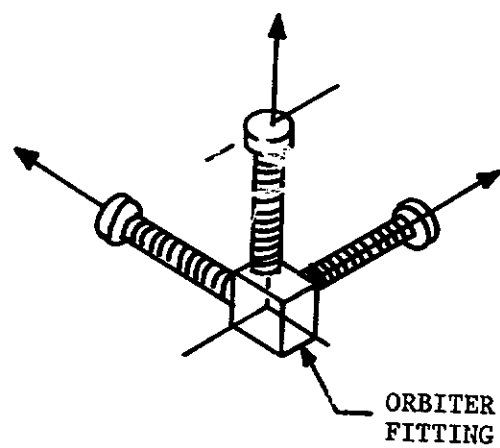
4.3.11.1 Four Point Suspension - The suspension system as shown in figure 4-9 will be evaluated. The natural frequencies and spring constants listed in table 4-9 are the same as section 4.3.7.1, configuration 3, listed in table 4-6. As defined in section 4.3.8 the critical damping equations are:

$$C_c = 2m\omega$$

for translation and

Table 4-8. Summary - Performance Characteristics of the Suspension Systems and Isolators

SINGLE POINT SUSPENSION	TWO POINT SUSPENSION	THREE POINT SUSPENSION	FOUR POINT SUSPENSION
<p><u>4.3.4.1 Containing the Center of Mass</u></p> <ul style="list-style-type: none"> <li>Decoupled Natural Frequencies</li> <li>Translational and Rotational Stiffness Required for Three Axes of the Isolator</li> </ul>  <ul style="list-style-type: none"> <li>Restricts Experiment Placement from the Central Portion of the Payload Volume</li> </ul>	<p><u>4.3.5.1 At the Sides of the Pallet</u></p> <ul style="list-style-type: none"> <li>Decoupled Natural Frequencies</li> <li>Translational Stiffness required for Three Axes and Rotational Stiffness required for One Axis of the Two Isolators.</li> </ul> 	<p><u>4.3.6.1 On a YZ Plane</u></p> <ul style="list-style-type: none"> <li>Decoupled Natural Frequencies</li> <li>Translational Stiffness required for Three Axes of the Two Inline Isolators</li> </ul>  <ul style="list-style-type: none"> <li>Translational Stiffness required for Two Axes of the Third Isolators</li> </ul>	<p><u>4.3.7.1 Containing the Center of Mass</u></p> <ul style="list-style-type: none"> <li>Decoupled Natural Frequencies</li> <li>Translational Stiffness required for Three Axes of the Four Isolators.</li> </ul> 
<p><u>4.3.4.2 Offset Below the Pallet</u></p> <ul style="list-style-type: none"> <li>Coupling: X Translation and Y Rotation</li> <li>Coupling: Y Translation and X Rotation</li> <li>Translational and Rotational Stiffness Required for Three Axes of the Isolator</li> </ul> 	<p><u>4.3.5.2 At the End of the Pallet</u></p> <ul style="list-style-type: none"> <li>Decoupled Natural Frequencies</li> <li>Translational Stiffness required for Three Axes and Rotational Stiffness required for One Axis of the Two Isolators</li> </ul>  <ul style="list-style-type: none"> <li>Restricts Experiment Placement from Both Ends of the Pallet</li> </ul>	<p><u>4.3.6.2 On a Skewed Plane</u></p> <ul style="list-style-type: none"> <li>Coupling: X Rotation and Z Rotation</li> <li>Translational Stiffness required for Three Axes of the Three Isolators</li> </ul>  <ul style="list-style-type: none"> <li>Low Natural Frequency for Y Axis Rotation</li> </ul>	<p><u>4.3.7.2 Offset Above the Pallet</u></p> <ul style="list-style-type: none"> <li>Coupling: X Translation and Y Rotation</li> <li>Coupling: Y Translation and X Rotation</li> <li>Translational Stiffness required for Three Axes of the Four Isolators</li> </ul> 
<p><u>4.3.4.3 Offset at the End of the Pallet</u></p> <ul style="list-style-type: none"> <li>Coupling: Y Translation and Z Rotation</li> <li>Coupling: Z Translation and Y Rotation</li> <li>Translational and Rotational Stiffness Required for Three Axes of the Isolator</li> </ul>  <ul style="list-style-type: none"> <li>Restricts Experiment Placement from One End of the Pallet</li> </ul>			
<p><u>4.3.9.1 Elastomeric Isolator</u></p> <ul style="list-style-type: none"> <li>Non Linear Load Versus Deflection</li> <li>Hysteretic Damping 5% to 15%</li> <li>Performance varies with Temperature Requiring Thermal Control</li> </ul>	<p><u>4.3.9.2 Wire Rope Helical Spring</u></p> <ul style="list-style-type: none"> <li>Non Linear Load Versus Deflection</li> <li>Friction Damping 15% to 20%</li> </ul>	<p><u>4.3.9.3 Solid Wire Helical Spring</u></p> <ul style="list-style-type: none"> <li>Linear Load Versus Deflection</li> <li>Hysteretic Damping 0.5%</li> <li>Requires Additional Damping</li> </ul>	<p><u>4.3.9.4 Gas Filled Bellows</u></p> <ul style="list-style-type: none"> <li>Linear Load Versus Deflection</li> <li>Viscous Damping 10%</li> </ul>



ISOLATOR - GAS BELLOWS  
ARRANGEMENT

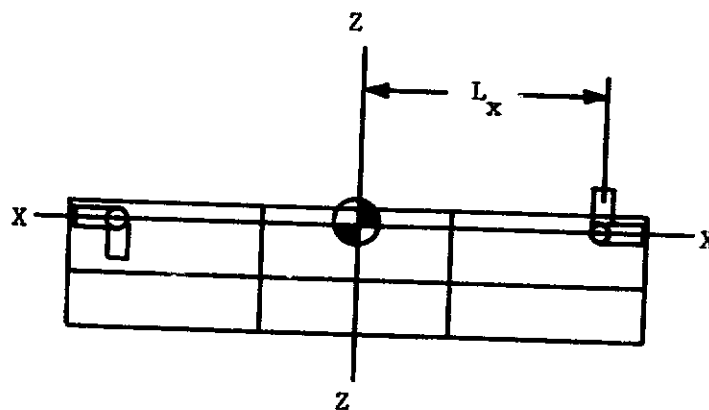
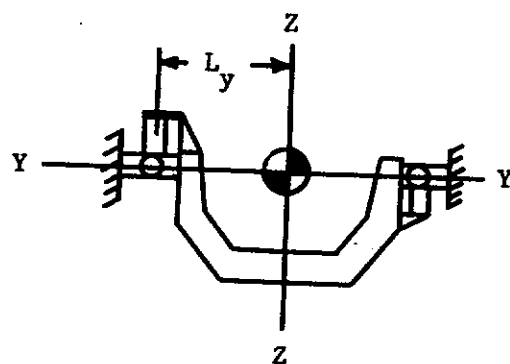
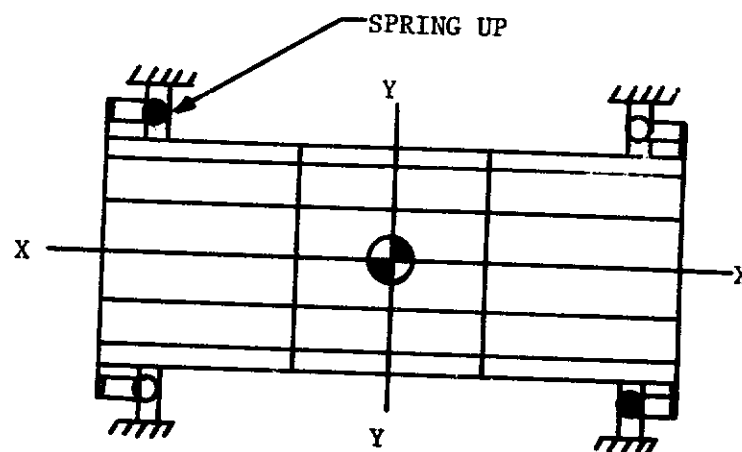


Figure 4-9. Four Point Suspension Containing the Center of Mass  
Gas Filled Bellows Isolaters

Table 4-9. Four Point Suspension - Gas Filled Bellows  
 Natural Frequencies, Damping Ratios, Spring Constants, Damping Constants

AXIS	SPACING m	TRANSLATIONAL NATURAL FREQUENCY Hz	ROTATIONAL NATURAL FREQUENCY Hz	AXIAL SPRING CONSTANT N/m	TRANSLATIONAL DAMPING RATIO $4C/C_c$	ROTATIONAL DAMPING RATIO $C_r/C_{rc}$	AXIAL DAMPING CONSTANT N-sec/m
X	3.66	0.08	0.10	719	0.08	0.10	229
Y	2.28	0.08	0.06	719	0.08	0.06	229
Z	0.00	0.06	0.10	404	0.06	0.10	129



$$C_{rc} = 2I\omega_r$$

for rotation. The system damping constants are:

$$4C_x = 2m\omega_x$$

for X translation,

$$4C_y = 2m\omega_y$$

for Y translation and

$$4C_z = 2m\omega_z$$

for Z translation. Because rotational damping is a function of spacing and translational damping two conditions exist.

From X axis rotation:

$$C_{rx} = 2I_{xx} \omega_{rx}$$

$$C_{rx} = 4L_y^2 C_z$$

From Y axis rotation:

$$C_{ry} = 2I_{yy} \omega_{ry}$$

$$C_{ry} = 4L_x^2 C_z$$

From Z axis rotation:

$$C_{rz} = 2I_{zz} \omega_{rz}$$

$$C_{rz} = 4L_x^2 C_y + 4L_y^2 C_x$$

The damping data listed in table 4-9 is based on X and Z axes equal damping ratios. This is in keeping with the configuration of the spring constants. It should be noted that various combinations of spring constants, damping constants, spacing and natural frequencies are possible with the four point suspension system.

4.3.11.2 Gas Filled Bellows - The design of the gas filled bellows is shown in figure 4-10. To facilitate the design, the calculations are in the American practice of units since the various equations and constants are defined in this system. The physical size of the bellows is easily converted to the metric units.

The approach to the design is based on the spring constant as a function of the gas and the metal bellows while damping is a function of the gas flow through a circular orifice.

The required damping force of a single bellows isolator is:

$$F = C \dot{\chi}$$

and is equal to the resisting force of the gas:

$$F = A_B \Delta P$$

where:

$F$  = the force (lb)

$C$  = the damping constant (lb-sec/in)

$\dot{\chi}$  = the velocity of the bellows motion (in/sec)

$A_B$  = the effective area of the bellows (in<sup>2</sup>)

$\Delta P$  = the change in the gas pressure (lb/in<sup>2</sup>)

The general equation of laminar gas flow through a circular orifice is:

$$v = \frac{D^2 \Delta P}{32 \mu \ell}$$

where:

$v$  = the gas flow rate (in/sec)

$D$  = the orifice diameter (in)

$\Delta P$  = the pressure drop across orifice (lb/in<sup>2</sup>)

$\mu$  = viscosity of the gas ( $3.33 \times 10^{-9}$  lb-sec/in<sup>2</sup> for air)

$\ell$  = the orifice length

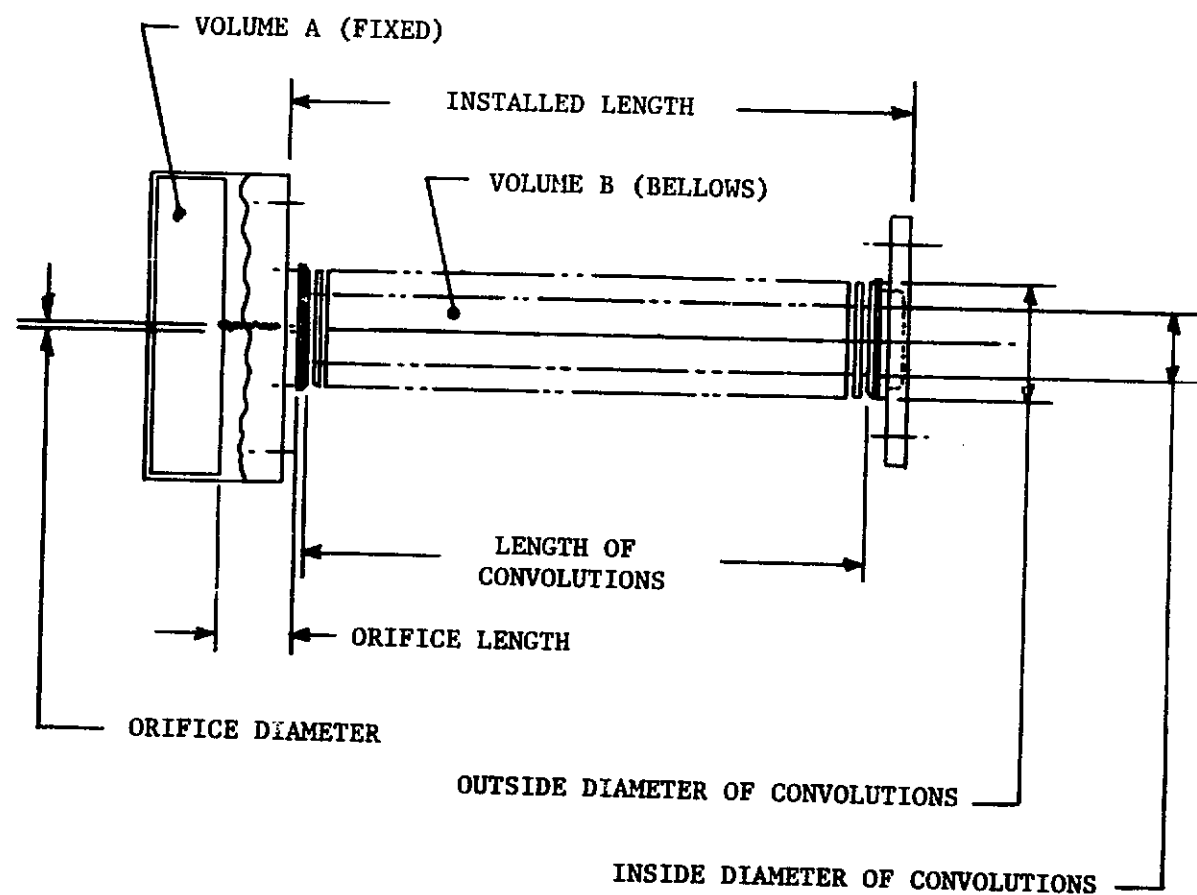


Figure 4-10. Gas Filled Bellows

And the gas flow rate as a function of the velocity of the bellows motion is:

$$vA_D = \dot{\chi}A_B$$

and

$$A_D = \frac{\pi D^2}{4}$$

$$v = \frac{4\dot{\chi}A_B}{\pi D^2}$$

where:

$A_D$  = the orifice area ( $\text{in}^2$ )

Combining these equations yields a relation between the damping constant and orifice:

$$C = \frac{128\mu l A_B^2}{\pi D^4}$$

Thus the orifice diameter and length can be chosen for various damping requirements.

The pressure change across the orifice as a function of the bellows velocity is determined from the two force equations:

$$F = C\dot{\chi} = A_B \Delta P$$

$$\Delta P = \frac{C}{A_B} \dot{\chi}$$

Bellows velocities are determined from the various pallet/orbiter disturbances. Man motion disturbance studies indicate bellows velocities of approximately .02 inches per second for a single spike. Gravity gradient studies indicate bellows velocities of approximately .09 inches per second. Experiment disturbances are not available at this time but the resulting bellows velocities can be expected to also be small. Therefore the bellows velocity of .10 inches per second will be used for the design. The general equation for air spring constants is:

$$K = \frac{\gamma P A^2}{V}$$

where:

K = the spring constant

$\gamma$  = the specific heat constant of gas (1.4 for air)

P = the pressure

A = the effective area

V = the volume

For the gas filled bellows the gas spring constant is:

$$K_G = \frac{\gamma P_o A_B^2}{V_A + V_B}$$

where:

$P_o$  = the initial pressure (lb/in<sup>2</sup>)

$V_A$  = the fixed volume A (in<sup>3</sup>)

$V_B$  = the initial bellows volume B (in<sup>3</sup>)

The pressure volume relations are:

$$P_o (V_A + V_B) = P_x (V_A + V_B + x A_B)$$

$$\Delta P = P_o - P_x$$

and:

$$\Delta P = \frac{x A_B P_o}{V_A + V_B}$$

The gas spring constant as a function of bellows displacement and pressure change is:

$$K_G = \frac{\gamma A_B \Delta P (V_A + V_B + x A_B)}{x (V_A + V_B)}$$

Bellows displacements (x) are expected to be small, less than .10 inch. Volumes A and B will be chosen large compared to the displacement volume  $x A_B$  so that:

$$\frac{V_A + V_B + x A_B}{V_A + V_B} \approx 1$$

Therefore:

$$K_G = \gamma A_B \frac{\Delta P}{x}$$

and

$$\Delta P = \frac{K_G}{\gamma A_B} x$$

The pressure change is now defined as functions of bellows displacement and velocity. Since the total spring rate required can be achieved by either the gas or the metal bellows, a reasonable isolator configuration can be achieved by determining the maximum pressure change from the damping velocity requirements and sizing the gas spring constant from the resulting initial pressure conditions.

The mathematical design of a bellows is based on Servometer Corporation literature, reference 4.

The spring rate of the metal bellows is based on the spring resistance due to bending of the convolution walls.

$$K_B = \frac{4.3E(OD+ID)t^3}{(OD-ID-t)^3 N}$$

where:

$K_B$  = the spring rate of the whole bellows (lb/in)

$E$  = Young's modulus of elasticity,  $23.35 \times 10^6$  for electrodeposited nickel

$OD$  = bellows outside diameter (in)

$ID$  = bellows inside diameter (in)

$t$  = bellows wall thickness (in)

$N$  = number of active convolutions

The stroke rating in tension is:

$$S = \frac{7.5 \times 10^{-4} (OD-ID-t)^2 N}{t}$$

where:

$S$  = maximum permissible stroke for the bellows (in)

The effective area is:

$$A_B = \frac{\pi}{16} (OD-ID)^2$$

The pressure rating is:

$$P_r = \frac{1.25 \times 10^6 t^2}{(OD-ID-t)^2}$$

where  $P_r$  is the nominal pressure rating (lb/in<sup>2</sup>).

Summary data for the X and Y axes bellows shown in figure 4-10 is listed in table 4-10. The pertinent design features are as follows.

For damping,  $\ell=1.00$  in. and:

$$D = \left( \frac{128 \mu \ell A_B^2}{\pi C} \right)^{1/4} = .0191 \text{ in}$$

The pressure change for damping is:

$$\Delta P = \frac{C}{A_B} \dot{x} = .12 \text{ lb/in}^2$$

The bellows volume is:

$$V_B = L_B A_B = (8)(1.13) = 9.04 \text{ in}^3$$

The volume A is sized to give:

$$V_A = 11.10 \text{ in}^3$$

Table 4-10. Bellows Design Features

FEATURES	X AND Y AXES	Z AXIS
Outside Diameter	1.50 in	1.50 in
Inside Diameter	.90 in	.90 in
Convolution Thickness	.0044 in	.0037 in
Convolution Pitch	.15 in	.15 in
Number of Convolutions	47	47
Effective Bellows Area	1.13 in <sup>2</sup>	1.13 in <sup>2</sup>
Bellows Volume	9.04 in <sup>3</sup>	9.04 in <sup>3</sup>
Fixed Volume	11.10 in <sup>3</sup>	11.10 in <sup>3</sup>
Orifice Diameter	.019 in	.022 in
Orifice Length	1.00 in	1.00 in
Bellows Pressure Rating	68.22 lb/in <sup>2</sup>	48.13 lb/in <sup>2</sup>
Initial (Fill) Pressure	21.51 lb/in <sup>2</sup>	12.55 lb/in <sup>2</sup>
Maximum Pressure	22.79 lb/in <sup>2</sup>	13.30 lb/in <sup>2</sup>
Bellows and Gas Weight	1.20 lb	1.01 lb
Free Length of Bellows	7.05 in	7.05 in
Maximum Stroke	2.84 in	3.39 in
Spring Constant	4.11 lb/in	2.31 lb/in
Damping Constant	1.31 lb-sec/in	.74 lb-sec/in



The initial pressure is

$$P_o = \frac{\Delta P(V_A + V_B + xA_B)}{xA_B} = 21.51 \text{ lb/in}^2$$

The gas spring rate is:

$$K_G = \gamma A_B \frac{\Delta P}{x} = 1.90 \text{ lb/in}$$

The bellows spring rate required is:

$$K_B = K - K_G = 2.21 \text{ lb/in}$$

Selection of the bellows wall thickness and number of active convolutions yields the bellows spring rate:

$$K_B = \frac{4.3E(OD-ID)t^3}{(OD-ID-t)^3 N} = 2.24 \text{ lb/in}$$

where:

$$t = .0044 \text{ in.}$$

$$N = 47$$

The bellows stroke rating is:

$$S = \frac{7.5 \times 10^{-4} (OD-ID-t)^2 N}{t} = 2.84 \text{ in}$$

The length of the convolutions is:

$$L = N(\text{pitch}) = 7.05 \text{ in}$$

where the pitch is .15 inch.

The pressure rating is:

$$P_r = \frac{1.25 \times 10^6 t^2}{(OD-ID-t)^2} = 68.22 \text{ lb/in}^2$$

The maximum pressure expected would occur at  $x = -1.0$  inch.

$$P_{\max} = \frac{P_o (V_A + V_B)}{(V_A + V_B - x_{AB})} = 22.79 \text{ lb/in}^2$$

The temperature effect on the pressure is:

$$P_o = P_i \left( \frac{T_o}{T_i} \right)^{\frac{k-1}{k}}$$

where:

$$T_o = 68^\circ\text{F} = 528^\circ\text{R}$$

$$T_{\max} = 160^\circ\text{F} = 620^\circ\text{R}$$

$$T_{\min} = -70^\circ\text{F} = 390^\circ\text{R}$$

$$k = 1.4$$

$$P_{\max} = \frac{P_o}{\left( \frac{T_o}{T_{\max}} \right)^{.286}} = 22.52 \text{ lb/in}^2$$

and:

$$P_{\min} = \frac{P_o}{\left( \frac{T_o}{T_{\min}} \right)^{.286}} = 19.72 \text{ lb/in}^2$$

The weight of just the gas filled bellows is:

$$W = \frac{\pi t d N}{2n} [ (OD-t)^2 - (ID+t)^2 + n((.75)(OD) + ID) ]$$

where:

$$d = .321 \text{ lb/in}^3 \text{ (the specific weight of nickel)}$$

$$n = .15 \text{ in (the pitch of the convolutions)}$$

$$W = 1.20 \text{ lb}$$

Summary data for the Z axis bellows shown in figure 4-10 is listed in table 4-10. The pertinent design features are as follows:

For damping,  $\ell=1.00$  in and:

$$D = \left( \frac{128\mu\ell A_B^2}{\pi C} \right)^{1/4} = .0220 \text{ in}$$

The pressure change for damping is:

$$\Delta P = \frac{C}{A_B} \dot{x} = .07 \text{ lb/in}^2$$

The bellows volume is:

$$V_B = L_B A_B = 9.04 \text{ in}^3$$

The volume A is sized to give:

$$V_A = 11.10 \text{ in}^3$$

The initial pressure is:

$$P_o = \frac{\Delta P (V_A + V_B + x A_B)}{x A_B} = 12.55 \text{ lb/in}^2$$

The gas spring rate is:

$$K_G = \gamma A_B \frac{\Delta P}{x} = 1.11 \text{ lb/in}$$

The bellows spring rate required is:

$$K_B = K - K_G = 1.20 \text{ lb/in}$$

Selection of the bellows wall thickness and number of active convolutions yields the bellows spring rate:

$$K_B = \frac{4.3E(OD-ID)t^3}{(OD-ID-t)^3 N} = 1.22 \text{ lb/in}$$

where:

$$t = .0037 \text{ in.}$$

$$N = 47$$

The bellows stroke rating is:

$$S = \frac{7.5 \times 10^{-4} (OD-ID-t)^2 N}{t} = 3.39 \text{ in.}$$

The length of the convolutions is:

$$L = N(\text{pitch}) = 7.05 \text{ in.}$$

where the pitch is .15 inch.

The pressure rating is:

$$P_r = \frac{1.25 \times 10^6 t^2}{(OD-ID-t)^2} = 48.13 \text{ lb/in}^2$$

The maximum pressure expected would occur at  $N = -1.0$  inch.

$$P_{\max} = \frac{P_o (V_A + V_B)}{(V_A + V_B - x A_B)} = 13.30 \text{ lb/in}^2$$

The temperature effect on the pressure is:

$$P_{\max} = \frac{P_o}{\left(\frac{T_o}{T_{\max}}\right) .286} = 13.07 \text{ lb/in}^2$$

and:

$$P_{\min} = \frac{P_o}{\left(\frac{T_o}{T_{\min}}\right) .286} = 11.51 \text{ lb/in}^2$$

The weight of just the gas filled bellow is:

$$W = \frac{\pi t d L}{2n} [(OD-t)^2 - (ID+t)^2 + n((.75)(OD) + ID)]$$

$$W = 1.01 \text{ lb}$$

The weight of the end fittings is not included at this time because the end fittings can be designed to meet a final installation configuration.

Installation of the bellows isolators between the pallet and orbiter stretches or preloads the isolators. The design was based on an installed length 1.25 inches greater than the bellows free length. This assures linear response characteristics plus allows the suspension system to float with orbiter/pallet deflections of plus or minus 1.0 inch along the three axes.

Since the bellows are always in tension, the bellows free length can be precompressed to reduce the free length; there is no effect on performance.

#### 4.3.12 Suspension System Evaluation

4.3.12.1 Center of Mass Offset Sensitivity - The center of mass is assumed to be offset from the true position in the center of the four point suspension as shown in figure 4-11. The offset is assumed to occur from tolerances associated with installing the suspension system to the pallet or from different payload arrangements. Any offset will result in coupling of various modes of response. The equations of motion are:

$$\Sigma F_x \quad x(-m\omega^2 + 4K_x) - \theta_y 4K_x Z + \theta_z 4K_x Y = F'_x$$

$$\Sigma F_y \quad y(-m\omega^2 + 4K_y) + \theta_x 4K_y Z - \theta_z 4K_y X = 0$$

$$\Sigma F_z \quad z(-m\omega^2 + 4K_z) + \theta_y 4K_z X - \theta_x 4K_z Y = 0$$

$$\Sigma M_x \quad \theta_x (-I_x \omega^2 + 4K_z L_y^2 + 4K_z Y^2 + 4K_y Z^2) \\ - \theta_z 4K_y XZ - \theta_y 4K_z XY + y 4K_z Z - z 4K_z Y = 0$$

$$\Sigma M_y \quad \theta_y (-I_y \omega^2 + 4K_z L_x^2 + 4K_z X^2 + 4K_x Z^2) \\ - \theta_x 4K_z XY - \theta_z 4K_x YZ - x 4K_z Z + z 4K_z X = 0$$

$$\Sigma M_z \quad \theta_z (-I_z \omega^2 + 4K_y L_x^2 + 4K_y L_y^2 + 4K_x Y^2 + 4K_x X^2) \\ - \theta_y 4K_x YZ - \theta_x 4K_y XZ - y 4K_y X + x 4K_y Y = 0$$

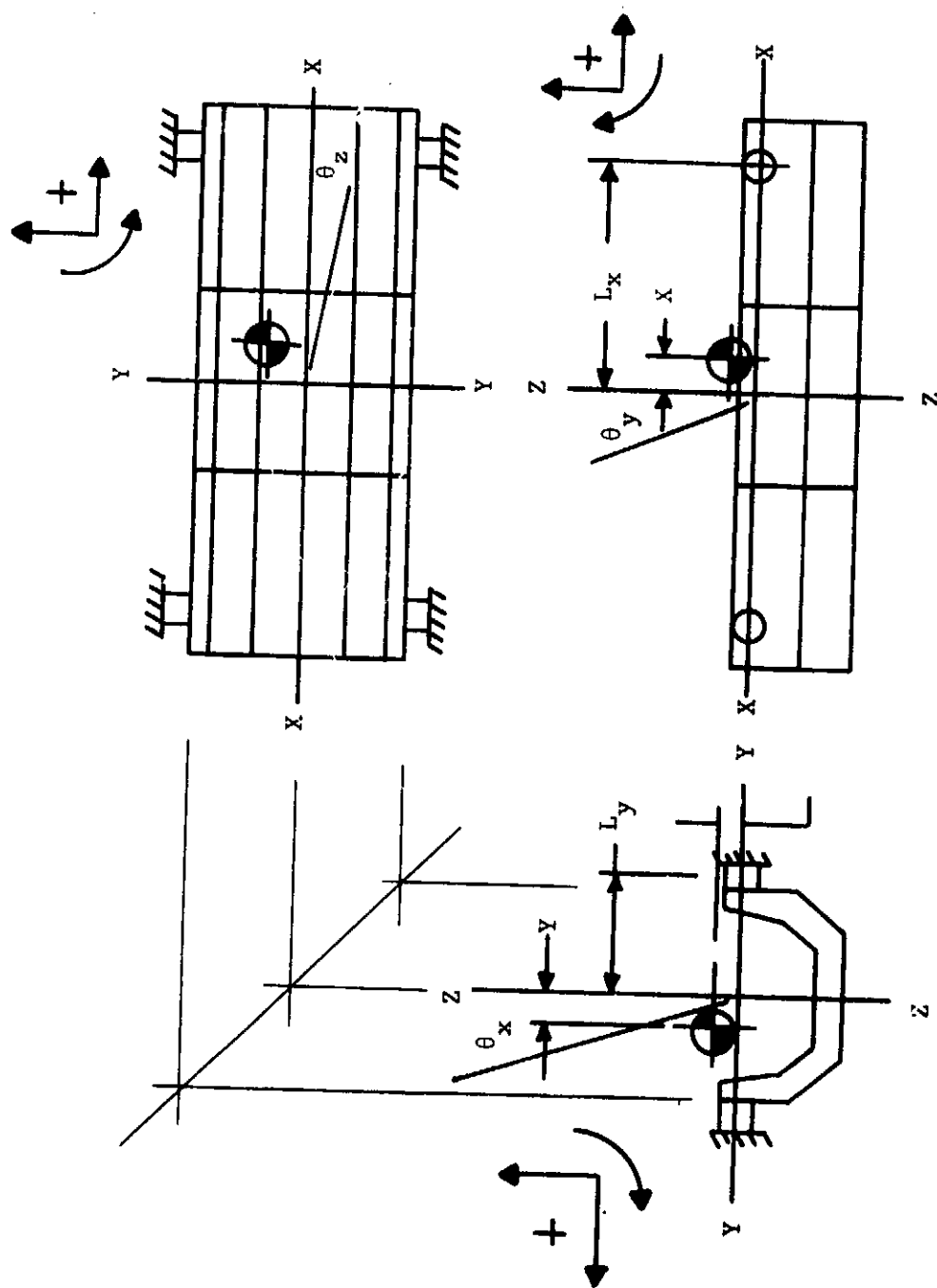


Figure 4-11. Center of Mass Offset

The coupling effects are investigated one axis at a time. By letting  $Y=Z=0$ , the X axis offset yields coupling of Z translation with Y rotation and Y translation with Z rotation. Solution of the equations of motion, using the data of the system and  $\omega$  in radians per second, yields:

$$\omega^4 - (.303 + .012X^2)\omega^2 + .023 = 0$$

For Z translation with Y rotation and:

$$\omega^4 - (.656 + .021X^2)\omega^2 + .103 = 0$$

For Y translation with Z rotation.

The natural frequencies are plotted as a function of the offset X in figure 4-12. The natural frequencies for X axis translation and rotation remain unaffected.

By letting  $X=Z=0$ , the Y axis offset yields coupling of X translation with Z rotation and Z translation with X rotation. Solution of the equations of motion, using the data of the system and  $\omega$  in radians per second, yields:

$$\omega^4 - (.656 + .021Y^2)\omega^2 + .103 = 0$$

For X translation with Z rotation and:

$$\omega^4 - (.542 + .076Y^2)\omega^2 + .058 = 0$$

For Z translation with X rotation. The natural frequencies are plotted as a function of the offset Y in figure 4-13. The natural frequencies for Y axis translation and rotation remain unaffected.

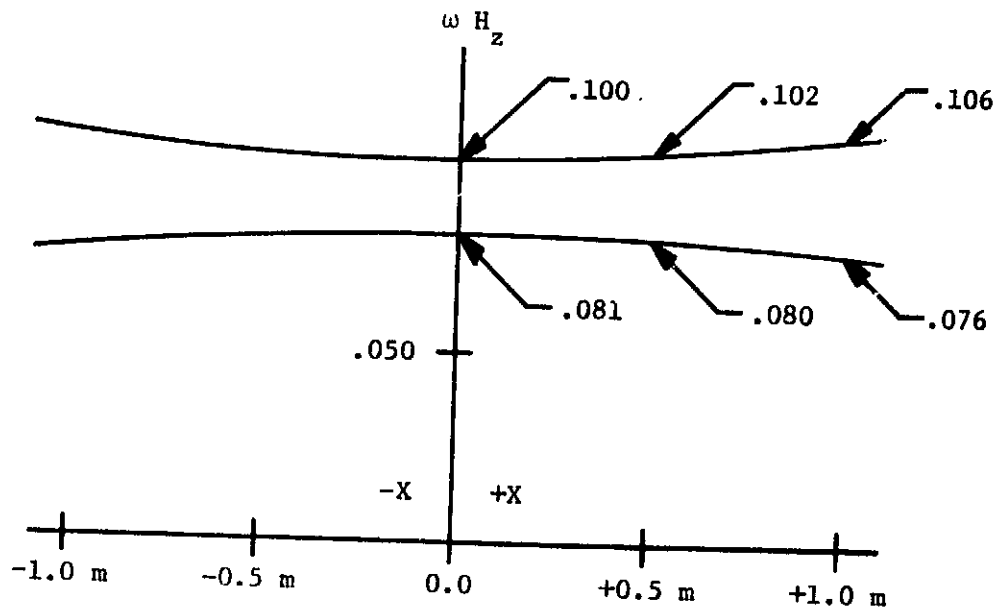
By letting  $X=Y=0$ , the Z axis offset yields coupling of X translation with Y rotation and Y translation with X rotation. Solution of the equations of motion, using the data of the system and  $\omega$  in radians per second, yields:

$$\omega^4 - (.419 + .021Z^2)\omega^2 + .041 = 0$$

For X translation with Y rotation and:

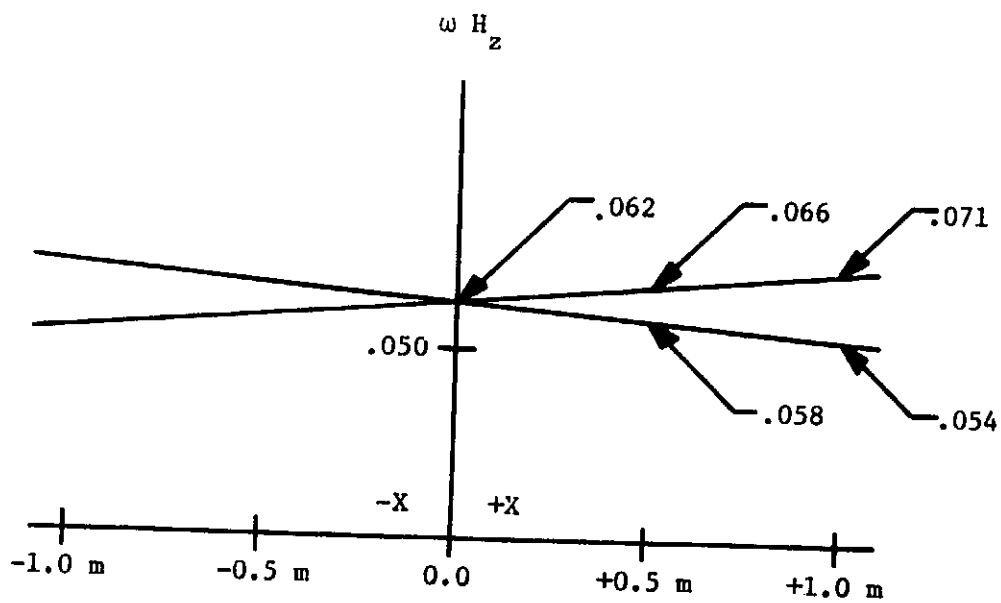
$$\omega^4 - (.657 + .135Z^2)\omega^2 + .103 = 0$$

For Y translation with X rotation. The natural frequencies are plotted as a function of the offset Z in figure 4-14. The natural frequencies for Z axis translation and rotation remain unaffected.



Y TRANSLATION WITH Z ROTATION

$$\omega^4 - (.656 + .021X^2)\omega^2 + .103 = 0$$

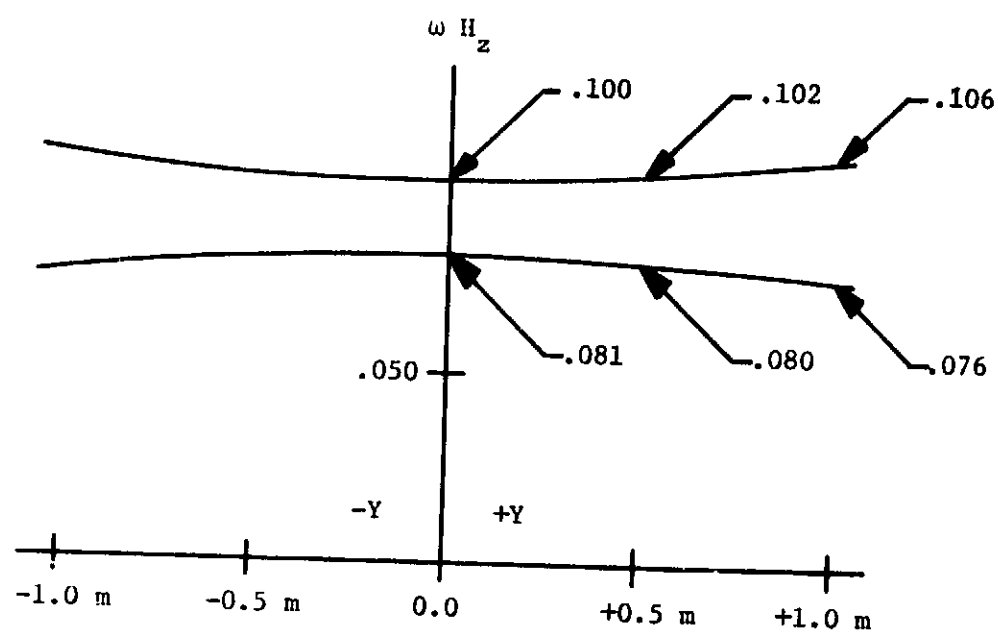


Z TRANSLATION WITH Y ROTATION

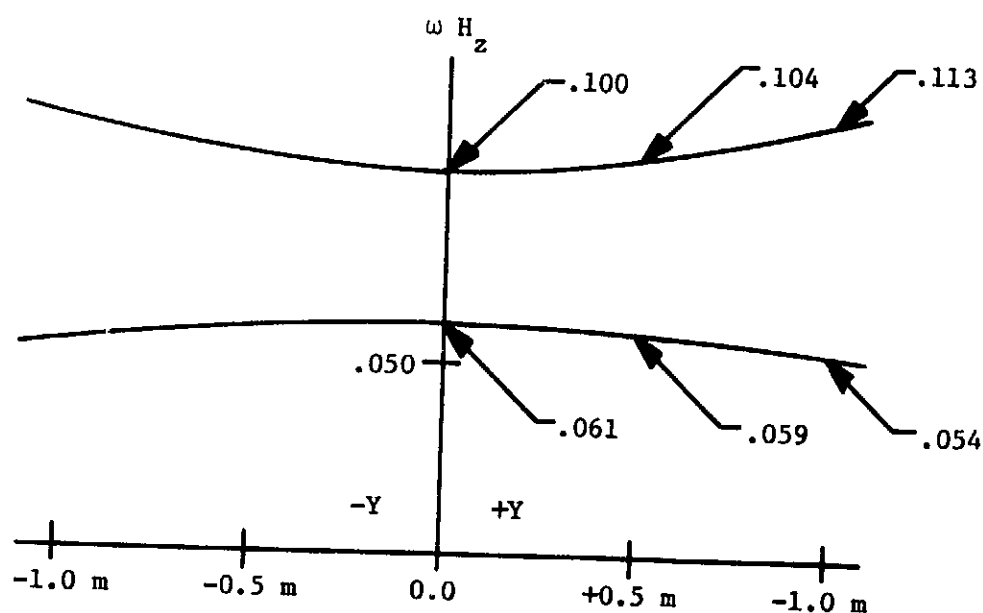
$$\omega^4 - (.303 + .012X^2)\omega^2 + .023 = 0$$

Figure 4-12. X Offset Center of Mass



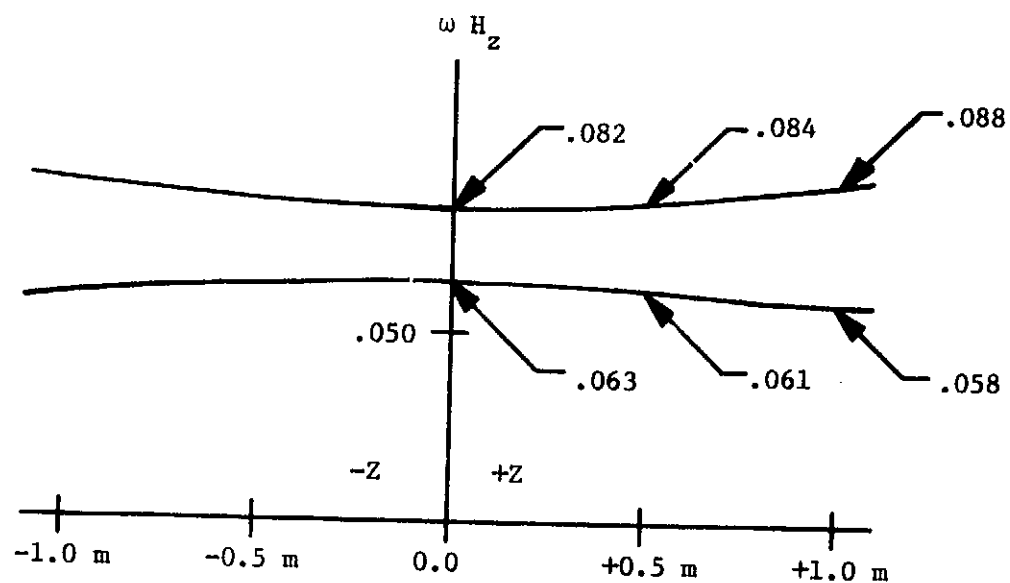


X TRANSLATION WITH Z ROTATION  
 $\omega^4 - (.656 + .021Y^2)\omega^2 + .103 = 0$

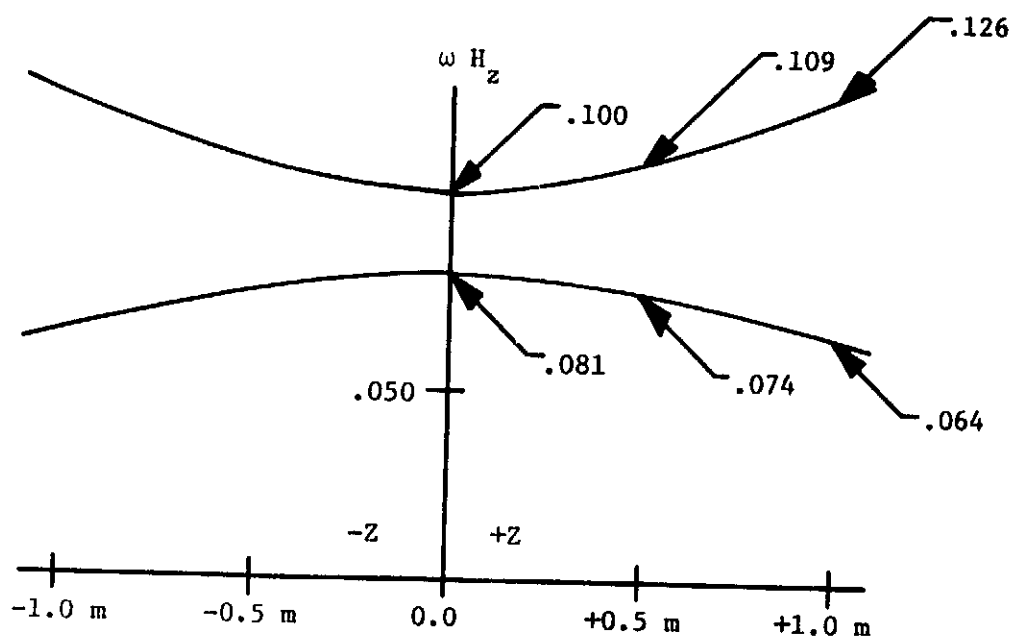


Z TRANSLATION WITH X ROTATION  
 $\omega^4 - (.542 + .076Y^2)\omega^2 + .058 = 0$

Figure 4-13. Y Offset Center of Mass



X TRANSLATION WITH Y ROTATION  
 $\omega^4 - (.419 + .021Z^2)\omega^2 + .041 = 0$



Y TRANSLATION WITH X ROTATION  
 $\omega^4 - (.657 + .135Z^2)\omega^2 + .103 = 0$

Figure 4-14. Z Offset Center of Mass

Center of mass offsets of:

$$X=\pm.75 \text{ m}$$

$$Y=\pm.75 \text{ m}$$

$$Z=\pm.50 \text{ m}$$

result in natural frequency changes less than 10 percent plus the noted coupling modes.

Coupling effects of combined axes offsets can also be investigated. However, the changes in natural frequencies can be expected to also be small, with the additional coupling modes. Therefore the suspension system can accommodate reasonable center of mass offsets without additional redesign for various payload arrangements.

4.3.12.2 Spring Constant Sensitivity - Variations in spring constants can occur from manufacturing tolerances of the bellows and loss of the gas from the assembled bellows. Investigation of spring constant sensitivity includes four cases:

1. The assembly spring constant varies  $\pm 10$  percent.
2. The bellows spring constant varies  $\pm 10$  percent.
3. Total loss of gas pressure.
4. Loss of gas pressure in one corner.

For this investigation the center of mass is assumed to be in its true position in the center of the suspension system. The data is listed in table 4-11.

For case 1, the assembly spring constants are varied  $\pm 10$  percent with the four spring constants per axis remaining equal.

For case 2, the bellows spring constants are varied  $\pm 10$  percent with the four spring constants per axis remaining equal.

For case 3, the total loss of gas pressure is assumed and only the nominal bellows spring constants are effective. This is clearly the worst case since damping will also be zero.

For case 4, the loss of gas pressure at one corner is assumed and only the nominal bellows spring constants of the corner are effective. The effects of coupling are neglected.

Table 4-11. Spring Constant Sensitivity

	X	Y	Z
Nominal Natural Translational Frequency, Hz	.081	.081	.061
Nominal Natural Rotational Frequency, Hz	.100	.063	.100
Nominal Bellows Spring Constant, N/m	387	387	210
Nominal Gas Spring Constant, N/m	332	332	194
Nominal Assembly Spring Constant, N/m	719	719	404

Case 1  $\pm 10\%$  Variation in Assembly Spring Constant

	+10%			-10%		
	X	Y	Z	X	Y	Z
Spring Constant, N/m	791	791	444	647	647	364
Translational Frequency, Hz	.085	.085	.064	.077	.077	.058
Rotational Frequency, Hz	.105	.066	.105	.095	.060	.095

Case 3 Loss of Gas Pressure

	X	Y	Z
Spring Constant, N/m	387	387	210
Translational Frequency, Hz	.059	.059	.044
Rotational Frequency, Hz	.073	.046	.072

Case 2  $\pm 10\%$  Variation in Bellows Spring Constant

	+10%			-10%		
	X	Y	Z	X	Y	Z
Bellows Spring Constant, N/m	426	426	231	348	348	189
Assembly Spring Constant, N/m	758	758	425	680	680	383
Translational Frequency, Hz	.083	.083	.063	.079	.079	.059
Rotational Frequency, Hz	.103	.065	.103	.097	.061	.097

Case 4 Loss of Gas Pressure in One Corner

	X	Y	Z
System Spring Constant, N/m	2,544	2,544	1,422
Translational Frequency, Hz	.076	.076	.057
Rotational Frequency, Hz	.094	.059	.094

Case 2 represents reasonable manufacturing tolerances resulting in natural frequency variations less than 5 percent. Case 4 represents a realistic failure mode resulting in natural frequency changes less than 10 percent.

4.3.12.3 Damping Sensitivity - Damping performance is a function of the damping constant and the gas pressure drop across the orifice. The damping constant is a function of the orifice length and hole diameter; the gas pressure drop is a function of the system disturbances. Therefore, if the initial gas pressure is greater than the required gas pressure drop, damping performance will not change.

Reasonable orifice length and hole diameter tolerances are:

Length  $\pm$  .010 inch

Hole Diameter  $\begin{matrix} + .0000 \\ - .0006 \end{matrix}$  inch

Using the damping constant equation of section 4.3.11.2:

$$C = \frac{128\mu l A_B^2}{\pi D^4}$$

the tolerance effect can be determined. The data for damping ratios as functions of tolerances is listed in table 4-12.

4.3.12.4 Pallet Excursion - Gravity gradient and orbiter disturbances impose moment loading upon the pallet causing relative motion between the pallet and orbiter. Approximately 2.54 cm of clearance between the pallet and orbiter is presently anticipated.

The lowest rotational natural frequency for the suspension system is about the Y axis. Using the relationship:

$$Z = \frac{TL_x}{(\omega_r)^2 I_{yy}}$$

Table 4-12. Damping Sensitivity

	X	Y	Z
Nominal Translational Damping Ratio $4C/C_c$	.081	.081	.061
Nominal Rotational Damping Ratio $C_r/C_{rc}$	.100	.063	.100
Maximum Translational Damping Ratio $4C_{max}/C_c$	.092	.092	.069
Maximum Rotational Damping Ratio $C_{rmax}/C_{rc}$	.112	.070	.112
Minimum Translational Damping Ratio $4C_{min}/C_c$	.080	.080	.060
Minimum Translational Damping Ratio $C_{rmin}/C_{rc}$	.099	.062	.099

where:

Z = excursion

T = applied gravity gradient torque

$L_x$  = distance from pallet center of mass to the suspension system

$\omega_r$  = natural rotational frequency

$I_{yy}$  = pallet moment of inertia

For gravity gradient torque of 10 N-m:

$$Z = \frac{(10)(3.66)}{((2\pi)(.06))^2(138,839)} = .19 \text{ cm}$$

Man motion disturbances indicate rotation of the orbiter about its center of mass of:

$$\theta = 2.51 \times 10^{-4} \text{ radians}$$

Using the relationship:

$$Z = L\theta$$

where:

Z = excursion

L = distance from orbiter center of mass to the suspension system

$\theta$  = rotational deflection of the orbiter

$$Z = (5.32)(2.51 \times 10^{-4}) = .134 \text{ cm}$$

The total excursion .32 cm is significantly below the 2.54 cm clearance.

4.3.12.5 Reliability - The reliability of the suspension system is expected to be high. This is due to the four point suspension utilizing three gas filled bellows per point of suspension.

Each bellows is seamless and end fittings are welded to the bellows. Operating gas pressures are low compared to the rated gas pressures. As investigated in section 4.3.12.2, loss of the gas from a single bellows does not create a mission abort mode.

4.3.12.6 Weight and Volume - The configuration of figure 8-2 is used for weight and volume estimates.

The weight of the bellows portion of the suspension system was calculated in section 4.3.12.2. The bellows end fittings are corrosion resistant steel. The interface structure is made from aluminum.

The volume required is based on a cube.

The weight and volume data is listed in table 4-13.

4.3.12.7 Cost - The configuration of figure 8-2 is used for cost assessment. The cost assessment of the total suspension system can be divided into three categories:

4.3.12.7.1 Bellows Assembly

4.3.12.7.2 Interface Structure

4.3.12.7.3 Installation

4.3.12.7.1 Bellows Assembly - The design approach to a bellows assembly will yield low development costs due in part to the manufacturing process: "electrodeposited bellows are manufactured by forming a mandrel to the shape of the inside of the bellows, depositing the proper thickness of spring quality metal onto this, trimming the ends and dissolving out the mandrel." The end fittings are machined from bar or plate stock and can be designed for standardization or custom made for unique considerations. Heli-arc or electron beam welding process can be used to join the end fittings to the bellows. Development testing of a single assembly is based on axial (tension) load versus deflection tests which can be accomplished on existing tension loading machines.

4.3.12.7.2 Interface Structure - The bellows to orbiter fittings can be machined from aluminum plate and designed to attach to existing orbiter retention side beams. The bellows to pallet structure is designed for stiffness and protection of the bellows; manufacturing is of the low cost formed aluminum sheet fabrication.



Table 4-13. Weight and Volume

	WEIGHT PER SUSPENSION POINT kg	TOTAL WEIGHT kg
Bellows	1.56	6.24
End Fittings	7.20	28.80
Structure	<u>2.24</u>	<u>8.96</u>
TOTAL	11.00	44.00

Volume Per Suspension Point

$$V = (0.35 \text{ m})^3 = 0.043 \text{ m}^3$$

4.3.12.7.3 Installation - The bellows to orbiter fitting is bolted to the orbiter retention side beams with a minimum quantity of threaded fasteners. Installation of the bellows/pallet structure to the pallet side panels or frames depends upon the local pallet stiffness. If the side panels are unstiffened aluminum sheet, beaming the support structure to the pallet frames may be required. Actual attachment can be accomplished with threaded fasteners.

4.4 Conclusion - The four point suspension system utilizing gas filled bellows nearly achieves the design goals of equal natural frequencies and equal damping ratios in all axes. While the system is designed as an uncoupled natural frequency system, various payload arrangements with reasonable center of mass offsets can be accommodated. The gas filled bellows, utilizing gas flow through a long circular orifice for damping, has linear performance; however, several other forms of viscous damping can be developed.

During launch and descent phases the suspension system will flex with the relative motion between the pallet and orbiter.

The system performance is stable over a wide temperature range without a thermal control system.

Since the design of the gas filled bellows and the integration of the system to the pallet/orbiter is based on state-of-the-art hardware, the system cost will be low.

## 5. PALLET RETENTION SYSTEM

5.1 General - This section specifically deals with the existing pallet retention system and modifications to allow the pallet to float on the suspension system once the orbiter is in orbit. Because the orbiter structure warps under aerodynamic flight loads, launch accelerations, and thermal differences, the pallet must be isolated from the relative motions of the mounting points. The existing pallet retention system was designed to overcome the problem. Two retention points are located on the cargo bay main longerons near the aft end of the pallet to react forward and aft loads plus up and down loads. Two retention points are located on the cargo bay main longerons near the forward end of the pallet to react up and down pitching loads. A fifth retention point on the lower centerline of the cargo bay reacts side loads. This approach prevents any relative motion of the orbiter structure from inducing destructive loads into the pallet/payload.

5.2 Summary - Retention system modifications investigated included the following:

5.3.2 Release at the orbiter trunnions

5.3.3 Splitting the mounting shaft

5.3.4 Movable mounting shaft

The modifications were investigated to determine if these configurations would be structurally equivalent to the existing design and would allow the pallet to float on the suspension system once the orbiter is in orbit. The movable mounting shaft arrangement was selected as the configuration which provides the stiffest structural interface plus provides the most adaptable characteristics to further design effort.

### 5.3 Discussion

5.3.1 Design Objectives - The modified retention system shall provide the support of the pallet to the orbiter during launch and descent. Once in orbit the retention system shall be disengaged to allow the pallet to float on the suspension system. Upon completion of the mission the retention system shall be engaged to support the pallet for descent. The modified retention system shall be adaptable to the existing pallet/orbiter interface structure.

5.3.2 Release At the Orbiter Trunnions - This approach would modify existing orbiter structure leaving the pallet mounting shafts unchanged. Orbiter hinged trunnions would be motor driven to allow opening and closing of the trunnions in orbit. A separate ejector or positioning mechanism would be required to allow the pallet to float on the suspension system with adequate clearances. This system would probably be an adaption of the system used for ejecting other large payloads into orbit. Therefore this system is identified as a possible solution without additional investigation.

### 5.3.3 Splitting the Mounting Shaft

5.3.3.1 Centerline Tension Member - This approach modifies the mounting shaft. The configuration as shown in figure 5-1 is the locked or launch position. The unlocked position is shown in figure 5-2.

The tension member holds the orbiter shaft and the pallet shaft together at the cone and socket interface. Separation is achieved by extending the tension member thus pushing the orbiter shaft outward. Partial retraction of the tension member completes the float clearance requirement. The tension member is also caged inside the orbiter shaft. Complete retraction of the tension member locks the shafts together for descent.

Analysis of this system shows the tension member to be critical to the load reaction path from the pallet to the orbiter, thus settling, relaxing or misalignment become major problems. Also the cone-socket interface is large compared to the bore of the orbiter trunnion; this is due to the loads and the in-orbit float clearance requirements.

5.3.3.2 External Latches - An attempt was made to configure a split shaft utilizing external latches. The high reaction loads plus the complexity of clamps, actuators and separation/caging mechanisms required indicated that this approach is not feasible.

5.3.4 Movable Mounting Shaft - This approach is based on moving the mounting shaft inside the pallet fitting. The cargo bay main longeron retention point with the mounting shaft in the extended position is shown in figure 5-3. The retracted position is shown in figure 5-4. Since the mounting shaft is sized for a free running fit to the orbiter trunnion, this feature is incorporated in the pallet fitting. The position of the mounting shaft is maintained through a positive friction device such as a set screw in the pallet fitting, plus the lead screw/nut combination.

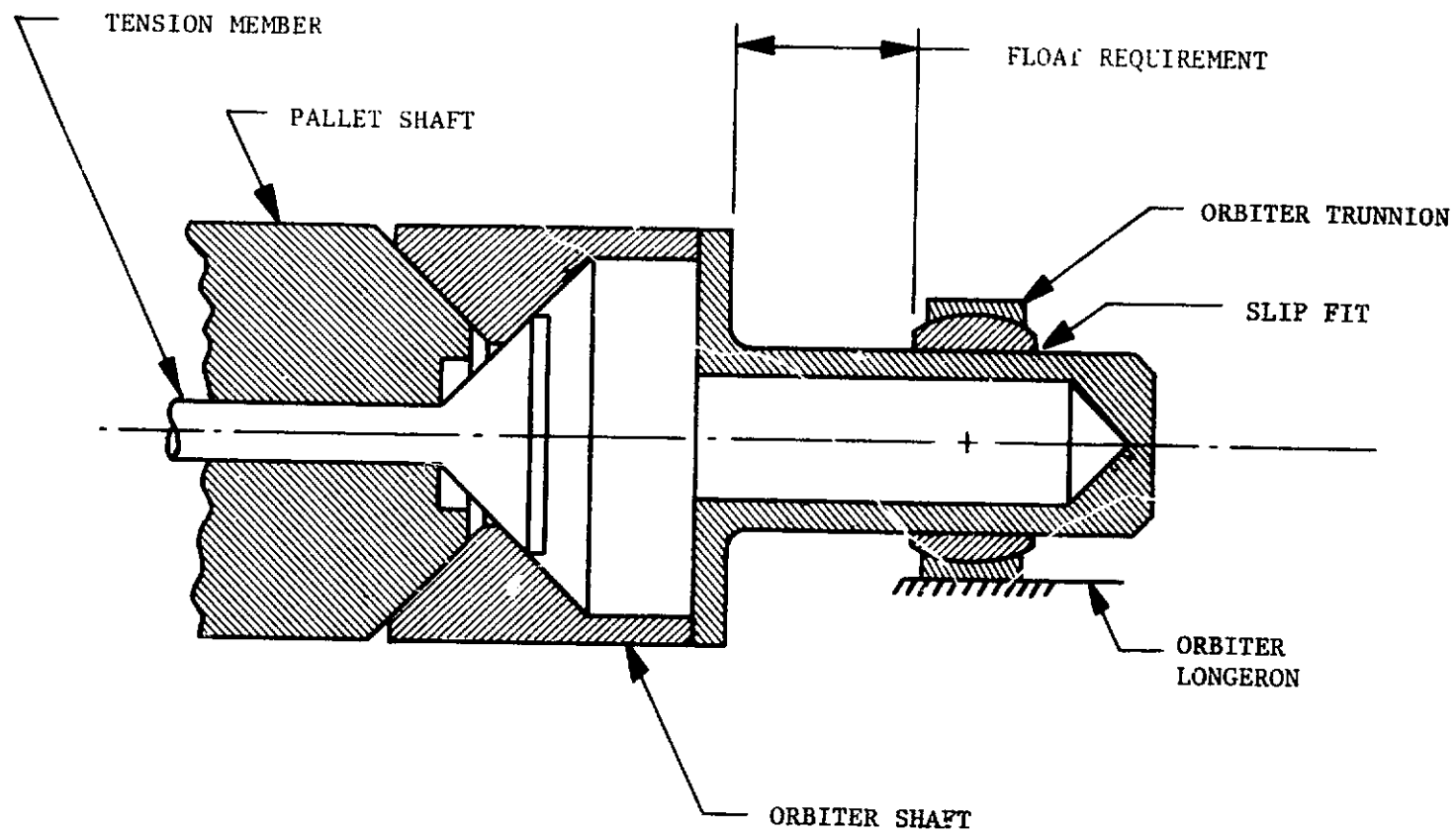


Figure 5-1. Locked Position

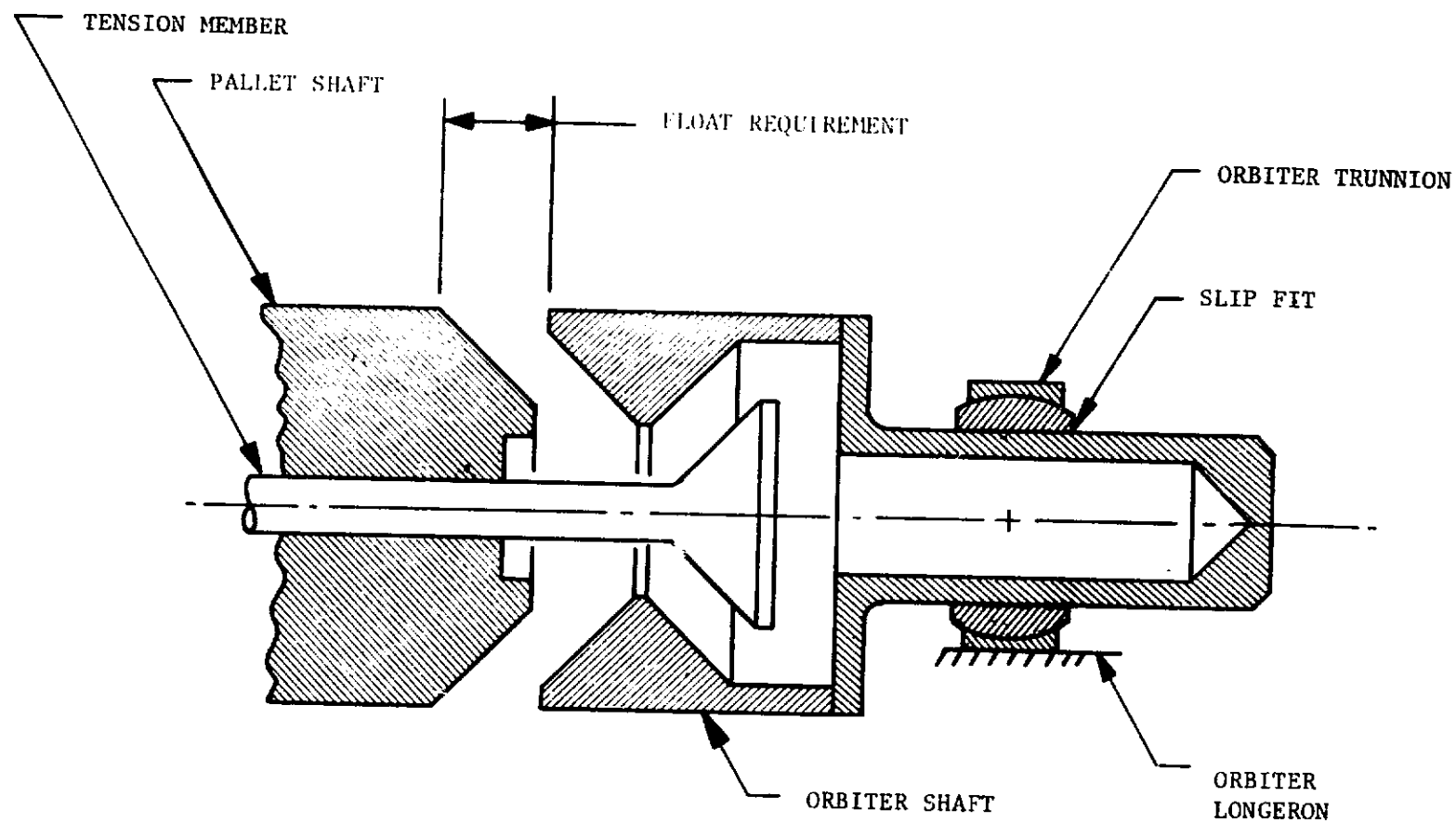


Figure 5-2. Unlocked Position

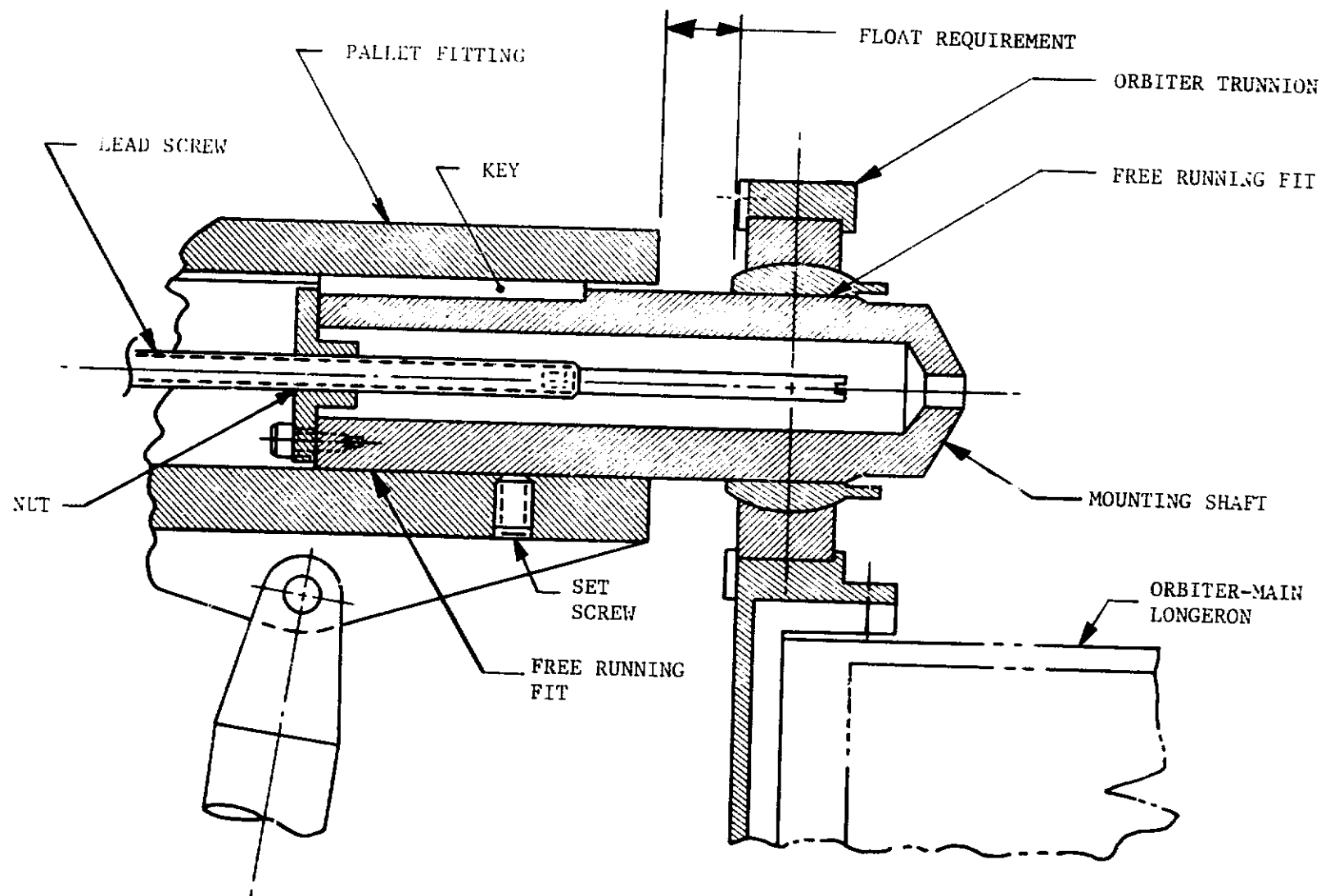


Figure 5-J. Cargo Bay Main Longeron Retention Point Mounting Shaft Extended Position

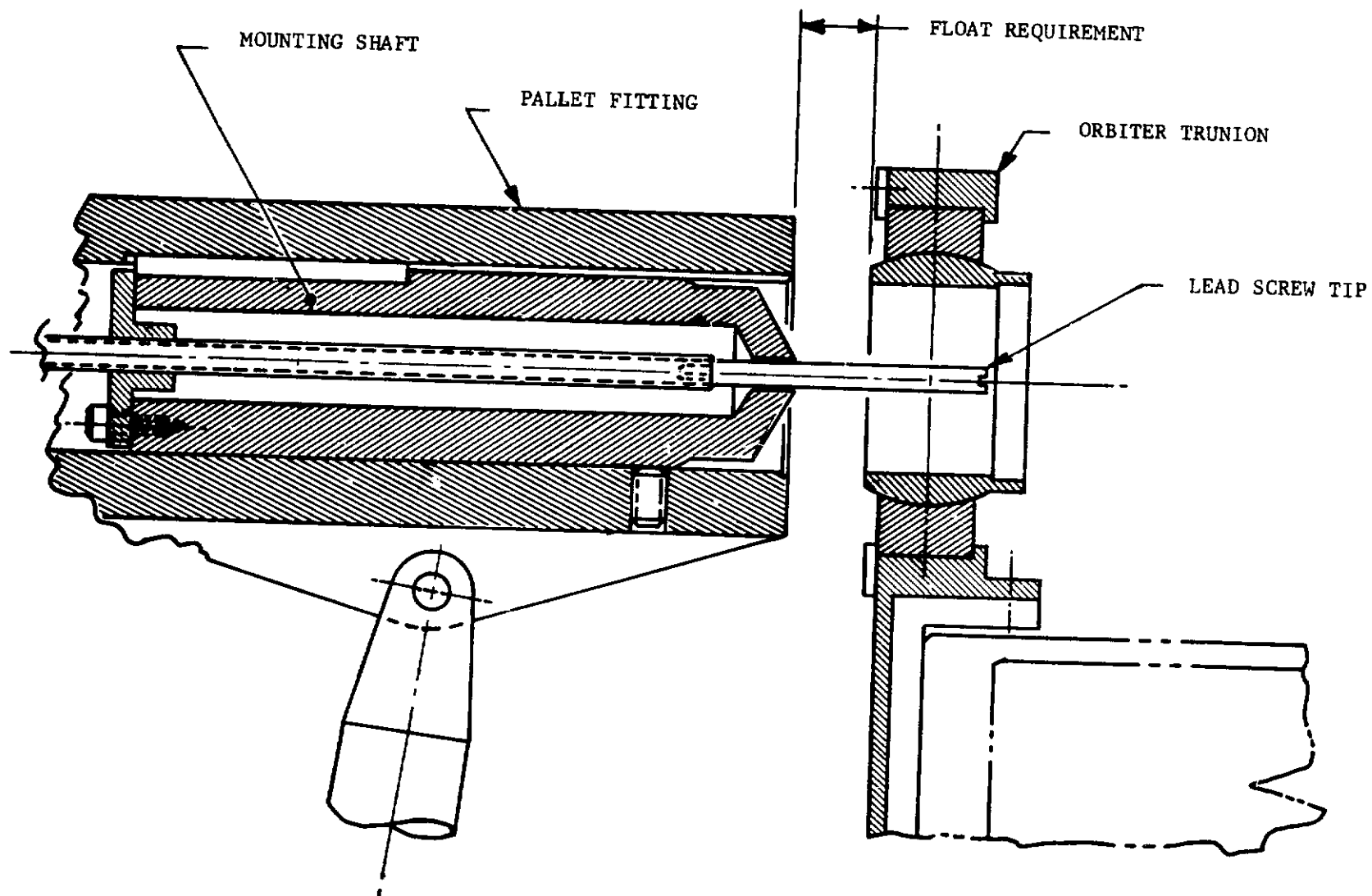


Figure 5-4. Cargo Bay Main Longeron Retention Point - Mounting Shaft Retracted Position



Retraction of the mounting shaft is accomplished by turning the lead screw with an actuator. As shown in figure 5-4 the lead screw tip remains inside the orbiter trunnion thus caging is achieved.

Extension of the mounting shaft is dependent upon engagement to the orbiter trunnion. Since the engagement sequence occurs in orbit, resistance will be from radial misalignment and the tendency of the orbiter trunnion spherical bushing to rotate. Forces necessary to overcome radial misalignment can be expected to be small compared to launch loads. The rotational misalignment of the spherical bushing is overcome by the configuration of the mounting shaft tip. A typical engagement sequence is shown in figure 5-5. Maximum radial misalignment (caging) is controlled by the size of the lead screw tip and is not necessary for engagement. Maximum rotation of the spherical bushing is controlled by the outer race of the trunnion. Position I shows initial contact of the shaft to the bushing at A. Extension of the shaft into the bushing continues along A and contact B is made as shown in position II. Contact at B causes the bushing to rotate until contact at C is made as shown in position III. The shaft lead diameter and lead length is determined at this position to assure a gap D. The spherical bushing is now centered about the shaft allowing further shaft extension as shown in position IV. The engagement sequence is completed when the shaft actuates a limit switch to stop the lead screw drive motor.

The mounting shaft drive mechanism is not critical to the integrity of the load reaction path from the pallet fitting through the mounting shaft into the orbiter trunnion. However, the lead screw must be locked to prevent the tendency to move the mounting shaft during launch or descent.

This arrangement would necessitate a new pallet fitting to house the mounting shaft and drive mechanism. However, since this system can be used for captive pallet missions as well as the floated pallet missions, a natural conclusion would be to incorporate the system on all pallet common modules.

The weight increase of this system over the existing system is estimated at 20 kg, based on the drive mechanism at 1 kg and the movable mounting shaft at 3 kg per retention point.

**5.4 Conclusion** - The movable mounting shaft arrangement maintains structural integrity of the retention system plus allows simple release and engagement in orbit. Incorporation of the system on all pallet common modules provides maximum usability without additional modifications for various missions.

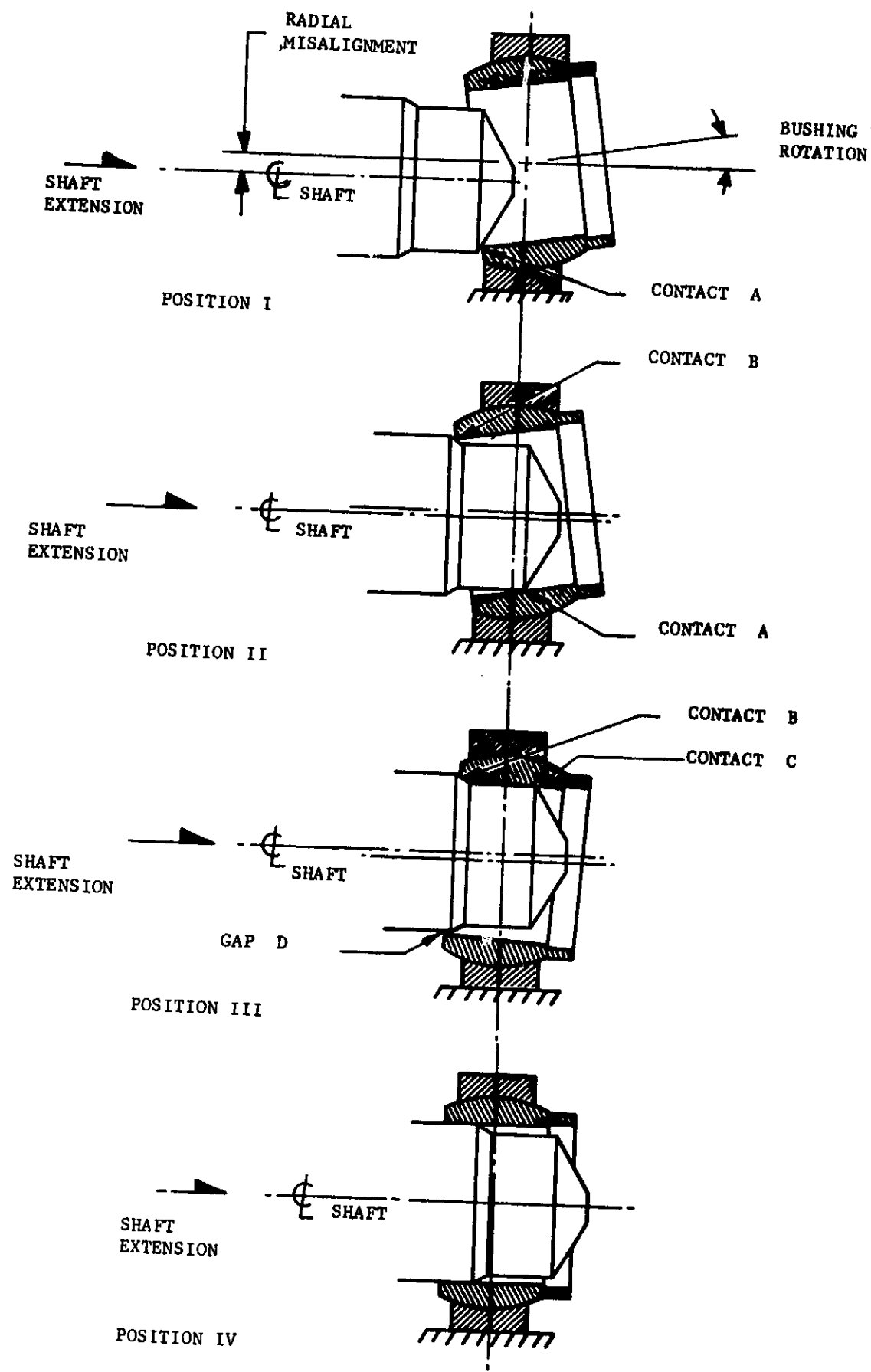


Figure 5-5. Engagement Sequence

## 6. CONTROL MOMENT GYROSCOPE (CMG) INSTALLATION

6.1 General - This section specifically deals with the installation of the four Bendix MA-2300 double gimbal CMGs to the pallet structure. The CMGs were selected as a result of the control system study performed in volume II.

6.2 Summary - Installation arrangements of the CMGs investigated included mounting two CMGs to a single support frame and mounting the four CMGs to a single support frame. The four CMGs on a single support frame was selected as the arrangement which provides the stiffest structural interface between the CMG cluster and the pallet.

### 6.3 Discussion

6.3.1 Design Objectives - The four CMGs shall be installed on the suspended pallet with the following considerations:

- a. Minimum structural modifications to the pallet.
- b. Each CMG shall be shock and vibration isolated with natural frequencies of approximately 20 Hz.
- c. Minimum structural modifications to the CMG attachment fittings.
- d. The installation shall be adaptable to various payload arrangements.

The existing CMG configuration is shown in figure 6-1. This configuration defines typical mounting hole patterns and locations with dimensions in inches.

6.3.2 Installation Study - The installation study performs analyses of these configurations:

6.3.4 Two support frames each containing two CMGs

6.3.5 One support frame containing four CMGs

One design objective is that the CMGs shall be isolated with natural frequencies of approximately 20 Hz. Since this objective is common to both configurations the isolation system is investigated in section 6.3.3.

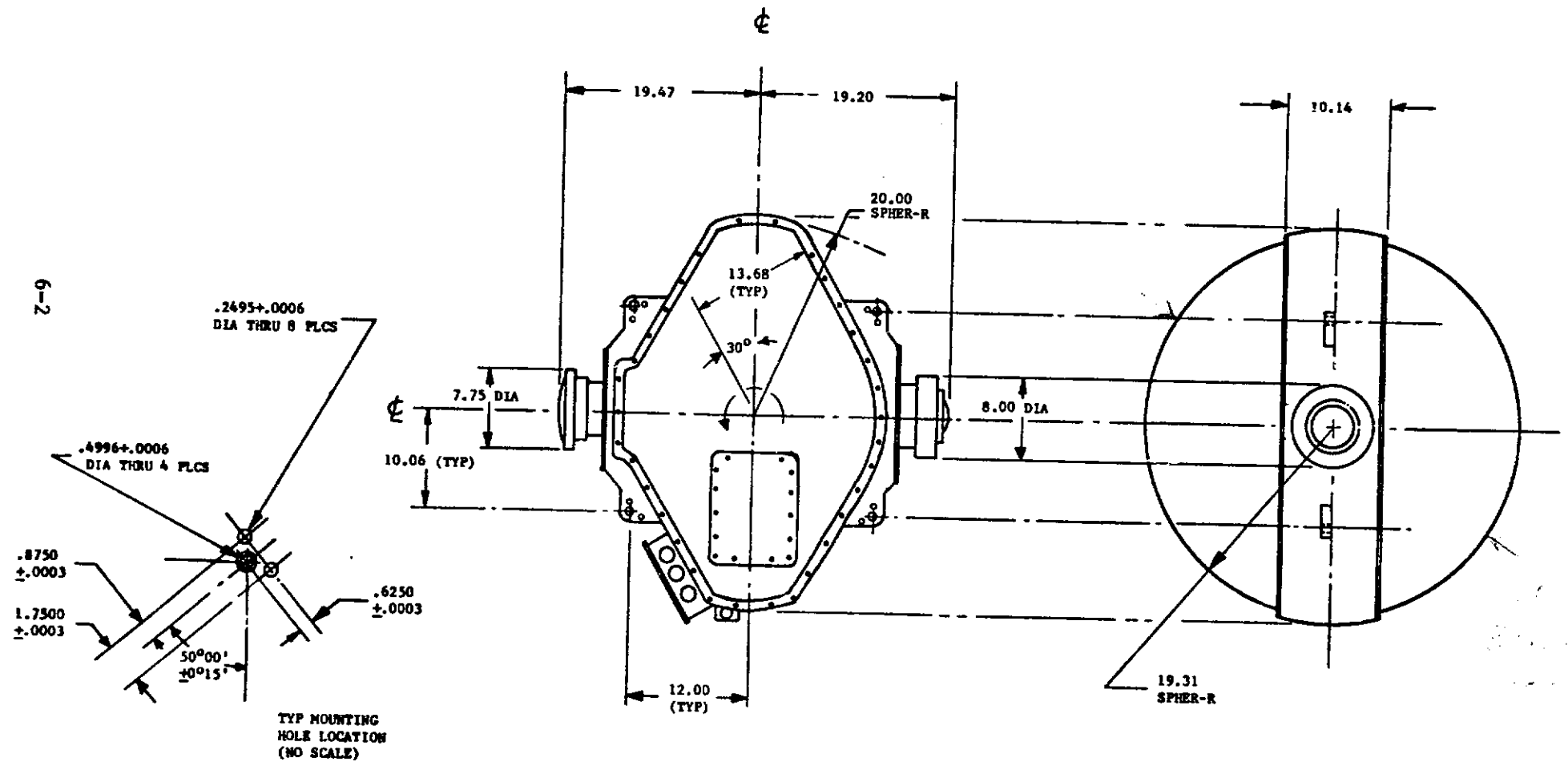


Figure 6-1. Bendix MA-2300 Double Gimbal Control Moment Gyroscope

The CMG is dimensioned and built to the American practice of units. The pallet is dimensioned and built to the metric units. No attempt is made at this time to define the CMG in the metric units. However, the actual design and fabrication of the support frame must address the conversion, particularly the CMG mounting holes and locations.

6.3.3 CMG Isolation System - The isolation requirements of 20 Hz indicates that off the shelf components are likely candidates. Barry Controls part number T94-AB-110 and Lord Corporation part number HTC-110 are military quality elastomer all-attitude mounts which meet the requirements. Also both mounts are physically interchangeable with nearly identical performance. Therefore a reasonable conclusion is to use the physical dimensions of these mounts and reserve final selection until procurement is required.

Adaption of the mounts to the CMG requires machine fittings due to the isolation float required and the CMG mounting fitting configurations. The design of the adapter fittings is straightforward and can be configured with the design of the support frame. The adapter fittings can also be bolted to the CMG so that no modification of existing CMGs is required until assembly to the support frame is made.

6.3.4 Support Frame With Two CMGs - The approach to the frame design is based on welded aluminum tubing with appropriate machined aluminum fittings. The configuration as shown in figure 6-2 shows the design parameters of pallet hard point locations, the isolator mounts and the isolator adapter fittings. The frame also supports the CMG electronics package as shown.

The weight of this frame is estimated at 45 kg, based on 5 cm square aluminum tubing with machined aluminum interface fittings.

Integration of this support frame utilizes the pallet hard points and does not require modification of the pallet structure.

This support frame can be located on the pallet according to the hard point pattern, giving maximum flexibility to experiment payload arrangements.

6.3.5 Support Frame With Four CMGs - The approach to the frame design is based on welded aluminum tubing with appropriate machined fittings. The configuration as shown in figure 6-3 shows the design parameters of pallet hard point locations, the isolator mounts and the isolator adapter fittings. The frame also supports the CMG electronic packages.

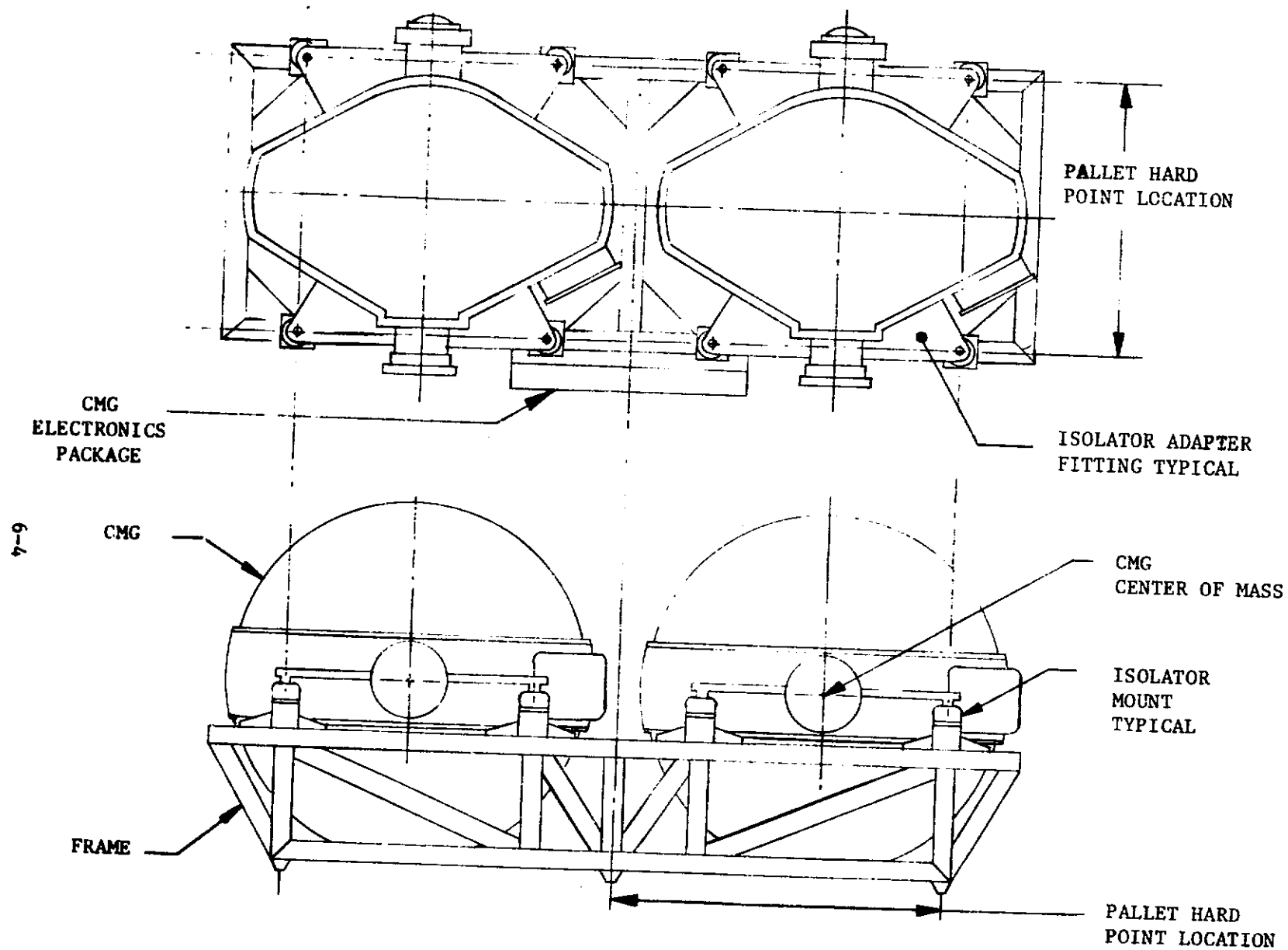


Figure 6-2. Support Frame With Two CMGs

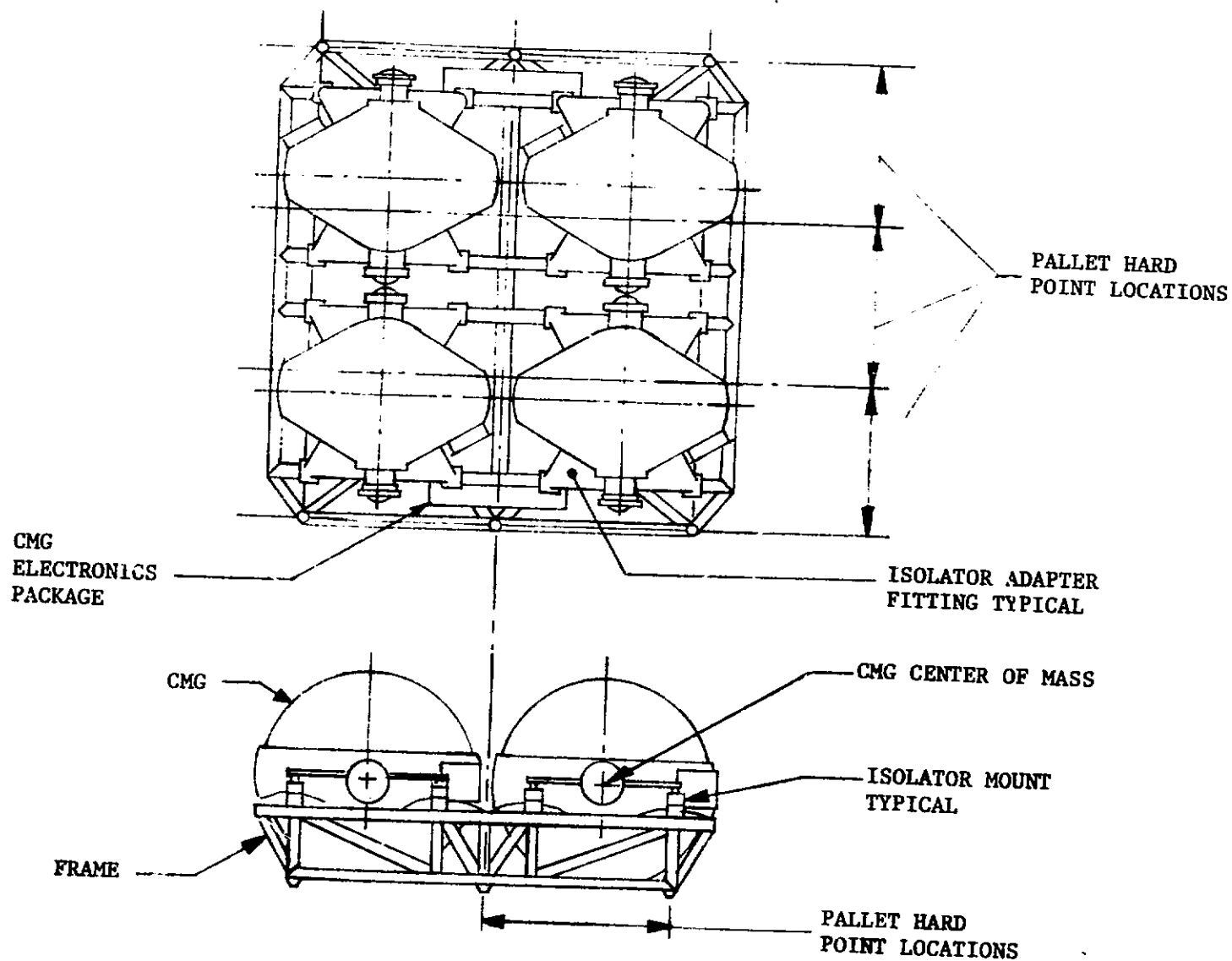


Figure 6-3. Support Frame With Four CMGs

The weight of this frame is estimated at 90 kg, based on 5 cm square aluminum tubing with machined aluminum interface fittings.

Integration of this support frame utilizes the pallet hard points and does not require modification of the pallet structure.

This support frame should be located on a single pallet. The tolerances associated with joining pallet segments together would present integration problems of locating this frame across the joint; further, control of the suspended pallet might be comprised if this frame were attached to two pallet segments. Therefore only three locations of this frame are available on a three segment pallet.

6.3.6 Installation - Since both CMG support frames are considered feasible, they are shown installed to the pallet in figure 8-1 and figure 8-4 of section 8. Actual pallet attachment is with threaded fasteners through the support frame base fittings into the standard hard point spherical nuts.

6.4 Conclusion - The single support frame containing the four CMGs is selected as the arrangement which provides the stiffest structural interface between the CMG cluster and the pallet. The design of the frame is that of conventional truss/frame designs.



## 7. EXPERIMENT MOUNT AND ERECTION

7.1 General - This section specifies the support frames for the specified Inside Out Gimbal System (IOG) and an alternative classical gimbal system for experiment pointing and defines alignment limits and gimbal motion thresholds for the experiment mounting system.

7.2 Summary - Two problems are treated in this section for each of the mounting arrangements, the first to determine the line of sight error due to gimbal and mount inaccuracies, the second to determine gimbal motions required to move the line of sight vector an arbitrary amount.

### 7.3 Experiment Base Mount Installation

7.3.1 Support Frame - The design of the support frame is that of conventional truss/frame designs. The two configurations, as shown in figure 7-1, clearly show the design parameters of pallet hard point locations, frame height, mount/frame interface. Experiment launch restraints are not shown since a restraint system would be unique to a particular experiment. The restraint system would consist of forward and aft supports. The aft support would interface with the experiment base plate and the frame. The forward support would interface with the experiment and the pallet hard points.

7.3.2 Installation - Frame attachment to the pallet is with threaded fasteners through the frame base fittings into the standard hard point spherical nuts. Alignment of the experiment/mount to the pallet reference system would require an adjustable interface between the mount and the frame; this can be achieved with the use of shims.

7.4 Line of Sight Errors Due to Mounting Misalignments - In general the ideal pointing of any instrument can only be approached due to various misalignments and inaccuracies in the mounting system. For an instrument with moderate power and resolution this would probably cause no difficulty, however, with an increase in magnification, the angular field of view decreases and it becomes important to examine the error in the line of sight due to physical inaccuracies. This would become extremely critical for limiting cases where faint objects are to be acquired and examined. In such cases the object should be near the center of the field of view to avoid vignetting and fine adjustments might be required to bring the line of sight back to the target point. A limiting line of sight error can be loosely defined as no greater than the minimum instrument field of view to insure that after gimbal action is commanded, that the target object is in the viewing field and can be brought near the optical axis by fine adjustment as required.

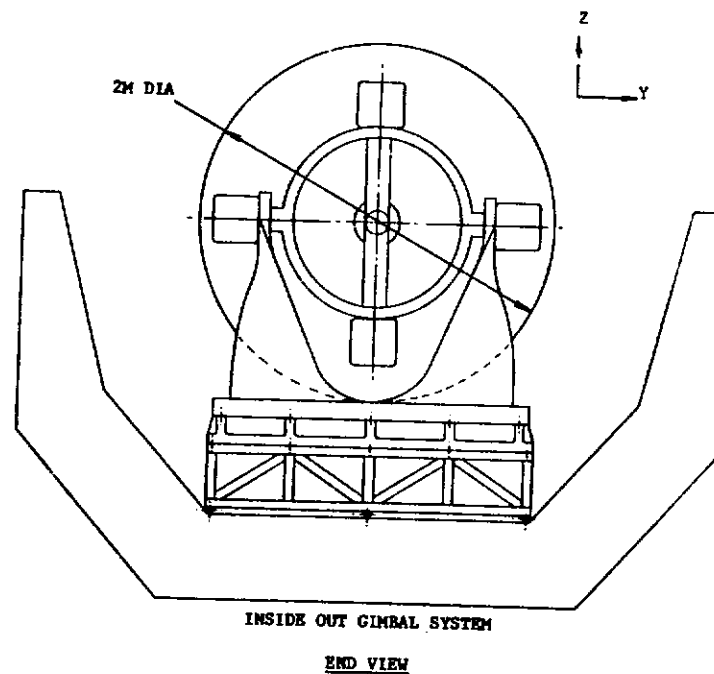
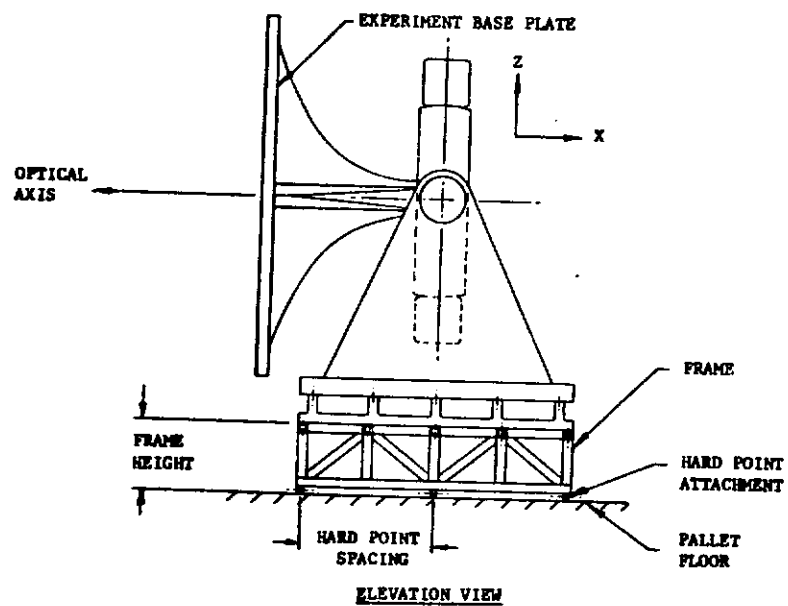
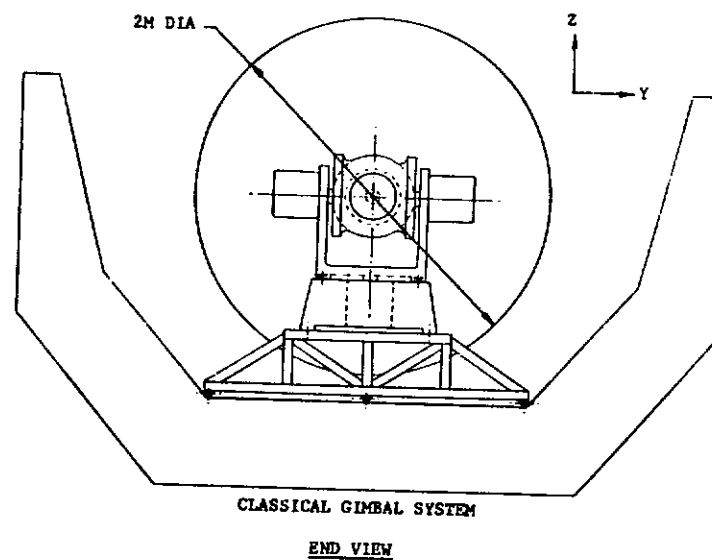
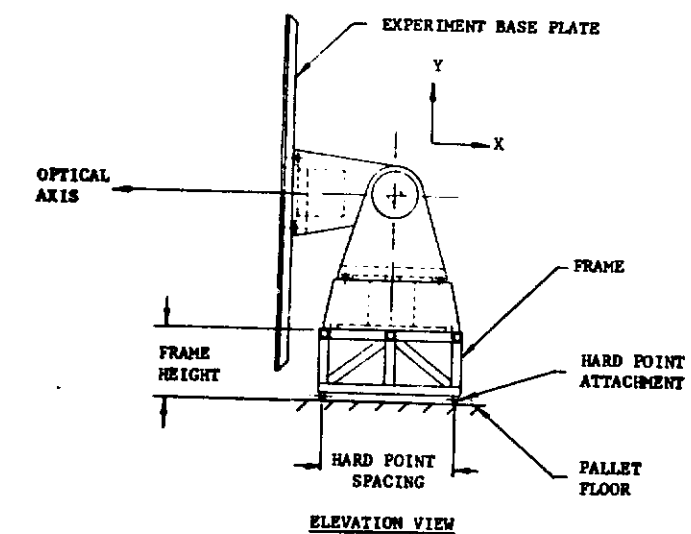


Figure 7-1. Experiment Base Mount Installation

The physical inaccuracies in the systems will be described by means of small angle transformations between the base and outer gimbal pivot, between the outer gimbal and inner gimbal pivot and between the inner gimbal and the instrument.

**7.4.1 Error Propagation for the Inside Out Gimbal System (IOG) -**  
The IOG system is shown in figure 7-2 with the mounting base in a stowed or launch position. For the purposes of this discussion it will be assumed that the zero gimbal angle state will occur when the optical axis is directed out along the pallet Z axis. The "P" (pointed) coordinate system is fixed in the base plate with the  $Z_p$  axis coinciding with the optical axis, the  $X_p$  axis along the ideal inner gimbal axis and the  $Y_p$  axis completing the triad. The "B" (base) system is a fixed reference system aligned with the pallet axes. The "P" and "B" systems coincide for zero gimbal angles with the  $Y_b$  axis being the ideal outer gimbal axis.

The relation between the ideal P and B axis systems is shown in figure 7-2, and is defined by an outer gimbal rotation  $\theta$  about the  $Y_b$  axis followed by an inner gimbal rotation  $\phi$  about the  $X_p$  axis. The transformations corresponding are:

$$\text{About } Y_b \text{ by } \theta: \quad [{}_I T_B] = \begin{bmatrix} \cos\theta & 0 & -\sin\theta \\ 0 & 1 & 0 \\ \sin\theta & 0 & \cos\theta \end{bmatrix}$$

$$\text{About } X_p \text{ by } \phi: \quad [{}_P T_I] = \begin{bmatrix} 1 & 0 & 0 \\ 0 & \cos\phi & \sin\phi \\ 0 & -\sin\phi & \cos\phi \end{bmatrix}$$

The unit vector along the optical axis in P coordinates is simply:

$$\hat{\rho}_p = (0, 0, 1)^T$$

Transforming to B space this becomes:

$$\hat{\rho}_b = [{}_B T_I][{}_I T_P]\hat{\rho}_p = \begin{bmatrix} \sin\theta\cos\phi \\ -\sin\phi \\ \cos\theta\cos\phi \end{bmatrix}$$

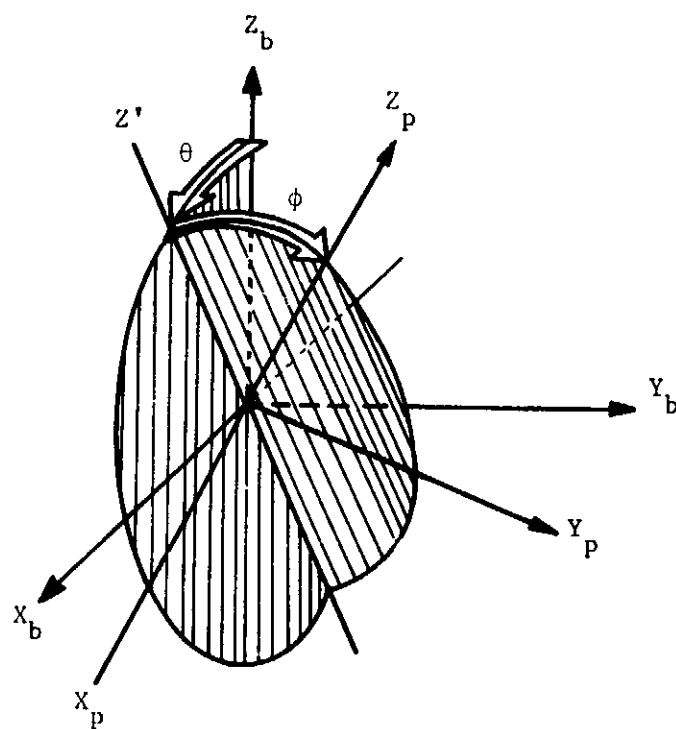


Figure 7-2. Relation of the Ideal Pointed Coordinates to the Base Coordinates For the Inside Out Gimbal

If the coordinates of a target on the celestial sphere are known in the base coordinate system, the ideal gimbal angles  $\theta$  and  $\phi$  required to direct the instrument can be calculated from the equation for  $\hat{\rho}_b$ . Alternatively, given gimbal angles  $\theta$  and  $\phi$  and an ideal gimbal system, the line of sight will be directed along  $\hat{\rho}_b$ .

In order to evaluate the effect of inaccuracies in the physical system, small angle transformations representing the various error possibilities will be added to the ideal transformation. Working from the base inward to the line of sight, the following transformation will be defined. The transformation from the base to the outer gimbal pivot space will be:

$$[{}_0T_B] = \begin{bmatrix} 1 & \epsilon_{zo} & -\epsilon_{yo} \\ -\epsilon_{zo} & 1 & \epsilon_{xo} \\ \epsilon_{yo} & -\epsilon_{xo} & 1 \end{bmatrix}$$

where the angles  $\epsilon_{xo}$  and  $\epsilon_{zo}$  represent the misalignments in the outer gimbal axis and  $\epsilon_{yo}$  is the error in the zero point of the outer gimbal. The transformation for the outer gimbal rotation  $\theta$  remains the same as before and will be designated as:

$$[{}_0T_O] \equiv [{}_IT_B]$$

The transformation from the outer gimbal to the inner gimbal pivot is:

$$[{}_IT_O] = \begin{bmatrix} 1 & \epsilon_{zi} & -\epsilon_{yi} \\ -\epsilon_{zi} & 1 & \epsilon_{xi} \\ \epsilon_{yi} & -\epsilon_{xi} & 1 \end{bmatrix}$$

where  $\epsilon_{zi}$  represents the nonorthogonality of the inner and outer gimbal axes,  $\epsilon_{xi}$  is the error in the zero point of the inner gimbal axis and  $\epsilon_{yi}$  represents an additional bias on the zero point of the outer gimbal. The transformation for the inner gimbal rotation  $\phi$  is the same as given earlier:

$$[I, T_I] \equiv [P^T I]$$

The transformation from the inner gimbal to the optical axis is:

$$[P^T I] = \begin{bmatrix} 1 & \epsilon_{zp} & -\epsilon_{yp} \\ -\epsilon_{zp} & 1 & \epsilon_{xp} \\ \epsilon_{yp} & -\epsilon_{xp} & 1 \end{bmatrix}$$

where  $\epsilon_{yp}$  is the nonorthogonality of the optical and inner gimbal axes,  $\epsilon_{xp}$  is an additional bias on the inner gimbal zero point and  $\epsilon_{zp}$  represents a rotation about the optical axis which will have no effect on the line of sight error. The actual unit vector along the line of sight expressed in base coordinates after arbitrary gimbal motions  $\theta$  and  $\phi$  is thus:

$$\hat{\rho}_a = [B^T O][O^T O][O^T I][I^T I][I^T P]\hat{\rho}_p$$

where as before the transformation with reversed indices represents the inverse of the direct transformation. The total error in the line of sight can be defined by a vector  $\vec{\epsilon} = \hat{\rho}_a - \hat{\rho}_b$ , the difference between the actual and desired lines of sight. The total angular error  $\epsilon$  is thus just the absolute value of  $\vec{\epsilon}$ . Expanding the above equation neglecting products of the  $\epsilon_{ij}$ :

$$\hat{\rho}_a = \begin{bmatrix} \sin\theta\cos\phi - (\epsilon_{xi} + \epsilon_{xp})\sin\theta\sin\phi + (\epsilon_{yi} + \epsilon_{yo})\cos\theta\cos\phi + (\epsilon_{zi}\sin\phi + \epsilon_{yp})\cos\theta + \epsilon_{zo}\sin\phi \\ -\sin\phi - (\epsilon_{xi} + \epsilon_{xp})\cos\phi + (\epsilon_{zo}\sin\theta - \epsilon_{xo}\cos\theta)\cos\phi \\ \cos\theta\cos\phi - (\epsilon_{xi} + \epsilon_{xp})\cos\theta\sin\phi - (\epsilon_{yi} + \epsilon_{yo})\sin\theta\cos\phi - (\epsilon_{zi}\sin\phi + \epsilon_{yp})\sin\theta - \epsilon_{xo}\sin\phi \end{bmatrix}$$

Note that as expected  $\epsilon_{zp}$  does not appear in  $\hat{\rho}_a$ , and further that the errors in definition of the zero gimbal angles  $\epsilon_{yi}, \epsilon_{yo}$  and  $\epsilon_{xi}, \epsilon_{xp}$  occur in pairs as would be expected. Defining the total zero gimbal angle offsets, using the subscript o for outer and i for inner:

$$\zeta_o \triangleq \epsilon_{yo} + \epsilon_{yi}$$

$$\zeta_i \triangleq \epsilon_{xi} + \epsilon_{xp}$$

The error vector  $\vec{\epsilon}$  can then be written as:

$$\begin{aligned} \vec{\epsilon} = & \begin{bmatrix} \epsilon_{zo} \sin \phi \\ (\epsilon_{zo} \cos \theta - \epsilon_{xo} \sin \theta) \cos \phi \\ -\epsilon_{xo} \sin \phi \end{bmatrix} + \begin{bmatrix} \zeta_o \cos \theta \cos \phi \\ 0 \\ -\zeta_o \sin \theta \cos \phi \end{bmatrix} + \begin{bmatrix} \epsilon_{zi} \cos \theta \sin \phi \\ 0 \\ -\epsilon_{zi} \sin \theta \sin \phi \end{bmatrix} \\ & + \begin{bmatrix} -\zeta_i \sin \theta \sin \phi \\ -\zeta_i \cos \phi \\ -\zeta_i \cos \theta \sin \phi \end{bmatrix} + \begin{bmatrix} \epsilon_{yp} \cos \theta \\ 0 \\ -\epsilon_{yp} \sin \theta \end{bmatrix} \end{aligned}$$

where the explicit vector components represent respectively the errors in line of sight due to outer gimbal axis misalignment with respect to the base  $\vec{m}_o$ , outer gimbal zero point error  $\vec{z}_o$ , outer gimbal/inner gimbal axis nonorthogonality  $\vec{n}_o$ , inner gimbal zero point error  $\vec{z}_i$  and inner gimbal/optical axis nonorthogonality  $\vec{n}_i$ . The magnitudes of these vectors represent the line of sight error due to each effect:

$$\begin{aligned} m_o = |\vec{m}_o| &= [(\epsilon_{xo}^2 + \epsilon_{zo}^2) \sin^2 \phi + (\epsilon_{zo} \cos \theta - \epsilon_{xo} \sin \theta)^2 \cos^2 \phi]^{1/2} \\ &= [\epsilon_{xo}^2 + \epsilon_{zo}^2 - (\epsilon_{zo} \sin \theta + \epsilon_{xo} \cos \theta)^2 \cos^2 \phi]^{1/2} \leq \sqrt{\epsilon_{xo}^2 + \epsilon_{zo}^2} \end{aligned}$$

$$z_o = |\vec{z}_o| = |\zeta_o \cos \phi| \leq |\zeta_o|$$

$$n_o = |\vec{n}_o| = |\epsilon_{zi} \sin \phi| \leq |\epsilon_{zi}|$$

$$z_i = |\vec{z}_i| = |\zeta_i|$$

$$n_i = |\vec{n}_i| = |\epsilon_{yp}|$$

The total error  $\epsilon$  is not so easily bounded, however, since it involves taking the root of the sum of the squares of the components of the vector  $\vec{\epsilon} = \vec{m}_0 + \vec{z}_0 + \vec{n}_0 + \vec{z}_1 + \vec{n}_1$ , clearly a difficult task. The worst case conceivable is that each individual error vector is in the same direction and each attains its maximum, clearly an impossible situation upon examination of the equations, however, it leads to an absolute bound:

$$\epsilon < |\vec{m}_0| + |\vec{z}_0| + |\vec{n}_0| + |\vec{z}_1| + |\vec{n}_1|$$

or,

$$\epsilon < \sqrt{\epsilon_{x0}^2 + \epsilon_{z0}^2} + |\zeta_0| + |\epsilon_{zi}| + |\zeta_1| + |\epsilon_{yp}|$$

The pointing error can be bounded somewhat more closely by noting that  $\vec{n}_0$  and  $\vec{z}_0$  cannot attain their maximum simultaneously, in fact:

$$|\vec{n}_0| + |\vec{z}_0| = |\zeta_0 \cos \phi| + |\epsilon_{zi} \sin \phi| \leq \sqrt{\zeta_0^2 + \epsilon_{zi}^2}$$

or,

$$\epsilon < \sqrt{\epsilon_{x0}^2 + \epsilon_{y0}^2} + \sqrt{\zeta_0^2 + \epsilon_{zi}^2} + |\zeta_1| + |\epsilon_{yp}|$$

Thus, the pointing error for the IOG can be bounded by the sum of the root-sum-square of outer gimbal axis misalignments with respect to the base, the root-sum-square of the outer gimbal/inner gimbal axis nonorthogonality and the outer gimbal zero offset, the inner gimbal zero offset and the inner gimbal/optical axis nonorthogonality.

**7.4.2 Error Propagation for the Classical Gimbal System** - Figure 7-1 shows the geometry for the classical gimbal system again with the mounting base in the stowed position. As before the zero gimbal angle state will occur when the optical axis and pallet Z axis are aligned. The "p" (pointed) coordinate system is fixed within the instrument with the  $Z_p$  axis directed out along the instrument line of sight. The  $Y_p$  axis is the ideal inner gimbal axis and the  $X_p$  axis completes the triad. The B (base) system is a fixed reference system with which the "p" system is aligned for zero gimbal angles. The  $Z_b$  axis is the ideal outer gimbal axis.



The relation between the P and B systems is shown in figure 7-3 and consists of the outer gimbal rotation  $\alpha$  about the  $Z_b$  axis followed by the inner gimbal rotation  $\beta$  about the  $Y_p$  axis to direct the  $Z_p$  axis toward the desired target point. The corresponding transformations are thus:

$$\text{About } Z_b \text{ by } \alpha: \quad [I^T_B] = \begin{bmatrix} \cos\alpha & \sin\alpha & 0 \\ -\sin\alpha & \cos\alpha & 0 \\ 0 & 0 & 1 \end{bmatrix}$$

$$\text{About } Y_i \text{ by } \beta: \quad [P^T_I] = \begin{bmatrix} \cos\beta & 0 & -\sin\beta \\ 0 & 1 & 0 \\ \sin\beta & 0 & \cos\beta \end{bmatrix}$$

The unit vector along the line of sight of the instrument will be designated as  $\hat{\rho}$  with the component in P coordinates simply:

$$\hat{\rho}_p = (0, 0, 1)^T$$

In the base space,

$$\hat{\rho}_b = [B^T_I][I^T_P]\hat{\rho}_p$$

where the transformation with reversed indices indicates the inverse (transpose) of the direct transformation. Explicitly:

$$\hat{\rho}_b = \begin{bmatrix} \cos\alpha \sin\beta \\ \sin\alpha \sin\beta \\ \cos\beta \end{bmatrix}$$

If the coordinates of a desired pointing target on the celestial sphere are known in the base coordinate system, the gimbal angles  $\alpha$  and  $\beta$  required to point the instrument can readily be calculated. Alternatively given gimbal angles  $\alpha$  and  $\beta$ , the instrument line of sight will be directed along the vector  $\hat{\rho}_b$  in the ideal case.

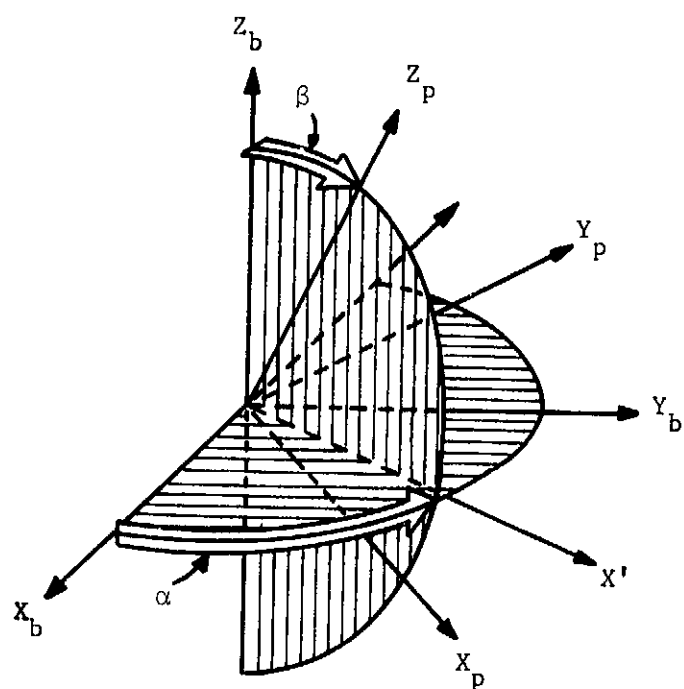


Figure 7-3. Relation of the Ideal Pointed Coordinates to the Base Coordinates For the Classical Gimbal Arrangement

The physical inaccuracies in the system will be described by means of small angle transformations between the base and outer gimbal pivot, between the outer gimbal and inner gimbal pivot and between the inner gimbal and the instrument. Working from the base inward to the line of sight, the transformation from the base to the outer gimbal pivot space will be:

$$[{}_0T_B] = \begin{bmatrix} 1 & \epsilon_{zo} & -\epsilon_{yo} \\ -\epsilon_{zo} & 1 & \epsilon_{xo} \\ \epsilon_{yo} & -\epsilon_{xo} & 1 \end{bmatrix}$$

where the angles  $\epsilon_{xo}$  and  $\epsilon_{yo}$  represent the misalignments in the outer gimbal axis and  $\epsilon_{zo}$  is the error in the zero point of the outer gimbal. The transformation for the outer gimbal rotation  $\alpha$  remains the same as before and will be designated as:

$$[{}_0T_O] = \begin{bmatrix} \cos\alpha & \sin\alpha & 0 \\ -\sin\alpha & \cos\alpha & 0 \\ 0 & 0 & 1 \end{bmatrix}$$

The transformation from the outer gimbal to the inner gimbal pivot is:

$$[{}_IT_O] = \begin{bmatrix} 1 & \epsilon_{zi} & -\epsilon_{yi} \\ -\epsilon_{zi} & 1 & \epsilon_{xi} \\ \epsilon_{yi} & -\epsilon_{xi} & 1 \end{bmatrix}$$

where  $\epsilon_{xi}$  represents the nonorthogonality of the inner and outer gimbal axes,  $\epsilon_{yi}$  is the error in the zero point of the inner gimbal axis and  $\epsilon_{zi}$  represents an additional bias on the zero point of the outer gimbal. The transformation for the inner gimbal rotation  $\beta$  remains:

$$[{}_IT_I] = \begin{bmatrix} \cos\beta & 0 & -\sin\beta \\ 0 & 1 & 0 \\ \sin\beta & 0 & \cos\beta \end{bmatrix}$$

The transformation from the inner gimbal to the instrument is:

$$[P^T_I] = \begin{bmatrix} 1 & \epsilon_{zp} & -\epsilon_{yp} \\ -\epsilon_{zp} & 1 & \epsilon_{xp} \\ \epsilon_{yp} & -\epsilon_{xp} & 1 \end{bmatrix}$$

where  $\epsilon_{xp}$  is the nonorthogonality of the optical and inner gimbal axes,  $\epsilon_{yp}$  is an additional bias on the inner gimbal zero point and  $\epsilon_{zp}$  represents a rotation about the optical axis which will have no effect on the line of sight error. The actual unit vector along the line of sight expressed in base coordinates after arbitrary gimbal motions  $\alpha$  and  $\beta$  is thus:

$$\hat{\rho}_a = [B^T_O][O^T_O][O^T_I][I^T_I][I^T_P]\vec{u}$$

where as before the transformation with reversed indices represents the inverse of the direct transformation. The total error in the line of sight can be defined by a vector  $\vec{\epsilon} = \hat{\rho}_a - \hat{\rho}_b$ , the difference between the actual and desired lines of sight. The total angular error  $\epsilon$  is thus just the absolute value of  $\vec{\epsilon}$ . Expanding the above equation neglecting products of the  $\epsilon_{ij}$ :

$$\hat{\rho}_a = \begin{bmatrix} \cos\alpha\sin\beta + (\epsilon_{yi} + \epsilon_{yp})\cos\alpha\cos\beta - (\epsilon_{zo} + \epsilon_{zi})\sin\alpha\sin\beta + (\epsilon_{xi}\cos\beta + \epsilon_{xp})\sin\alpha + \epsilon_{yo}\cos\beta \\ \sin\alpha\sin\beta + (\epsilon_{yi} + \epsilon_{yp})\sin\alpha\cos\beta + (\epsilon_{zo} + \epsilon_{zi})\cos\alpha\sin\beta - (\epsilon_{xi}\cos\beta + \epsilon_{xp})\cos\alpha - \epsilon_{xo}\cos\beta \\ \cos\beta - (\epsilon_{yi} + \epsilon_{yp})\sin\beta + (\epsilon_{xo}\sin\alpha - \epsilon_{yo}\cos\alpha)\sin\beta \end{bmatrix}$$

Note that as expected  $\epsilon_{zp}$  does not appear in  $\hat{\rho}_a$  and further that the zero point errors  $\epsilon_{yi}, \epsilon_{yp}$  and  $\epsilon_{zo}, \epsilon_{zi}$  appear only in pairs, thus define:

$$\zeta_o \triangleq \epsilon_{zo} + \epsilon_{zi}$$

$$\zeta_i \triangleq \epsilon_{yi} + \epsilon_{yp}$$

where  $\zeta_o$  is the total zero point error in the outer gimbal and  $\zeta_i$  is that for the inner gimbal. Thus,

$$\begin{aligned} \hat{\rho}_a = \hat{\rho}_b + & \begin{bmatrix} \epsilon_{yo} \cos \beta \\ -\epsilon_{xo} \sin \beta \\ (\epsilon_{xo} \sin \alpha - \epsilon_{yo} \cos \alpha) \sin \beta \end{bmatrix} + \begin{bmatrix} -\zeta_o \sin \beta \sin \alpha \\ \zeta_o \sin \beta \cos \alpha \\ 0 \end{bmatrix} + \begin{bmatrix} \epsilon_{xi} \cos \beta \sin \alpha \\ -\epsilon_{xi} \cos \beta \cos \alpha \\ 0 \end{bmatrix} \\ & + \begin{bmatrix} \zeta_i \cos \alpha \cos \beta \\ \zeta_i \sin \alpha \cos \beta \\ -\zeta_i \sin \beta \end{bmatrix} + \begin{bmatrix} \epsilon_{xp} \sin \alpha \\ -\epsilon_{xp} \cos \alpha \\ 0 \end{bmatrix} \end{aligned}$$

where the explicit vector components represent respectively the errors in line of sight due to outer gimbal axis misalignment with respect to the base  $\vec{m}_o$ , outer gimbal zero point error  $\vec{z}_o$ , outer gimbal/inner gimbal axis nonorthogonality  $\vec{n}_o$ , inner gimbal zero point error  $\vec{z}_i$  and inner gimbal/optical axis nonorthogonality  $\vec{n}_i$ . The magnitudes of these vectors represent the line of sight error due to each effect:

$$\begin{aligned} m_o = |\vec{m}_o| &= [(\epsilon_{yo}^2 + \epsilon_{xo}^2) \cos^2 \beta + (\epsilon_{xo} \sin \alpha - \epsilon_{yo} \cos \alpha)^2 \sin^2 \beta]^{1/2} \\ &= [\epsilon_{xo}^2 + \epsilon_{yo}^2 - (\epsilon_{xo} \cos \alpha + \epsilon_{yo} \sin \alpha)^2 \sin^2 \beta]^{1/2} \leq \sqrt{\epsilon_{xo}^2 + \epsilon_{yo}^2} \\ z_o = |\vec{z}_o| &= |\zeta_o \sin \beta| \leq |\zeta_o| \\ n_o = |\vec{n}_o| &= |\epsilon_{xi} \cos \beta| \leq |\epsilon_{xi}| \\ z_i = |\vec{z}_i| &= |\zeta_i| \\ n_i = |\vec{n}_i| &= |\epsilon_{xp}| \end{aligned}$$

The total error  $\epsilon$  is not so easily bounded, however, since it involves taking the root of the sum of the squares of the components of the vector  $\vec{\epsilon} = \vec{m}_o + \vec{z}_o + \vec{n}_o + \vec{z}_i + \vec{n}_i$ , clearly a difficult task. The worst case conceivable is that each individual error vector is in the same direction

and each attains its maximum, clearly an impossible situation upon examination of the equations, however, it leads to an absolute bound:

$$\epsilon < |\vec{m}_0| + |\vec{z}_0| + |\vec{n}_0| + |\vec{z}_1| + |\vec{n}_1|$$

or,

$$\epsilon < \sqrt{\epsilon_{x0}^2 + \epsilon_{y0}^2} + |\zeta_0| + |\epsilon_{x1}| + |\zeta_1| + |\epsilon_{xp}|$$

The pointing error can, however, be bounded somewhat more closely by noting that  $\vec{n}_0$  and  $\vec{z}_0$  cannot attain their maxima simultaneously, in fact:

$$|\vec{n}_0| + |\vec{z}_0| = |\zeta_0 \sin \beta| + |\epsilon_{x1} \cos \beta| \leq \sqrt{\zeta_0^2 + \epsilon_{x1}^2}$$

Thus, the line of sight error  $\epsilon$  can be bounded as follows:

$$\epsilon < \sqrt{\epsilon_{x0}^2 + \epsilon_{y0}^2} + \sqrt{\zeta_0^2 + \epsilon_{x1}^2} + |\zeta_1| + |\epsilon_{xp}|$$

**7.5 Gimbal Motions Required for an Arbitrary Line of Sight Adjustment** - Definition of the line of sight error caused by physical misalignments in the gimbal system immediately indicates that some fine pointing capability is required to bring the desired target point into alignment with the optical axis. Regardless of the implementation of the fine pointing control, the magnitude of gimbal motion required to move the optical axis by a small amount to center a target is an item of interest.

The gimbal motions required for an arbitrary change in the line of sight can be determined quite generally by considering the locus of all possible unit vectors  $\hat{\rho}_0$  making an angle  $\epsilon$  with an arbitrary line of sight vector  $\rho$ . In P coordinates this locus can be expressed in terms of a parameter  $\gamma$  which is merely the ccw rotation of the  $\hat{\rho}_0$  vector away from the  $X_Z$  plane as shown in figure 7-4. In P coordinates the general offset vector is thus:

$$\hat{\rho}_{op} = \begin{bmatrix} \sin \epsilon \cos \gamma \\ \sin \epsilon \sin \gamma \\ \cos \epsilon \end{bmatrix}$$

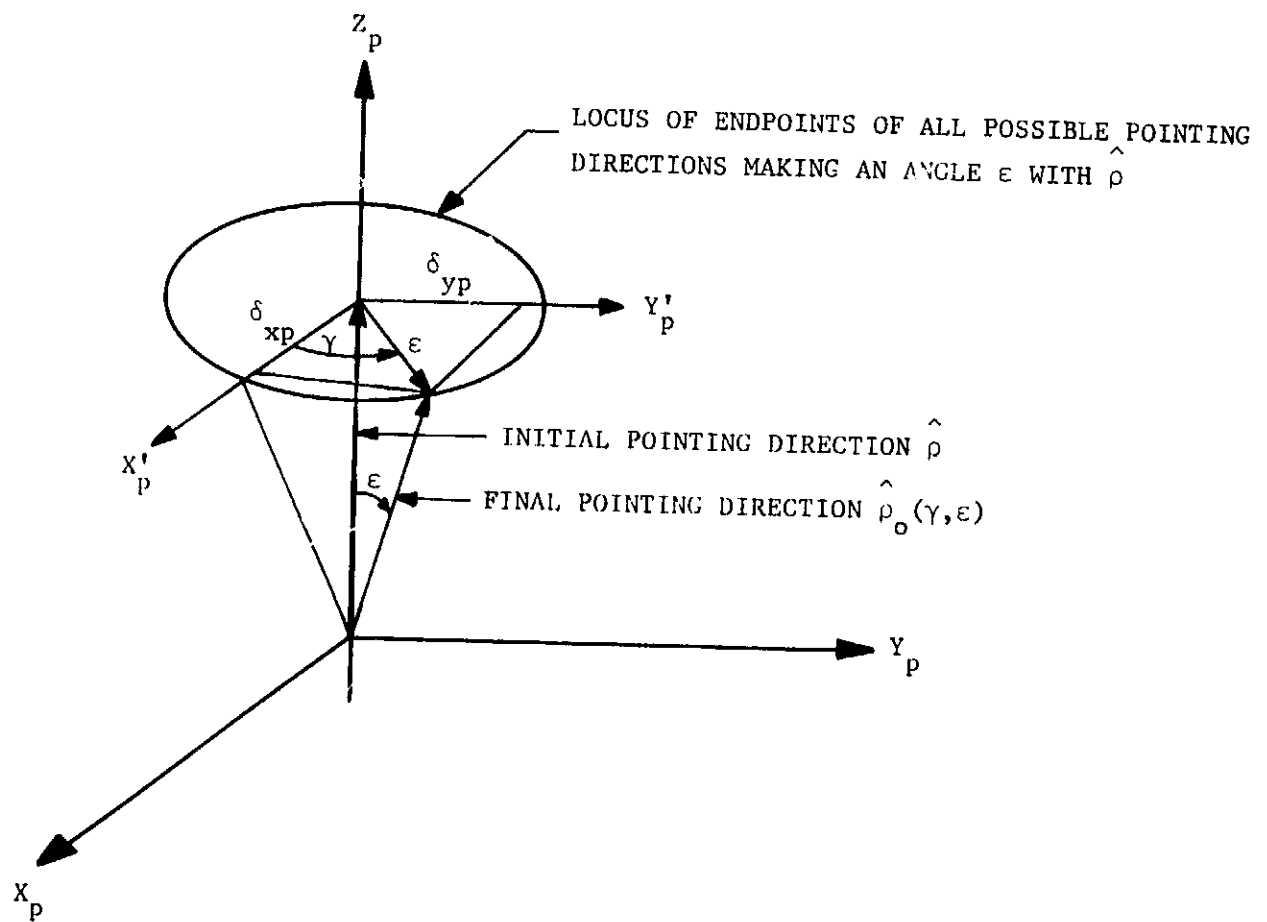


Figure 7-4. Relation of the Initial and Adjusted Lines of Sight

where the angle  $\epsilon$  is specified and the parameter  $\gamma$  can vary from 0 to  $2\pi$ .

With reference to figure 7-4, it is evident that for  $\epsilon$  small,  $\epsilon \cos \gamma$  is the change in the line of sight in the  $X_p$  direction and  $\epsilon \sin \gamma$  is that in the  $Y_p$  direction. Defining:

$$\delta_{xp} \triangleq \epsilon \cos \gamma$$

$$\delta_{yp} \triangleq \epsilon \sin \gamma$$

Then:

$$\sqrt{\delta_{xp}^2 + \delta_{yp}^2} = \epsilon$$

and the change in the line of sight can be alternatively defined by specifying the offsets  $\delta_{xp}$  and  $\delta_{yp}$ .

**7.5.1 Gimbal Motions of the IOG System** - To define the gimbal motions  $\delta\theta$  and  $\delta\psi$  required to move the optical axis from  $\hat{\rho}_p$  to  $\hat{\rho}_o$ , we need to find the gimbal angles  $\theta + \delta\theta$  and  $\phi + \delta\phi$  that will place the  $Z_p$  axis along  $\hat{\rho}_o$ . In base coordinates the vector  $\hat{\rho}_o$  is:

$$\hat{\rho}_{ob} = \begin{bmatrix} \cos(\theta + \delta\theta) & 0 & \sin(\theta + \delta\theta) \\ 0 & 1 & 0 \\ -\sin(\theta + \delta\theta) & 0 & \cos(\theta + \delta\theta) \end{bmatrix} \begin{bmatrix} 1 & 0 & 0 \\ 0 & \cos(\phi + \delta\phi) & -\sin(\phi + \delta\phi) \\ 0 & \sin(\phi + \delta\phi) & \cos(\phi + \delta\phi) \end{bmatrix} \begin{bmatrix} 0 \\ 0 \\ 1 \end{bmatrix}$$

Alternatively,  $\hat{\rho}_{ob}$  can be expressed in terms of the preexisting gimbal angles  $\theta$  and  $\phi$  and the parameters  $\epsilon$  and  $\gamma$  as:

$$\hat{\rho}_{ob} = \begin{bmatrix} \cos\theta & 0 & \sin\theta \\ 0 & 1 & 0 \\ -\sin\theta & 0 & \cos\theta \end{bmatrix} \begin{bmatrix} 1 & 0 & 0 \\ 0 & \cos\phi & -\sin\phi \\ 0 & \sin\phi & \cos\phi \end{bmatrix} \begin{bmatrix} \sin\epsilon \cos\gamma \\ \sin\epsilon \sin\gamma \\ \cos\epsilon \end{bmatrix}$$



Equating the two expressions:

$$\begin{bmatrix} \cos\theta & 0 & \sin\theta \\ 0 & 1 & 0 \\ -\sin\theta & 0 & \cos\theta \end{bmatrix} \begin{bmatrix} 1 & 0 & 0 \\ 0 & \cos\phi & -\sin\phi \\ 0 & \sin\phi & \cos\phi \end{bmatrix} \begin{bmatrix} \sin\epsilon\cos\gamma \\ \sin\epsilon\sin\gamma \\ \cos\epsilon \end{bmatrix} =$$

$$\begin{bmatrix} \cos\theta & 0 & \sin\theta \\ 0 & 1 & 0 \\ -\sin\theta & 0 & \cos\theta \end{bmatrix} \begin{bmatrix} \cos\delta\theta & 0 & \sin\delta\theta \\ 0 & 1 & 0 \\ -\sin\delta\theta & 0 & \cos\delta\theta \end{bmatrix} \begin{bmatrix} 0 \\ -\sin(\phi+\delta\phi) \\ \cos(\phi+\delta\phi) \end{bmatrix}$$

Clearly, the matrices involving  $\theta$  may be removed by premultiplying by the inverse transformation, thus illustrating the independence of the differential motions  $\delta\alpha$  and  $\delta\beta$  from the outer gimbal angle  $\theta$ . Doing this and premultiplying by the inverse of the  $\delta\theta$  matrix gives:

$$\begin{bmatrix} \sin\epsilon\cos\gamma\cos\delta\phi - (\sin\epsilon\sin\gamma\sin\phi + \cos\epsilon\cos\phi)\sin\delta\theta \\ \sin\epsilon\sin\gamma\cos\phi - \cos\epsilon\sin\phi \\ \sin\epsilon\cos\gamma\sin\delta\theta + (\sin\epsilon\sin\gamma\sin\phi + \cos\epsilon\cos\phi)\cos\delta\theta \end{bmatrix} = \begin{bmatrix} 0 \\ -\sin(\phi+\delta\phi) \\ \cos(\phi+\delta\phi) \end{bmatrix}$$

For an arbitrary angle  $\epsilon$ , this vector equation may be solved first for  $\delta\theta$  by using the X components, then for  $\delta\phi$  by using the Y components and checking with the Z components, all by means of standard trigonometric techniques.

However, since  $\epsilon$  will in general be sufficiently small to allow use of the small angle approximations and since in this case both  $\delta\theta$  and  $\delta\phi$  will be bounded by  $\epsilon$  for all  $\phi < \pi/2 - \epsilon$ , the above equation can be written as:

$$\begin{bmatrix} \epsilon\cos\gamma - \delta\theta\cos\phi \\ \epsilon\sin\gamma\cos\phi - \sin\phi \\ \delta\theta\cos\phi \end{bmatrix} = \begin{bmatrix} 0 \\ -\sin\phi - \delta\phi\cos\phi \\ \cos\phi - \delta\phi\sin\phi \end{bmatrix}$$

from which the required motions are:

$$\delta\phi = -\epsilon \sin\gamma$$

$$\delta\theta = \frac{\epsilon \cos\gamma}{\cos\gamma}$$

The denominator of the expression for  $\delta\theta$  approaches 0 as  $\phi$  approaches  $\pi/2$ , however, a physical stop will occur for an angle some degrees less than  $\pi/2$ , thus the above expressions can be considered valid for any allowable gimbal angles  $\theta$  and  $\phi$ . The result could indeed have been inferred directly from figure 7-4.

**7.5.2 Gimbal Motions of the Classical System** - In a similar development it is necessary to define the gimbal motions  $\delta\alpha$  and  $\delta\beta$  required to move the line of sight from  $\hat{\rho}$  to  $\hat{\rho}_o$  for the classical gimbal system. We require that the gimbal angles  $\alpha+\delta\alpha$ ,  $\beta+\delta\beta$  will place the line of sight along the  $Z_p$  axis, or:

$$\hat{\rho}_{ob} = \begin{bmatrix} \cos(\alpha+\delta\alpha) & -\sin(\alpha+\delta\alpha) & 0 \\ \sin(\alpha+\delta\alpha) & \cos(\alpha+\delta\alpha) & 0 \\ 0 & 0 & 1 \end{bmatrix} \begin{bmatrix} \cos(\beta+\delta\beta) & 0 & \sin(\beta+\delta\beta) \\ 0 & 1 & 0 \\ -\sin(\beta+\delta\beta) & 0 & \cos(\beta+\delta\beta) \end{bmatrix} \begin{bmatrix} 0 \\ 0 \\ 1 \end{bmatrix}$$

Equating the two expressions for  $\hat{\rho}_{ob}$  after performing the second multiplication and separating the first matrix of the preceding equation:

$$\begin{bmatrix} \cos\alpha & -\sin\alpha & 0 \\ \sin\alpha & \cos\alpha & 0 \\ 0 & 0 & 1 \end{bmatrix} \begin{bmatrix} \cos\beta & 0 & \sin\beta \\ 0 & 1 & 0 \\ -\sin\beta & 0 & \cos\beta \end{bmatrix} \begin{bmatrix} \sin\epsilon \cos\gamma \\ \sin\epsilon \sin\gamma \\ \cos\epsilon \end{bmatrix} =$$

$$\begin{bmatrix} \cos\alpha & -\sin\alpha & 0 \\ \sin\alpha & \cos\alpha & 0 \\ 0 & 0 & 1 \end{bmatrix} \begin{bmatrix} \cos\delta\alpha & -\sin\delta\alpha & 0 \\ \sin\delta\alpha & \cos\delta\alpha & 0 \\ 0 & 0 & 1 \end{bmatrix} \begin{bmatrix} \sin(\beta+\delta\beta) \\ 0 \\ \cos(\beta+\delta\beta) \end{bmatrix}$$

Clearly, the  $\alpha$  matrices may be removed (i.e., premultiply by  $[I_B]$ ) and as might have been expected, the differential motions  $\delta\alpha$  and  $\delta\beta$  are independent of the outer gimbal angle  $\alpha$ . Doing this and premultiplying both sides by the  $\delta\alpha$  transformation inverse:

$$\begin{bmatrix} (\sin\epsilon\cos\gamma\cos\beta+\cos\epsilon\sin\beta)\cos\delta\alpha+\sin\epsilon\sin\gamma\sin\delta\alpha \\ -(\sin\epsilon\cos\gamma\cos\beta+\cos\epsilon\sin\beta)\sin\delta\alpha+\sin\epsilon\sin\gamma\cos\delta\alpha \\ -\sin\epsilon\cos\gamma\sin\beta+\cos\epsilon\cos\beta \end{bmatrix} = \begin{bmatrix} \sin(\beta+\delta\beta) \\ 0 \\ \cos(\beta+\delta\beta) \end{bmatrix}$$

For any arbitrary angle  $\epsilon$ , this equation may be solved first for  $\delta\beta$  as a function of  $\beta$ ,  $\epsilon$  and the parameter  $\gamma$  using the Z components then for  $\delta\alpha$  using the Y components, and checking with the remaining X components, all by means of standard trigonometric techniques. In addition it can be shown from the equation or directly from the geometry of the problem that:

$$\delta\beta < \epsilon$$

$$\sin\delta\alpha < \frac{\sin\epsilon}{\sin\beta} \text{ for } \beta > \epsilon$$

The solutions for  $\delta\alpha$  and  $\delta\beta$  can be greatly simplified by specifying  $\epsilon$  sufficiently small that  $\sin\epsilon \approx \tan\epsilon \approx \epsilon$ ,  $\cos\epsilon \approx 1$ . In this case since  $\delta\beta < \epsilon$ ,  $\sin\delta\beta \approx \delta\beta$ ,  $\cos\delta\beta \approx 1$ :

$$\begin{bmatrix} (\sin\beta+\epsilon\cos\gamma\cos\beta)\cos\delta\alpha+\epsilon\sin\gamma\sin\delta\alpha \\ -(\sin\beta+\epsilon\cos\gamma\cos\beta)\sin\delta\alpha+\epsilon\sin\gamma\cos\delta\alpha \\ -\epsilon\cos\gamma\sin\beta+\cos\beta \end{bmatrix} = \begin{bmatrix} \sin\beta+\delta\beta\cos\beta \\ 0 \\ \cos\beta-\delta\beta\sin\beta \end{bmatrix}$$

Equating the Z components:

$$\delta\beta = \epsilon\cos\gamma$$

Equating the Y components:

$$\epsilon\sin\gamma\cos\delta\alpha - (\sin\beta+\epsilon\cos\gamma\cos\beta)\sin\delta\alpha = 0$$

Although  $\delta\beta$  is always small when  $\epsilon$  is small,  $\delta\alpha$  can be as large as  $\pm\pi$  when the inner gimbal angle is less than  $\epsilon$ , thus additional simplification must proceed in stages. First, for  $\beta < \epsilon$ , the small angle approximations can be used for  $\beta$  and:

$$\left. \begin{aligned} \delta\alpha &= \tan^{-1} \frac{\epsilon \sin \gamma}{\beta + \epsilon \cos \gamma}, \quad \beta + \epsilon \cos \gamma > 0 \\ &= \tan^{-1} \frac{\epsilon \sin \gamma}{\beta + \epsilon \cos \gamma} + \pi \operatorname{sgn}\{\sin \gamma\}, \quad \beta + \epsilon \cos \gamma < 0 \end{aligned} \right\} \beta < \epsilon$$

For  $\beta$  greater than or equal  $\epsilon$ ,  $\delta\alpha$  cannot exceed  $\pi/2$ , thus the principal arc-tangent can be used and:

$$\delta\alpha = \tan^{-1} \frac{\epsilon \sin \gamma}{\beta + \epsilon \cos \gamma}, \quad \beta \geq \epsilon$$

As  $\beta$  increases, the limit on  $\sin \delta\alpha$  decreases according, indeed for  $\sin \beta = 15\epsilon$ ,  $\sin \delta\alpha \leq \frac{1}{15}$  and  $\sin \delta\alpha = \delta\alpha$  to three significant figures, thus:

$$\delta\alpha = \frac{\epsilon \sin \gamma}{\beta + \epsilon \cos \gamma}, \quad \beta \geq 15\epsilon$$

Expressing  $\beta$  as  $k\epsilon$ ,  $k \geq 1$ ,  $\delta\alpha = \sin \gamma / (k + \cos \gamma)$  and for  $k$  greater than 60,  $\sin \gamma / k = \sin \gamma / (k + \cos \gamma)$  to three significant figures and:

$$\delta\alpha = \frac{\epsilon \sin \gamma}{\beta}, \quad \beta \geq 60\epsilon$$

Finally, as  $\beta$  increases to around 4 degrees, the denominator of the above equation must be replaced by  $\sin \beta$  in order to maintain three significant figure accuracy:

$$\delta\alpha = \frac{\epsilon \sin \gamma}{\sin \beta}, \quad \beta \geq 4^\circ$$

**7.6 Conclusions** - Support frames are shown for the IOG experiment mounting system and an alternate classical gimbal experiment mounting system. Attachment of base mount to support frame and frame to pallet is discussed for both systems.

Bounds are established for line of sight errors caused by angular misalignments in the mounting systems. In both cases the line of sight error bound is of the following form:

$$\epsilon < m_0 + \sqrt{Z_0^2 + n_0^2} + Z_1 + n_1$$

where  $m_0$  is the total (two axis) angular misalignment of the gimbal base with respect to the pallet,  $Z_0$  and  $Z_1$  are the bias errors of the

zero points of the outer and inner gimbals, respectively, and  $n_o$  and  $n_i$  are the outer gimbal/inner gimbal and inner gimbal/optical axis nonorthogonalities.

Differential gimbal motions required to move the optical axis through small angles  $\delta_{xp}$  and  $\delta_{yp}$  from an initial pointing direction are derived for both mounting arrangements. For the IOG the differential motions  $\delta\theta$  (outer gimbal) and  $\delta\phi$  (inner gimbal) are:

$$\delta\phi = -\delta_{yp}$$

$$\delta\theta = \frac{\delta_{xp}}{\cos\phi}$$

For the classical system the motions  $\delta\alpha$  (outer gimbal) and  $\delta\beta$  (inner gimbal) are:

$$\delta\beta = \delta_{xp}$$

$$\epsilon = \sqrt{\delta_{xp}^2 + \delta_{yp}^2}$$

$$\left. \begin{aligned} \delta\alpha &= \tan^{-1} \frac{\delta_{yp}}{\beta + \delta_{xp}}, \quad \beta + \delta_{xp} > 0 \\ &= \tan^{-1} \frac{\delta_{yp}}{\beta + \delta_{xp}} + \pi \sin\{\delta_{yp}\}, \quad \beta + \delta_{xp} < 0 \end{aligned} \right\} \beta < \epsilon$$

$$\begin{aligned} &= \tan^{-1} \frac{\delta_{yp}}{\beta + \delta_{xp}} && \epsilon \leq \beta < 15\epsilon \\ &= \frac{\delta_{yp}}{\beta + \delta_{xp}} && 15\epsilon \leq \beta < 60\epsilon \\ &= \frac{\delta_{yp}}{\beta} && 60\epsilon \leq \beta < 4^\circ \\ &= \frac{\delta_{yp}}{\sin\beta} && \beta > 4^\circ \end{aligned}$$

The complexity of the expressions for the classical system arise from the gimbal singularity at the 0,0 gimbal angles. The corresponding singularity for the IOG occurs for an inner gimbal angle of  $\pm 90^\circ$ , which is outside the range of allowable motion.

## 8. PALLET COMMON MODULE CONFIGURATION

8.1 General - This section specifically deals with a pallet common module developed from existing pallet segments and modified to incorporate those features required for a suspended experiment platform. The basic pallet segment is 3 meters in length with a U-shaped cross section of typical aeronautical construction. Three segments are interconnected forming a pallet. An integral pattern of hard points are provided for mounting heavy experiments while lighter experiments can be mounted on inner floor panels and side wall panels via inserts with self-locking threads.

8.2 Summary - The pallet common module resulted from the investigations of sections 4, 5, and 6, plus the basic three segment pallet. The suspension system, section 4, provides the necessary in orbit isolation of the pallet from the orbiter. The retention system, section 5, provides the support of the pallet to the orbiter during launch and descent. The installation of the control moment gyroscopes, section 6, provides the stabilization of the suspended pallet to meet the various experiment requirements. The pallet common module as shown in figure 8-1 incorporates these systems.

### 8.3 Discussion

8.3.1 Design Objectives - The pallet common module shall provide means of supporting various experiment arrangements. The pallet common module shall incorporate a suspension system capable of supporting the pallet during in orbit data acquisition and will isolate the pallet from orbiter vibrational disturbances. The pallet common module shall incorporate a retention system capable of supporting the pallet during launch and descent, disengaging in orbit to allow the pallet to float on the suspension system. The pallet common module shall incorporate a control system capable of stabilizing the pallet to meet the various experiment requirements.

8.3.2 Suspension System Installation - The suspension system installation as shown in figure 8-1 is based on the gas filled bellows defined in section 4. Figure 8-2 defines the arrangement of the aft left hand location; the three remaining locations have a similar arrangement.

The space between the orbiter side beam and the pallet outer panel is utilized to minimize structural modification. The orbiter attachment fitting as shown is a detail, machined from aluminum plate; the final design would depend upon the orbiter side beam configuration. The pallet attachment details are formed aluminum sheet metal

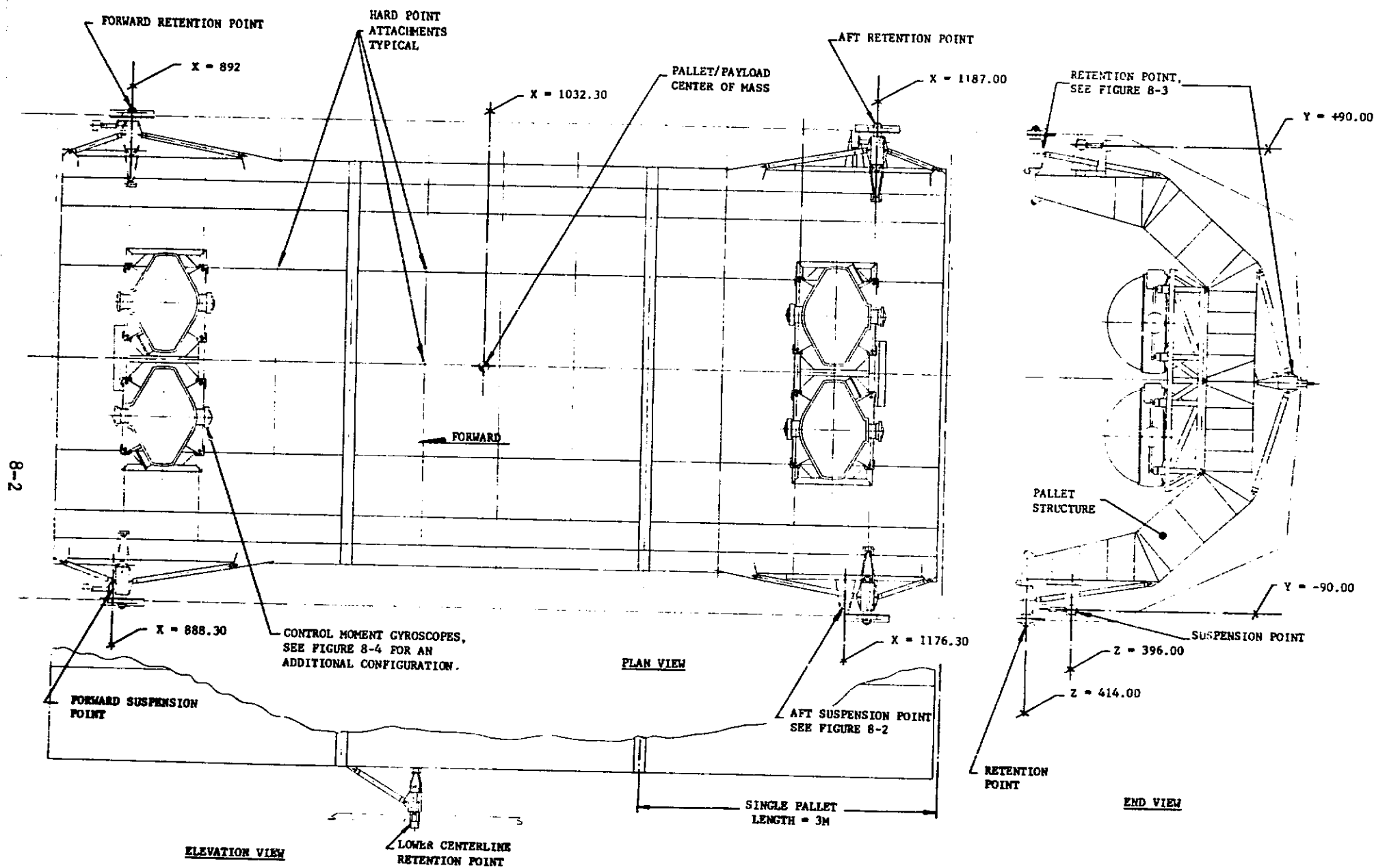


Figure 8-1. Pallet Common Module



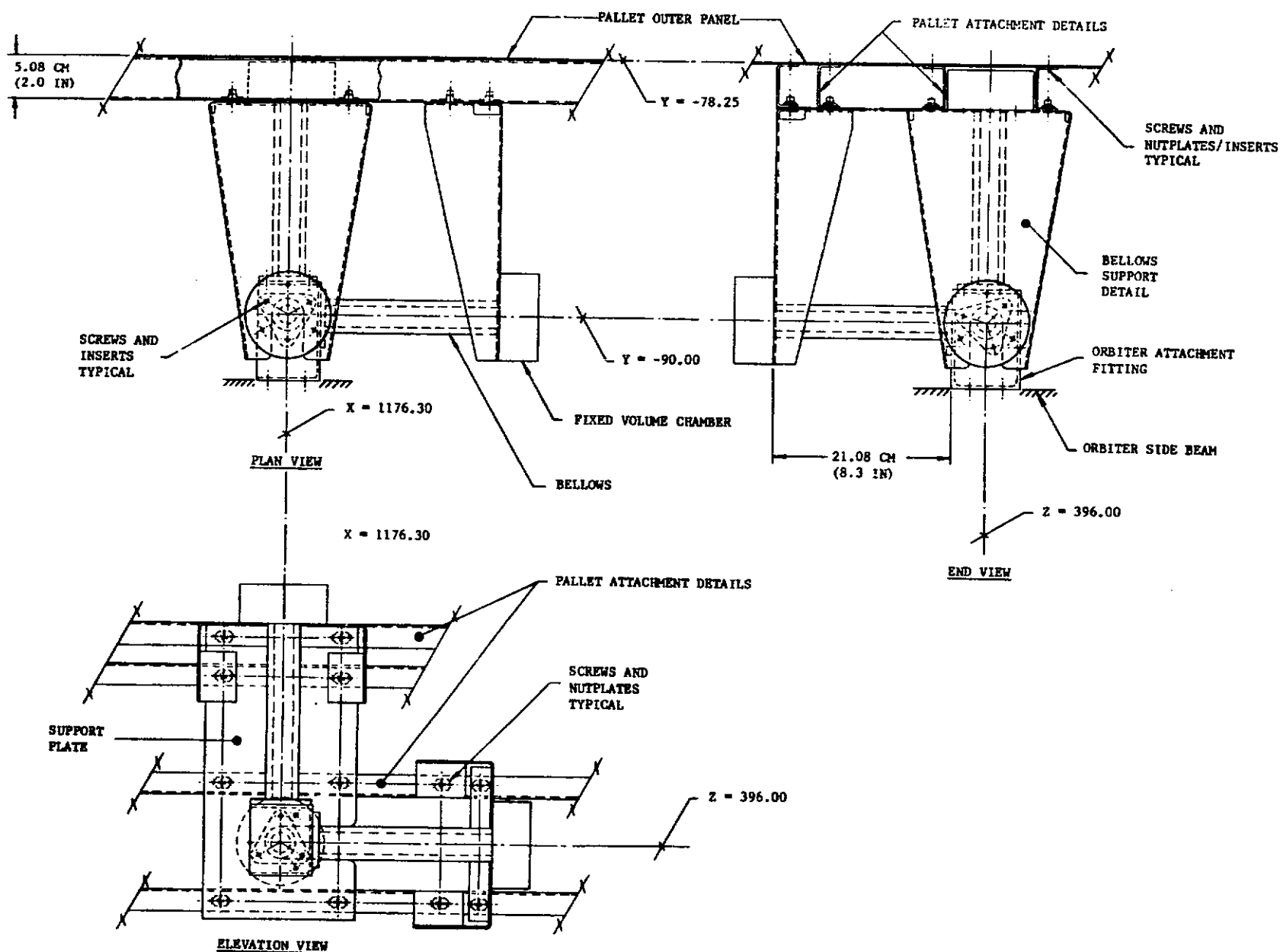


Figure 8-2. Suspension System - Gas Filled Bellows  
Aft Left-Hand Location

channels. These details stiffen the outer panel as required and can be configured to span the distance between the pallet frames if required. The bellows support details are formed aluminum sheet metal parts sized to provide reasonable stiffness. All assembly and installation hardware utilize screws, nutplates/inserts combinations. The installation can be controlled with normal tolerances associated with this type of construction.

8.3.3 Retention System Installation - The retention system installation as shown in figure 8-3 is based on the movable mounting shaft configuration defined in section 5. Figure 8-3 defines the arrangement of the aft right-hand location of the cargo bay main longeron retention points and the low centerline retention point.

The pallet fittings, machined parts, are similar to existing fittings but require a smooth bore for the movable mounting shafts and drive mechanism motor actuator attachments. The various struts from the pallet fittings to the pallet structure are either existing struts or new shorter struts depending upon final design. All assembly and installation hardware to the pallet utilizes existing attachment locations and bolts, nutplates/nuts combinations.

8.3.4 Control Moment Gyroscope Installation - The CMG installation is based on the two support frame configurations defined in section 6. Figure 8-1 shows the two support frames located on the end pallets. Figure 8-4 shows the single support frame located on one end of the pallet train. Both installations utilize bolts, through the frames, engaging existing pallet hard points. Both installations show the versatility of integrating the CMGs to the pallet train. Final location would depend upon payload integration requirements.

8.4 Pallet Modifications/Improvements - The pallet structure must be modified to accept the suspension system. Actual modification depends upon the stiffness of the pallet outer panels. If the pallet outer panels are of honeycomb construction with adequate attachments to the pallet framework, modification requirements are merely bonding threaded inserts into the panels. If the pallet outer panels are aluminum sheet webs, modification requirements are based on stiffening the web with the attachment channels spanning the distance between pallet frames. As indicated, major modifications are not required and can be accomplished with simple tools at the time of installing the suspension system.

The existing pallet retention fittings can not be modified and must be replaced with new fittings. Since the existing fittings are probably forgings made from high strength materials replacement expense would involve forging tooling and procurement lead time. Therefore a reasonable improvement would be to incorporate the recommended retention system with movable mounting shafts on all pallets.

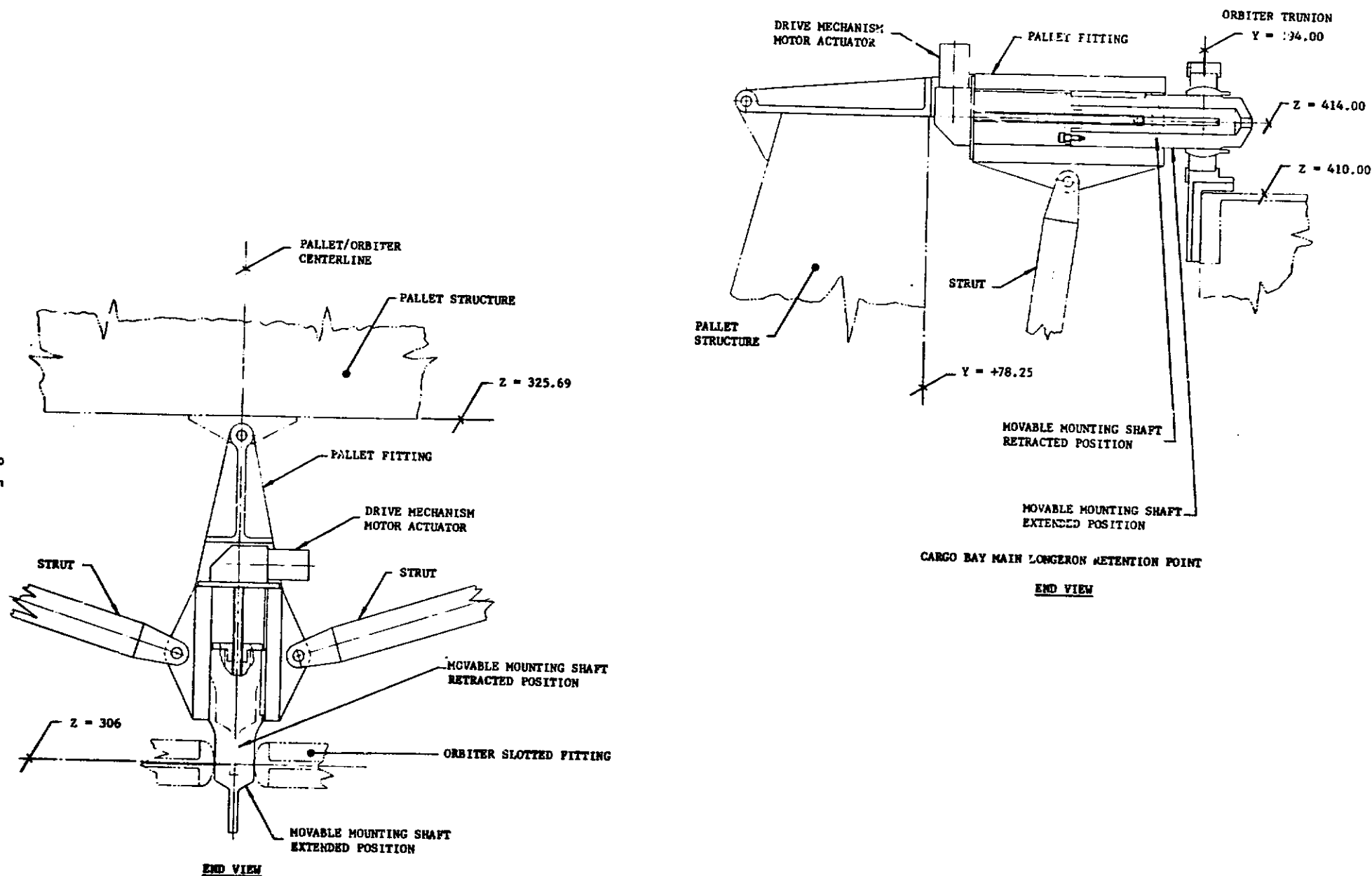


Figure 8-3. Retention System - Movable Mounting Shafts

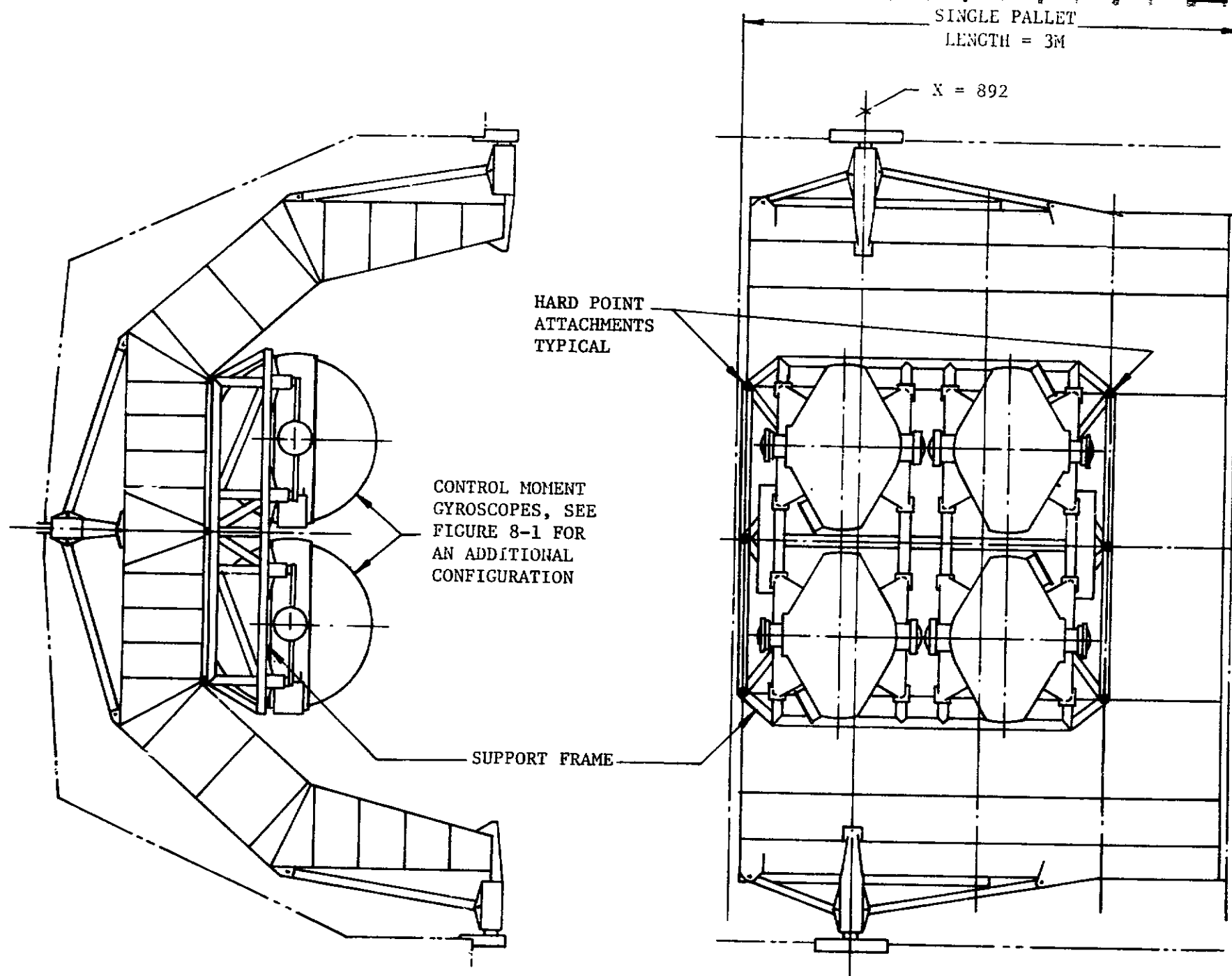


Figure 8-4. Four Control Moment Gyroscopes on a Single Pallet

8.5 Conclusion - The installation of the suspension system requires simple pallet modifications which can be incorporated during payload integration.

Incorporation of the recommended retention system will result in lower program costs, as the retention system with movable mounting shafts can accommodate missions with or without the suspension system.

Since the installation of the CMGs utilizes existing pallet hard points, pallet modifications are not required and payload experiment arrangements can be maximized.

9. REFERENCES

1. Bendix Navigation and Control Division, Internal Memorandum No. BA-5265 (telephone data transmittal from Messrs. J. Howell and P. D. Nicaisse of NASA-MSFC).
2. MCR 277, Payload Structural Attachments (Parametric Analysis) as contained in J. C. Heberling (NASA-Houston) to T. J. Lee (NASA-MSFC) data transmittal of March 9, 1974, reference LP-8-241.
3. Mechanical Spring Design Manual, North American Rockwell, 1972, page 18.
4. Miniature Metal Bellows, Servometer Corporation, Clifton, New Jersey.
5. Mechanical Design and Systems Handbook, McGraw-Hill Book Company, 1964, sections 34 and 36.